

FOR OFFICIAL USE ONLY

JPRS L/10511

12 May 1982

# USSR Report

EARTH SCIENCES

(FOUO 2/82)



FOREIGN BROADCAST INFORMATION SERVICE

FOR OFFICIAL USE ONLY

NOTE

JPRS publications contain information primarily from foreign newspapers, periodicals and books, but also from news agency transmissions and broadcasts. Materials from foreign-language sources are translated; those from English-language sources are transcribed or reprinted, with the original phrasing and other characteristics retained.

Headlines, editorial reports, and material enclosed in brackets [] are supplied by JPRS. Processing indicators such as [Text] or [Excerpt] in the first line of each item, or following the last line of a brief, indicate how the original information was processed. Where no processing indicator is given, the information was summarized or extracted.

Unfamiliar names rendered phonetically or transliterated are enclosed in parentheses. Words or names preceded by a question mark and enclosed in parentheses were not clear in the original but have been supplied as appropriate in context. Other unattributed parenthetical notes within the body of an item originate with the source. Times within items are as given by source.

The contents of this publication in no way represent the policies, views or attitudes of the U.S. Government.

COPYRIGHT LAWS AND REGULATIONS GOVERNING OWNERSHIP OF  
MATERIALS REPRODUCED HEREIN REQUIRE THAT DISSEMINATION  
OF THIS PUBLICATION BE RESTRICTED FOR OFFICIAL USE ONLY.

JPRS L/10511

12 May 1982

USSR REPORT  
EARTH SCIENCES

(FOUO 2/82)

CONTENTS

OCEANOGRAPHY

Estimating Level of Microscale Turbulence Using Empirical Correlation With Richardson Number .....	1
New Data on Structure of Ampere Seamount .....	8
Effect of Sensor Size on Estimation of Rate of Dissipation of Turbulent Energy in Ocean .....	14
Physical Aspects of Remote Sensing of Ocean-Atmosphere System .....	20
Effective Range of Hydroacoustic Apparatus .....	22
Geology of World Ocean Floor According to Deep-Water Drilling..	26
Study of Caribbean-Gulf of Mexico Basin .....	33
New Monograph on Oceanic Turbulence .....	39
Propagation of Internal Waves in Stratified Medium With Flow Velocity Shear .....	41
Effect of Thermal Structure of Upper Ocean Layer on Turbulence Development .....	51
Spectral Dependences of Light Scattering by Sea Water .....	60
Radar Observations of Wind Waves at Sea .....	67
Determination of Spectrum of Sea Waves by Spectral Analysis of Aerial Photographs .....	73

- a - [III - USSR - 21K S&T FOUO]

FOR OFFICIAL USE ONLY

**FOR OFFICIAL USE ONLY**

Investigation of Surface Wind Current on Sea .....	76
Adiabatic Interaction of Surface and Internal Waves .....	81
Organization of Computer-Instrument Interaction in Systems for Automation of Scientific Research With Variable Structure .....	87
Interaction of Computing Processes in Automated Research Vessels .....	101
Black Sea Hydrophysical, Hydrochemical Expedition Results .....	114
Marine Geophysical Exploration .....	117
Annotation, Abstracts of Articles in Collection 'Physical Aspects of Remote Sounding of Ocean- Atmosphere System' .....	119
<b>TERRESTRIAL GEOPHYSICS</b>	
One-Dimensional Computations of Displacements During Blast in Problems With Weak Two-Dimensionality .....	125

- b -

**FOR OFFICIAL USE ONLY**

FOR OFFICIAL USE ONLY

OCEANOGRAPHY

UDC 551.465.15

ESTIMATING LEVEL OF MICROSCALE TURBULENCE USING EMPIRICAL CORRELATION WITH RICHARDSON NUMBER

Moscow OKEANOLOGIYA in Russian Vol 22, No 1, Jan-Feb 82 (manuscript received 15 Oct 80, after revision 11 Feb 81) pp 30-34

[Article by V. D. Pozdynin, Institute of Oceanology imeni P. P. Shirshov, USSR Academy of Sciences, Moscow]

[Text]

Abstract: On the basis of the results of synchronous measurements of microscale velocity fluctuations of a current, its vertical gradients and the vertical gradients of water density a study was made of the empirical dependence of the mean square turbulence level  $\sqrt{u'^2}$  on the Richardson number in the form  $\sqrt{u'^2} = aRi^{-n}$ . It was found that with  $\sqrt{u'^2} < 0.3$  cm sec<sup>-1</sup> the correlation between  $\sqrt{u'^2}$  and Ri is lacking. For  $\sqrt{u'^2} > 0.3$  cm·sec<sup>-1</sup>  $n = 0.11$ ,  $a = 0.33$  cm·sec<sup>-1</sup>. An algorithm is proposed for computing the distributions  $\sqrt{u'^2}$  on the basis of the known Ri distribution. An example of computation of the  $\sqrt{u'^2}$  distribution is given in a system of equatorial currents in the central part of the Pacific Ocean.

The authors of [1, 9] gives empirical formulas expressing the dependence of the level of microscale turbulence  $\sqrt{u'^2}$  on the Richardson number:

$$Ri = - \frac{g}{\rho} \frac{d\rho/dz}{(dU/dz)^2}, \quad (1)$$

where  $\rho$  and  $d\rho/dz$  is water density and its vertical gradient,  $dU/dz$  is the vertical gradient of current velocity,  $g$  is the acceleration of gravity.

The empirical dependence of  $\sqrt{u'^2}$  on Ri was sought in [1, 9] in the form

$$\sqrt{u'^2} = aRi^{-n}, \quad (2)$$

## FOR OFFICIAL USE ONLY

where the  $a$  and  $n$  evaluations must be found using the results of in situ measurements of  $\sqrt{u'^2}$  and  $Ri$ .

With the present-day status of study of turbulence in the ocean an attractive side of the use of  $Ri$  in empirical correlations is the ease in obtaining its quantitative estimates with the use of existing standard oceanological instruments and as indicated by (1), its direct correlation with some of the principal characteristics of hydrological conditions.

Specialists at the Marine Turbulence Laboratory of the Institute of Oceanology, USSR Academy of Sciences, made measurements of  $\sqrt{u'^2}$  and  $Ri$  on several voyages beginning in 1971. A summary of evaluations of the parameters  $a$  and  $n$  in (2), obtained using materials from these measurements, is given in Table 1. The data in this table show that the values of the  $a$  parameter differ appreciably from one another. If they are interpreted, in accordance with (2), as the mean square turbulence levels existing in the ocean when  $Ri = 1$ , they all seem exaggerated, except for the last  $a$  evaluation. The tabulated  $n$  values indicate essentially different evaluations of the influence of  $Ri$  on the turbulence level. However, the value  $n = 0.25$  nevertheless is closer to the  $n$  evaluations obtained in equatorial polygons in the Atlantic and Pacific Oceans, and the very fact of a virtual coincidence of the latter need not necessarily be mere chance. In this connection it makes sense to discuss in greater detail the results of measurements made in 1980 in the Pacific Ocean.

During February-March 1980, in an equatorial polygon in the central part of the Pacific Ocean (24th voyage of the scientific research ship "Dmitriy Mendeleev"), it was possible to collect empirical material specially intended for refining the  $a$  and  $n$  parameters in (2). The initial data for  $Ri$  were determined on the basis of the results of bathometric series and special gradient measurements of current velocity carried out using strings of BPV current meters which were lowered from aboard a drifting ship. The depth distance between current meters was 10 m, but in a number of cases the distance was increased to 15 and 20 m. The exposures of the current meters at the horizons were 1 hour, in individual cases -- a half-hour. Computation of the vertical gradients of current velocity for  $Ri$  evaluations was carried out using the method described in [7]. Synchronously with current measurements in these same water layers measurements were made of turbulence characteristics using a freely falling sonde. The sonde was developed at the Atlantic Division of the Institute of Oceanology, USSR Academy of Sciences, under the direction of V. T. Paka and registers turbulence in the range of vertical scales from 2 to 25 cm.

The resulting  $\sqrt{u'^2}$  and  $Ri$  estimates were plotted on a graph with the coordinate axes  $\ln \sqrt{u'^2}$  and  $\ln Ri$ . It was found that with  $\sqrt{u'^2} < 0.3$  cm·sec<sup>-1</sup> there are no directed changes in  $\sqrt{u'^2}$  with a decrease or increase in  $Ri$ . For  $\sqrt{u'^2} > 0.3$  cm·sec<sup>-1</sup> values such a dependence is missing (Fig. 1). The data in Fig. 1 correspond to evaluations  $a = 0.33$  cm·sec<sup>-1</sup> and  $n = 0.11$ . The  $n$  value virtually coincided with its evaluation in the equatorial polygon in the Atlantic ( $n = 0.15$ ). However, the absence of a correlation between  $Ri$  and  $\sqrt{u'^2} < 0.3$  cm·sec<sup>-1</sup> can be attributed to the following factors.

## FOR OFFICIAL USE ONLY

The mean hourly Ri values, relating to water layers with a thickness of 10 meters or more, are too approximate for detecting a dependence between Ri and low turbulence levels; it is possible that for finding such a dependence it is necessary to use data on the fine structure of the vertical Ri profile, but it is probable that the sought-for dependence on Ri with  $\sqrt{u'^2} < 0.3 \text{ cm} \cdot \text{sec}^{-1}$  does not exist at all because the current becomes virtually laminar.

The measurements of internal waves in the equatorial polygon in the Pacific Ocean indicated their weak development: the probability of the collapse of the crests of such waves is small and the contribution of this mechanism for the generation of turbulence was absent at its observed level. In this case the value  $a = 0.33 \text{ cm} \cdot \text{sec}^{-1}$  can be regarded as an evaluation of the mean square turbulence level attributable primarily to the shear instability of current velocity and existing with  $Ri = 1$ . Thus, the formula

$$\sqrt{u'^2} = 0.33 Ri^{0.1}, \quad (3)$$

somewhat modified and refined in comparison with [9], makes it possible to obtain an evaluation of the mean square turbulence level  $\sqrt{u'^2} \geq 0.3 \cdot \text{sec}^{-1}$ . In this case, to be sure, there should be a certain assurance that the shear instability of a current is the predominant mechanism of generation of turbulence under given hydrological conditions.

Obtaining  $\sqrt{u'^2}$  evaluations on the basis of formulas of type (2) is dependent at the present time on the availability of data on Ri relating to different hydrological conditions in the ocean. During recent years considerable interest has been shown in determination of Ri values in the ocean. This is done both in an investigation of internal waves and in the study of the fine vertical structure of hydrophysical fields. There are studies in which sets of Ri evaluations have already been represented by empirical and theoretical distributions [2, 3].

On the 24th voyage of the scientific research ship "Dmitriy Mendeleev" Ri evaluations were obtained on five meridional sections in the equatorial polygon. They were given in the form of five meridional sections of the Ri field and in the form of a distribution for the three investigated layers of the ocean: upper quasihomogeneous layer, pycnocline layer and the layer situated directly beneath it with the lower limit of the measurements at a depth of 300 m [4]. These empirical Ri distributions agree with the exponential and hyperexponential (with two terms) distributions [5]. For the upper quasihomogeneous layer and the layer with its lower boundary at a depth of 300 m the Ri distribution has the form

$$f_1(Ri) = 2.4 \exp [-2.4 Ri], \quad (4)$$

for the pycnocline layer

$$f_2(Ri) = 0.5[2.4 \exp (-2.4 Ri) + 0.3 \exp (-0.3 Ri)]. \quad (5)$$

If the initial information on Ri is similar, for example, to (4) or (5), the results of the  $\sqrt{u'^2}$  computations can be represented in the form of the distribution  $g(\sqrt{u'^2})$ . The law of distribution of this particular function is found from the known law of distribution of its argument by transformation of the distribution of

## FOR OFFICIAL USE ONLY

the latter [10]; in our case with the use of (3), (4) and (5) we have

$$g(\sqrt{u'^2}) = f_i[\psi(\sqrt{u'^2})]|\psi'(\sqrt{u'^2})|, \quad i = 1, 2, \quad (6)$$

where  $\psi(\sqrt{u'^2})$  is a function, the inverse of (3);  $|\psi'(\sqrt{u'^2})|$  is the absolute value of its derivative. The concept "function, the inverse of (3)" requires an explanation. Formula (3) was derived as a regression equation for  $\sqrt{u'^2}$  relative to  $Ri$ . It is logical to assume that the "function, the inverse of (3)" in this case should be a regression equation for  $Ri$  relative to  $\sqrt{u'^2}$ , derived on the basis of the same empirical data as (3). This empirical dependence has the form  $Ri = 0.05(\sqrt{u'^2})^{-2.4}$ . It was used in computations made on the basis of formula (6).

Figure 2 shows the probability density function curves for  $\sqrt{u'^2}$  computed on the basis of formula (6) with the use of (4) and (5). As indicated by the shape of the curves in Fig. 2, the most probable mean square turbulence levels fall in the range 0.3-0.4 cm·sec<sup>-1</sup>. The distributions in Fig. 2 cannot be identified with the distributions describing the actual state of the turbulence level under given hydrological conditions and in a definite range of vertical scales of inhomogeneities.

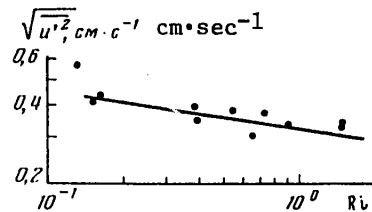


Fig. 1. Empirical dependence between  $Ri$  and  $\sqrt{u'^2}$  according to measurement data for equatorial polygon in central part of Pacific Ocean in February-March 1980.

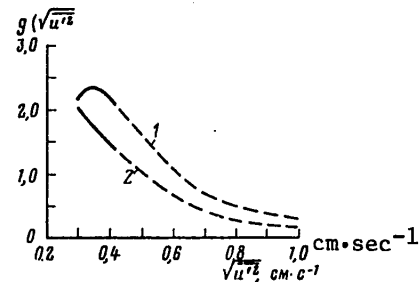


Fig. 2. Probability density curves  $\sqrt{u'^2}$  computed using (4)-(6). 1) upper quasi-homogeneous layer and layer with lower limit at a depth of 300 m; 2) pycnocline layer. The segments of the curves represented by solid lines show the  $\sqrt{u'^2}$  range in which the empirical dependence (3) was obtained making use of  $\sqrt{u'^2}$  and  $Ri$  measurements in the equatorial polygon.

The distributions in Fig. 2 do not contain information on turbulence levels less than 0.3 cm·sec<sup>-1</sup> because (3) is valid only for  $\sqrt{u'^2} \geq 0.3$  cm·sec<sup>-1</sup>. The dashed segments of the curves in Fig. 2 must be regarded as preferable because (3) was derived for the range  $0.3 \leq \sqrt{u'^2} < 0.5$  cm·sec<sup>-1</sup>, as indicated in Fig. 1. In this case the formal extrapolation of (3) in the direction  $Ri < 0.15$  seems premature. The  $Ri < 0.15$  values may be critical for ocean conditions and it is not precluded that in the initial stages of loss of stability by the current the relationships

## FOR OFFICIAL USE ONLY

between  $Ri$  and  $\sqrt{u'^2}$  have a great scatter, which with  $Ri < 0.15$  makes (3) unsuitable for practical use. For  $Ri < 0.15$  the empirical formula (3) requires experimental checking. At the present time distributions similar to those cited in Fig. 2 are more correctly interpreted as distributions of the mean square levels of turbulent disturbances which may exist with the observed distributions of Richardson numbers simultaneously with weaker turbulence or even in its absence in individual water layers.

Evaluations of  $a$  and  $n$  Parameters According to Measurements of  $\sqrt{u'^2}$  and  $Ri$ 

Region	Time	Method	Scales of measured inhomogeneities	Evaluation of parameters $a, \text{cm} \cdot \text{sec}^{-1}$ $n$		Source
Equatorial, in central Atlantic	Feb 1971	Horizontal towing	2-150	1.3	0.15	[8, 9]
Equatorial, in central Indian Ocean	Feb 1974	Vertical sounding	2-150	2.2	0.50	[1]
Region of Kuroshio Current	Aug 1977	Approximation by theoretical dependence	2-150	4.7	0.25	[6]
Equatorial, in central part of Pacific Ocean	Mar 1980	Vertical sounding	2-25	0.33	0.11	This paper

In order to use (3) for obtaining  $\sqrt{u'^2}$  evaluations under the influence of one or several mechanisms for the generation of turbulence in the ocean it is necessary to take into account the scatter of  $a$  evaluations in the form of the  $\varphi(a)$  distribution with  $Ri = 1$  corresponding to a definite range in the scales of turbulent disturbances. There are no fundamental difficulties in obtaining this distribution. Then the determination of  $\sqrt{u'^2}$  on the basis of individual data on  $Ri$  and on its distribution law, for example, in the form (4) and (5), must be accomplished using formulas (3) and (6), substituting into them the modal or mean value  $a$ , in accordance with the distribution  $\varphi(a)$  with  $Ri = 1$ . There is also a more general approach to obtaining the  $\sqrt{u'^2}$  distribution as the quotient by dividing two independent random values, each of which conforms to definite distribution laws [11]. In our case the most probable types of these distributions can be a normal distribution for the  $a$  evaluations [10] and an exponential distribution for  $Ri$ , as follows from [3] and data from the 24th voyage of the scientific research ship "Dmitriy Mendeleev." The practical implementation of such computations will evidently become possible after clarifying the real form of the  $\varphi(a)$  distribution and an evaluation of its parameters.

Judging from the ever-increasing interest in the real values of the Richardson numbers in the ocean associated primarily with an analysis of the stability of movements, and bearing in mind the tendency in modern oceanological instrument making to produce multipurpose and multichannel instruments, it seems timely to raise the question of creation of a special "Ri-meter." By the use of such an instrument

## FOR OFFICIAL USE ONLY

the procedure of determining  $Ri$  would become in the practice of oceanological investigations as ordinary, for example, as the measurement of temperature or current velocity. The mass of  $Ri$  data for the ocean will find immediate multipurpose application.

In this paper we used empirical data obtained on the 24th voyage of the scientific research vessel "Dmitriy Mendeleev." The turbulence measurements were made by a detachment headed by V. N. Nabatov under the immediate direction of the head of this voyage, V. T. Paka. The primary processing of these data on a shipboard electronic computer was carried out by A. L. Sukhov. Gradient measurements of the current were made by a detachment headed by V. D. Yegorikhin. Computations of the  $Ri$  evaluations were made by A. N. Gezentsvey.

The author expresses appreciation to V. S. Belyayev and A. Yu. Benilov, whose critical comments assisted in introducing refinements into the text of the paper and simplifying the proposed computation procedure.

## BIBLIOGRAPHY

1. Belyayev, V. S., Lozovatskiy, I. D. and Ozmidov, R. V., "Correlation Between the Parameters of Microscale Turbulence and Local Conditions of Ocean Stratification," *IZV. AN SSSR: FIZIKA ATMOSFERY I OKEANA* (News of the USSR Academy of Sciences: Physics of the Atmosphere and Ocean), Vol 11, No 7, pp 718-725, 1975.
2. Belyayev, V. S. and Gezentsvey, A. N., "Shear Instability of Internal Waves in the Ocean," *IZV. AN SSSR: FIZIKA ATMOSFERY I OKEANA*, Vol 14, No 6, pp 648-655, 1978.
3. Varlatyy, Ye. P., Ozmidov, R. V. and Pyzhevich, M. L., "Values of the Local Richardson Numbers in the Ocean," *OKEANOLOGIYA* (Oceanology), Vol 21, No 2, pp 211-216, 1981.
4. Gezentsvey, A. N. and Pozdynin, V. D., "Evaluation of the Richardson Number From Measurements in the Equatorial Currents of the Central Part of the Pacific Ocean," *OKEANOLOGIYA* (Oceanology), Vol 21, No 4, pp 587-591, 1981.
5. Kofman, A. and Kryuon, R., *MASSOVOYE OBSLUZHIVANIYE, TEORIYA I PRIMENENIYE* (Mass Servicing, Theory and Application), Moscow, Mir, 1965.
6. Lozovatskiy, I. D. and Ozmidov, R. V., "Correlation Between the Characteristics of Microscale Turbulence and Water Stratification Parameters in the Ocean," *OKEANOLOGIYA*, Vol 19, No 6, pp 982-991, 1979.
7. Pozdynin, V. D., "Determination of Vertical Current Velocity Gradients in the Ocean According to Data From BPV-2 Current Meters," *ISSEDOVANIYE OKEANICHESKOY TURBULENTNOSTI* (Investigations of Ocean Turbulence), Moscow, Nauka, pp 79-86, 1973.
8. Pozdynin, V. D., "Statistical Evaluations of Parameters of Microscale Oceanic Turbulence," *ISSEDOVANIYE IZMENCHIVOSTI GIDROFIZICHESKIKH POLEY V OKEANE* (Investigation of Variability of Hydrophysical Fields in the Ocean), Moscow, Nauka, pp 50-61, 1974.

FOR OFFICIAL USE ONLY

9. Pozdynin, V. D., "Some Statistical Patterns of Microscale Turbulence," OKEANOLOGIYA, Vol 16, No 5, pp 791-797, 1976.
10. Khal'd, A., MATEMATICHESKAYA STATISTIKA S TEKHNICHESKIMI PRILOZHENIYAM (Mathematical Statistics With Technical Applications), Moscow, Izd-vo Inostr. Lit., 1956.
11. Khan, G. and Shapiro, S., STATISTICHESKIYE MODELI V INZHENERNYKH ZADACHAKH (Statistical Models in Engineering Problems), Moscow, Mir, 1969.

COPYRIGHT: Izdatel'stvo "Nauka", "Okeanologiya", 1982

5303

CSO: 1865/106

7  
FOR OFFICIAL USE ONLY

FOR OFFICIAL USE ONLY

UDC 551.462.64

NEW DATA ON STRUCTURE OF AMPERE SEAMOUNT

Moscow OKEANOLOGIYA in Russian Vol 22, No 1, Jan-Feb 82 (manuscript received 29 Sep 80, after revision 25 Mar 81) pp 87-90

[Article by V. M. Litvin, V. V. Matveyenkov, E. L. Onishchenko, M. V. Rudenko and A. M. Sagalevich, Institute of Oceanology imeni P. P. Shirshov, USSR Academy of Sciences, Moscow]

[Text]

Abstract: The Ampere seamount was studied using the "Paysis" manned vehicle and the "Zvuk-4m" complex. The seamount is made up of volcanic rocks, including trachytes. The latter are exposed in the form of narrow, linear ridges. Conglomerates dissected by scour and cavernous limestones were discovered at the seamount peak.

The Ampere seamount, situated to the west of the Strait of Gibraltar, has long been known [8]. At different times Soviet and foreign expeditions have carried out surveys of bottom relief and the magnetic field, as well as underwater photography and the collection of samples of bottom sediments and rocks [1, 4, 6, 7]. Accordingly, the general features of its structure have been studied and the seamount is shown on all maps. During recent years new research methods and apparatus have appeared, including towed and manned underwater vehicles which make it possible to obtain qualitatively new information on the structure of the ocean floor. Such work is being intensively developed at the Institute of Oceanology, USSR Academy of Sciences.

On the 30th voyage of the scientific research ship "Akademik Kurchatov" in December 1979 and March 1980 specialists carried out an echo sounding survey over the Ampere seamount, together with photographing of the floor with a camera attached to a cable, trawling with a biological trawl, and at the same time, and what is most important, work with the "Paysis" underwater manned vehicle and the "Zvuk-4m" towed underwater vehicle (Fig. 1). During the submergence of the "Paysis" vehicle, which makes it possible to carry out a broad complex of investigations [5], a crew consisting of A. M. Sagalevich and V. S. Kuzin carried out visual observations, television videorecording with a duration of 30 minutes, photographing of the bottom, measurement of hydrophysical parameters and sampling of bedrocks by means of a manipulator. The vehicle moved a distance of about 200 m over the bottom and investigated an area up to 1000 m<sup>2</sup>. The "Zvuk-4m" apparatus, developed in the Deep-Water Research Technology Section of the Institute of Oceanology, USSR Academy of

## FOR OFFICIAL USE ONLY

Sciences under the direction of V. S. Yastrevov and constituting a system towed on a supporting-electrical cable, was used in photography, television scanning and side-looking sonar survey of the seamount peak. Photographs were taken at a distance of 1-3 m from the bottom in an automatic regime each 15 seconds. A total of about 400 photographs were taken with a rate of towing of the vehicle up to 1 knot. A survey with the side-looking sonar was made over a period of 30 minutes. The width of the surveyed zone was 370 m (185 m to the right and left of the vehicle). Inspection of the videorecord obtained by the "Paysis," petrographic study of bedrock samples and analysis of the record from the side-looking sonar and photographs of the bottom made it possible to obtain new data on structure of Ampere seamount.

The seamount rises above the surrounding bottom more than 400 m and enters into the southern branch of the horseshoe-shaped Hosshu "7" rise. The seamount peak extends in a latitudinal direction and measures 1 x 3.5 miles; at the base it measures 35 x 45 miles. The seamount slopes are steep and almost undissected. Individual small side peaks are encountered only locally. The steepness of the slopes to a depth of about 1500 m attains 40-50°; lower it gradually decreases to 20-15°. The eastern part of the seamount peak is somewhat uplifted. The depths here are 60-90 m; the relief is uneven with depth fluctuations of 5-10 m. A slightly sloping, more levelled surface with depths from 100 to 180 m, on which hills with a height up to 20 m with steep lateral slopes rise, extends westward.

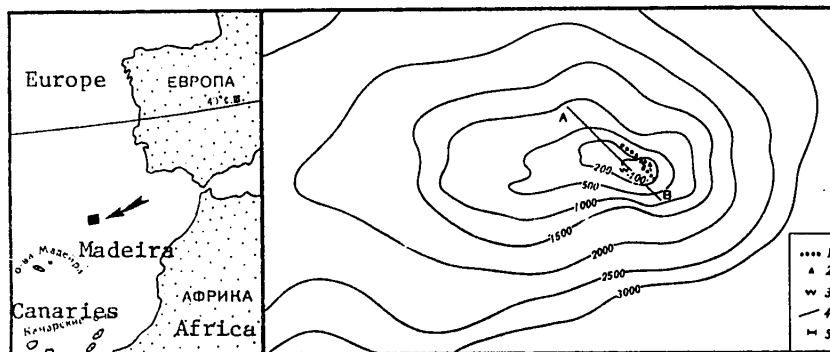


Fig. 1. Schematic map of Ampere seamount and its location (at left). 1) track of towed "Zvuk-4m" vehicle; 2) region of "Paysis" submergence; 3) trawling; 4) echo sounding profile; 5) side-looking sonar survey.

Observations from the "Paysis" underwater vehicle were made over a small sector of the bottom, near the peak, at a depth of 80-90 m (Fig. 1). At the upper part of the gentle slope there were low ridges, constituting outcrops of strata of dense rocks gently sloping to the horizon (10-15°) with a thickness from 0.5-1 (Fig. 2) to 10-15 m. These are characterized by a rectangular fracturing, creating the impression of laid bricks. The outcrops of the described rocks were photographed in the region of submergence of the "Paysis" using the "Zvuk-4m" apparatus (Fig. 2). In the southern part of the seamount peak a trawl raised platy blocks measuring

## FOR OFFICIAL USE ONLY

10 x 20 cm and with a thickness of 4-5 cm, consisting of reddish-ochreous trachyte with a clearly expressed fluidal texture from a depth of 130-170 m. The upper part of the blocks was covered with a crust of lithothamnium, whereas the lower part was free of overgrowth. This same trawl contained numerous fragments of dead and living madreporal corals and a great quantity of calcareous ooze with fragments of shells. The trawl also contained pieces of very bubbly alkaline basalt with large phenocrysts of titanite and olivine. The surface of the block was rough and uneven. This sort of surface can be observed on underwater photographs of bedrock.

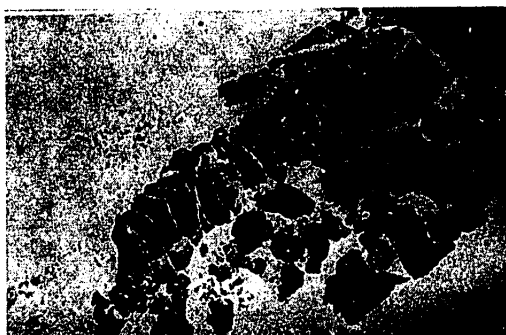


Fig. 2. Ridge consisting of trachytes and surrounded by light-colored calcareous sediments.

Downslope observations from the "Paysis" made it possible to detect highly dissected relief. In this section of the bottom the bedrock is represented by strata of conglomerates dissected by troughs with a depth of 1.5-2 m and with a width of several tens of meters (Fig. 3). Using its manipulator, the "Paysis" sampled from the exposure of conglomerates two well-rounded pebbles (measuring 10 x 8, 10 x 6 cm), covered with a rather thick (1-5 mm) rosy-violet crust of lithothamnium. Persisting on the surface of the pebbles were remnants of cement, represented by calcareous detritus. Both pebbles consisted of alkaline basalts differing in their petrographic composition. One sample was represented by magnophyric dense basalt with impregnations of augite and plagioclase. The second sample consisted of aphyric basalt with small bubbles.

The record of the side-looking sonar (Fig. 4) shows that at the seamount peak it is easy to trace two systems of ridges oriented almost perpendicularly to one another; the submeridional ridge seemingly overlaps the sublatitudinal ridge. The first system is evidently represented by outcrops of conglomerates. Here the ridges have distinct boundaries and different widths. The second system is characterized by rather distinct outlines and probably consists of layers of dense rock of the trachyte type.

FOR OFFICIAL USE ONLY



Fig. 3. Outcrops of conglomerates. A scour with a width of about 0.5 m is visible at the center of the frame.

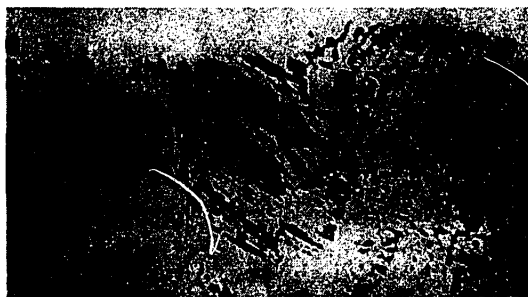


Fig. 4. Record of side-looking sonar.

11  
FOR OFFICIAL USE ONLY

## FOR OFFICIAL USE ONLY

The width of the ridges was 10 m or less and the distances between them were about 10-15 m, as is confirmed by visual observations from the "Paysis."

Summing the data cited above, the following conclusions can be drawn concerning the structure and development of the Ampere seamount. The seamount itself is unquestionably a volcanic formation consisting of alkaline basalts and their derivatives, like the overwhelming majority of the seamounts in the Atlantic Ocean [3]. The seamount peak has the form of a small, scarcely sloping bowl and probably constitutes a partially filled-in crater. Along its edges a stratified layer consisting of volcanites of different hardness is laid bare. Denser rocks of the trachyte type rise above the bottom surface, creating a system of ridges parallel to the edge of the volcano. During glacial times, when the ocean level was lower than at present [2], the seamount peak protruded above the water, constituting a volcanic island. The action of storm waves led to a partial destruction of the rocks and the formation of volcanic-pebbly beaches around the seamount peak. With subsequent rising of the ocean level the seamount peak sank and the accumulation of calcareous sediments began here. The cementing of the pebbles by fine detritus and lithothamnium algae led to the formation of conglomerates. As a result of repeated depressions of the ocean level during the Pleistocene the highest parts of the seamount reached the sea surface and even rose above it, being exposed to the action of the waves and surface waters. This led to the partial erosion of poorly cemented conglomerates and the creation of scours and small canyons in their strata, for the most part directed downslope. On the deeper western part of the seamount peak, during the Pleistocene at virtually all times being under water, on the contrary, there was an accumulation of calcareous detritus and a sand shoal was formed here. The post-glacial uplifting of the ocean level led to the modern underwater position of the peak of the Ampere seamount. Judging from observations from the "Paysis," in the eastern part of the seamount there is a weak effect of storm waves and swell at depths as great as 80-90 m, stirring up the fine sedimentary material which is transported onto its slopes. Accordingly, here there is exposure of volcanic bed-rocks; conglomerates and sedimentary material are found only in relief depressions.

## BIBLIOGRAPHY

1. Gorodnitskiy, A. M., Litvinov, E. M. and Valyasko, G. M., "The Anomalous Magnetic Field Over the Ampere and Horridge Seamounts," GEOFIZICHESKIYE METODY RAZVEDKI V ARKTIKE (Geophysical Reconnaissance Methods in the Arctic), No 10, pp 154-156, 1975.
2. Leont'yev, O. K., "Changes in World Ocean Level During the Mesozoic-Cenozoic," OKEANOLOGIYA (Oceanology), Vol 10, No 2, pp 276-286, 1970.
3. Litvin, V. M., Rudenko, M. V. and Kharin, G. S., "Role of Volcanism in the Formation of Bottom Relief of the Atlantic Ocean," GEOMORFOLOGIYA (Geomorphology), No 4, pp 92-98, 1976.
4. Rudenko, M. V., "Atlantic Ocean Seamounts," IZV. VSESOYUZN. GEOGRAF. O-VA (News of the All-Union Geographical Society), Vol 107, No 4, pp 295-301, 1975.

FOR OFFICIAL USE ONLY

5. Sagalevich, A. M. and Podrazhanskiy, A. M., "'Paysis' Underwater Manned Scientific Research Complex," OKEANOLOGIYA (Oceanology), Vol 19, No 5, pp 911-919, 1977.
6. Heezen, B. C., Tharp, M. and Ewing, M., THE FLOOR OF THE OCEANS. I. THE NORTH ATLANTIC. GEOL. SOC. AMER. SPEC. PAPER, Vol 65, 1959.
7. Laughton, A. S., Roberts, D. G. and Graves, R., "Bathymetry of the Northeast Atlantic: Mid-Atlantic Ridge to Southwest Europe," DEEP-SEA RES., Vol 22, No 12, pp 91-810, 1975.
8. Tolstoy, I., "Submarine Topography in the North Atlantic," BULL. GEOL. SOC. AMER., Vol 62, No 5, pp 441-450, 1951.

COPYRIGHT: Izdatel'stvo "Nauka", "Okeanologiya", 1982

5303

CSO: 1865/106

13  
FOR OFFICIAL USE ONLY

FOR OFFICIAL USE ONLY

UDC 551.46:681.1/4

EFFECT OF SENSOR SIZE ON ESTIMATION OF RATE OF DISSIPATION OF TURBULENT ENERGY IN OCEAN

Moscow OKEANOLOGIYA in Russian Vol 22, No 1, Jan-Feb 82 (manuscript received 4 Mar 81) pp 153-157

[Article by V. M. Zhurbas and V. N. Nabatov, Institute of Oceanology imeni P. P. Shirshov, USSR Academy of Sciences, Moscow]

[Text]

Abstract: The influence of the size of the sensing element of a conduction-type magnetohydrodynamic anemometer (CMA) on estimates of the rate of dissipation of turbulent energy  $\varepsilon$  in the ocean is analyzed on the basis of data from field measurements. It was found that for the CMA variants used in oceanological research the understatement of  $\varepsilon$  estimates associated with finiteness of sensor size attains a factor of 2-3. An empirical estimate of the CMA spectral characteristic, obtained on the basis of in situ measurement data, is presented.

An important characteristic of oceanic turbulence is the rate of dissipation of turbulent energy  $\varepsilon$ . Estimates of this parameter on the basis of measurements of velocity fluctuations can be obtained by several methods [1]. With the assumption of a local isotropicity of small-scale velocity fluctuations the expression for  $\varepsilon$  can be written in the form

$$\varepsilon = 15\nu \overline{(\partial u' / \partial x)^2}, \quad (1)$$

where  $x$  is the coordinate along the motion of the sensor;  $u'$  is the longitudinal component of velocity fluctuations;  $\nu$  is the kinematic viscosity of water. The formula (1) in a spectral representation is equivalent to the expression

$$\varepsilon = 15\nu \int_0^\infty k^2 E(k) dk, \quad (1')$$

where  $E(k)$  is the spectral density of the longitudinal component of velocity  $u'$ ;  $k$  is the wave number. The use of expressions (1) and (1') for  $\varepsilon$  estimates assumes a sufficiently reliable measurement of velocity fluctuations with wave numbers of

11  
FOR OFFICIAL USE ONLY

## FOR OFFICIAL USE ONLY

the order of  $k = 0.1/\eta$  ( $\eta = (\nu^3/\varepsilon)^{1/4}$  is the Kolmogorov internal scale), where the dissipation spectrum  $k^2 E(k)$  has a maximum [5]. Typical estimates of the scale  $\eta$  for the ocean fall in the range 0.1-0.2 cm [4] and the maximum of the dissipation spectrum is attained with extremely high values of the wave number  $k = 0.5-1 \text{ rad}\cdot\text{cm}^{-1}$ , where there can be an understatement of the empirical estimates of the spectrum level as a result of averaging of velocity fluctuations in the working volume of the sensor sensing element. The latter circumstance is particularly important when measuring velocity fluctuations by a conduction-type magnetohydrodynamic anemometer (CMA) [2], used during recent years in Soviet oceanological investigations. The CMA, together with indisputable advantages (insensitivity to transverse velocity fluctuations and changes in medium temperature) has greater geometrical dimensions than sensors of the thermoanemometric type. The spectral characteristic of the CMA  $H^2(k) = E(k)/E_{\text{true}}(k)$ , where  $E(k)$  and  $E_{\text{true}}(k)$  are the spectral densities of the signal at the CMA output and longitudinal fluctuations of velocity of the medium, was estimated in laboratory conditions [7] by a comparison of the spectra of the output signal with the spectrum obtained with the thermoanemometer. It was noted that the influence of the averaging volume of the CMA as a function of the type of spectrum of velocity fluctuations began with scales  $\lambda = 2\pi/k = 2-4 \text{ cm}$ , where the  $\lambda$  scale was determined at the 0.5-level of the sensor spectral characteristic:  $H^2(2\pi/\lambda) = 0.5$ . We will analyze the errors in estimates of  $\varepsilon$  in the ocean as a result of averaging of velocity fluctuations in the working volume of the CMA on the basis of data from in situ measurements on the 24th voyage of the scientific research ship "Dmitriy Mendeleyev."

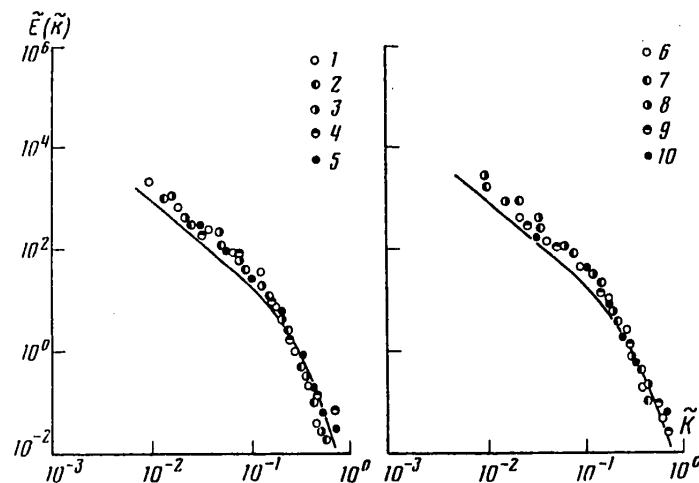


Fig. 1. Dimensionless spectral densities of longitudinal velocity fluctuations in upper quasihomogeneous layer of ocean according to CMA measurements. The numbers in the figure correspond to the numbers of the sectors in the table.

The measurements were made in an equatorial polygon in the central part of the Pacific Ocean using the turbulence meter-sonde of the Atlantic Division of the Institute of Oceanology, USSR Academy of Sciences [6]. The diameter of the CMA

## FOR OFFICIAL USE ONLY

sensing element head was 40 mm; the distance between electrodes was 10 mm. The noise level in the measurements did not exceed  $0.7 \text{ mm} \cdot \text{sec}^{-1}$  with a mean square amplitude in the frequency range of the sensor 4-64 Hz with a rate of sonde submergence  $V \approx 1 \text{ m} \cdot \text{sec}^{-1}$ . The analysis was made using 10 sectors of vertical profiles of velocity fluctuations with an increased signal dispersion level in the upper quasihomogeneous layer of the ocean (the numbers of the stations, soundings and depth ranges are indicated in Table 1). Figure 1 shows the spectral densities of the longitudinal component of velocity fluctuations in these sectors in the dimensional form

$$E(k) = \varphi(k), \quad (2)$$

where  $\tilde{E} = E/(\varepsilon \nu^5)^{1/4}$ ,  $\tilde{k} = k \eta$ . In normalizing the spectra use was made of  $\varepsilon$  estimates using formula (1). The solid curve in Fig. 1 gives the empirical universal dependence  $\varphi(k)$  for the inertial-viscous turbulence interval [5]. Figure 1 shows that dimensionless spectra with a relatively small scatter fell on one another and in general agree fairly well with the universal dependence. However, in a more detailed examination it is easy to find that with  $\tilde{k} < 10^{-1}$  the estimates of the spectra systematically lie above the universal curve; with an increase in  $\tilde{k}$  the spectra drop off more steeply than the universal dependence, and in the neighborhood  $\tilde{k} = 0.3$  the experimental points are already situated below it. This peculiarity of the spectra is still more conspicuous in Fig. 2,a, which shows the result of averaging of these same 10 spectra (denoted by the digit 1). It is natural to relate the exaggeration of the levels of the dimensionless spectra with  $\tilde{k} < 0.1$  to the use in the normalization of  $\varepsilon$  estimates made using formula (1), which may be too low as a result of the averaging of velocity fluctuations in the working volume of the sensor. In this situation the  $\varepsilon$  estimates for the level of the sector of the "-5/3" spectrum are more reliable.

Table 1

Stations and Ranges of Sounding Depths Used in Estimating Energy Dissipation Rate

Sector	Stations	Sounding	Measurement layer meters	Evaluation $\varepsilon$ , $\text{cm}^2 \cdot \text{sec}^{-3}$	
				using formula (1)	using spectrum level
1	1961	1	48-56	$1,3 \cdot 10^{-3}$	$3,2 \cdot 10^{-3}$
2	1961	1	15-20	$3,6 \cdot 10^{-3}$	$7,5 \cdot 10^{-3}$
3	1960	4	14-19	$6,9 \cdot 10^{-3}$	$2,6 \cdot 10^{-3}$
4	1961	2	58-65	$8,9 \cdot 10^{-3}$	$2,9 \cdot 10^{-3}$
5	1951	2	17-22	$2,0 \cdot 10^{-3}$	$4,3 \cdot 10^{-3}$
6	1961	3	17-21	$1,9 \cdot 10^{-3}$	$3,1 \cdot 10^{-3}$
7	1961	3	40-48	$1,3 \cdot 10^{-3}$	$3,5 \cdot 10^{-3}$
8	1961	4	52-61	$1,4 \cdot 10^{-3}$	$4,3 \cdot 10^{-3}$
9	1961	5	102-104	$1,8 \cdot 10^{-3}$	$3,4 \cdot 10^{-3}$
10	1948	2	90-94	$1,8 \cdot 10^{-3}$	$4,7 \cdot 10^{-3}$
Mean $\varepsilon$ value				$6,7 \cdot 10^{-3}$	$1,9 \cdot 10^{-3}$

## FOR OFFICIAL USE ONLY

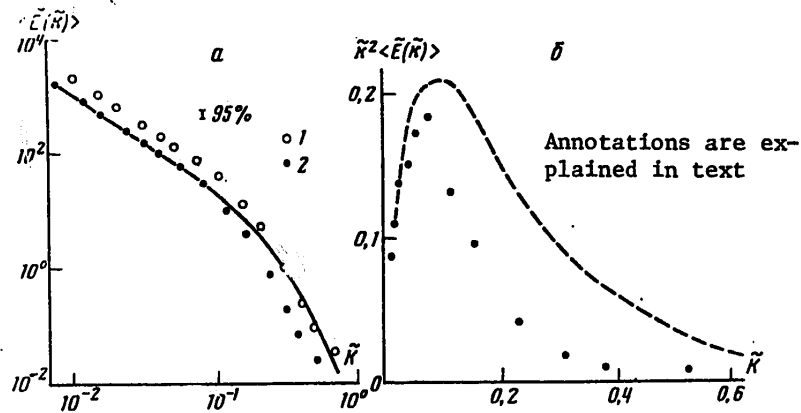


Fig. 2. Averaged dimensionless spectral density of longitudinal velocity fluctuations (a) and dissipation spectrum (b) in upper quasihomogeneous layer of ocean according to CMA measurement data.

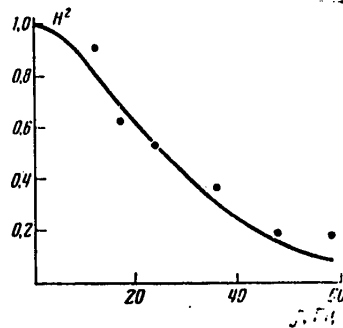


Fig. 3. Empirical estimate of spectral characteristic of CMA according to data from in situ measurements.

The table gives  $\mathcal{E}$  estimates made using both formula (1) and using the "-5/3" spectrum sector level. In order to obtain the latter by the least squares method we carried out an approximation of the low-frequency part of each spectrum ( $\tilde{k} < 10^{-1}$ ) by the dependence  $E = C \mathcal{E}^{2/3} k^{-5/3}$ , where the C constant was selected equal to 0.48 [5]. The table indicates that  $\mathcal{E}$  estimates for the level of the "-5/3" spectrum level averaged 2.8 times greater than the estimates using formula (1). In estimates of  $\mathcal{E}$  at the "-5/3" level the dimensionless averaged spectrum was displaced downward and to the left (denoted by the digit 2 in Fig. 2,a); its low-frequency part coincided with the universal curve, whereas with  $\tilde{k} > 10^{-1}$  (that is, in the viscous interval) the experimental points fell lower. The corresponding averaged dissipation spectrum  $\tilde{k}^2 \langle \bar{E}(\tilde{k}) \rangle$  is shown in Fig. 2,b. The dashed curve in Fig. 2,b represents the result of averaging of the empirical dissipation spectra of this type according to data in the literature which were cited in [5]. The averaged dissipation spectrum, according to CMA measurement data, passes considerably below the dashed curve and

## FOR OFFICIAL USE ONLY

the area under it is 0.031, which is less than half the theoretical value  $1/15$  [5]. This circumstance also explains the difference in the  $\varepsilon$  estimates made using formula (1) and the level of the "-5/3" spectrum sector.

An estimate of the spectral characteristic and characteristic scale of averaging of the CMA sensing element can be made much as was done in [8] by a comparison of the averaged dimensionless spectrum  $\langle \tilde{E}(\tilde{k}) \rangle$  obtained using data from in situ measurements with the universal curve for the inertial-viscous interval. The result of such a determination of the CMA spectral characteristic as a function of the cyclic frequency  $f = Uk/2\pi$  is shown in Fig. 3. The solid curve in Fig. 3 shows the results of theoretical computations [3] of the  $H^2(f)$  function for a spherical sensor in the field of locally isotropic velocity fluctuations with a spectrum dropping off in conformity to the "-5/3" law (the velocity fluctuations were averaged for the volume of a sphere with the diameter  $a = 1.4$  cm). The choice of the spectral characteristic for a spherical sensor for estimating the characteristic averaging scale for the CMA is related to the fact that it virtually coincides with the spectral characteristic of a two-dimensional longitudinal orientation sensor [3] and accordingly can serve as a satisfactory approximation of the spectral characteristic of real sensors with a different configuration of the averaging volume.

Thus, according to data from in situ measurements, the CMA spectral characteristic is satisfactorily approximated by the characteristic of a spherical sensor with a diameter of the averaging volume  $a = 1.4$  cm. As follows from Fig. 3, the "steep drop" of the spectra, determined for the 0.5-level of the  $H^2(f)$  characteristic, begins at frequencies 25-30 Hz, which corresponds to values of velocity fluctuations  $\lambda = U/f = 3-4$  cm, close to the diameter of the CMA sensing element head. This estimate of the CMA resolution scale is in good agreement with data from laboratory tests [7]. It is impossible to determine the precise form of the  $H^2(f)$  function and carry out a correction of the observational data as a result of the dependence of the  $H^2(f)$  function on the spectral makeup of the measured velocity fluctuations [3]. However, it must be remembered that when using existing CMA variants for estimating the rate of dissipation of turbulent energy in the ocean the results may prove to be too low by a factor of 2-3 as a result of spatial averaging of the velocity fluctuations by the sensor in the dissipative part of the spectrum.

In order to reduce the errors in  $\varepsilon$  estimates associated with the finite size of the sensor it is evidently necessary to design sensors with a lesser averaging volume. Accordingly, the question arises as to what extent it is necessary to reduce the geometrical dimensions of the CMA so that when measuring velocity fluctuations in the ocean the relative understatement of  $\varepsilon$  estimates will not exceed the stipulated value  $\delta = \varepsilon_{\text{true}}/\varepsilon$ . The answering of this question requires stipulation of the maximum  $\varepsilon_{\text{max}}$  value which, according to modern concepts, can be observed in the ocean and corresponding computations must be made using the empirical universal dependence for the spectrum of velocity fluctuations (2) and estimates of the spectral characteristic of the sensor, taken, for example, from Fig. 3. If it is assumed that  $\varepsilon_{\text{max}} = 0.1 \text{ cm}^2 \cdot \text{sec}^{-3}$  [4], such computations show that for the CMA employed in the measurements on the 24th voyage of the "Dmitriy Mendeleev" scientific research ship ( $a = 1.4$  cm),  $\delta_{\varepsilon} \leq 3.2$ , with  $a = 0.7$  cm (decrease in the geometrical dimensions of the CMA by half)  $\delta_{\varepsilon} \leq 1.9$ , whereas with  $a = 0.47$  cm (decrease in the size of the CMA by a factor of 3) the estimates in the ocean will be understated by not more than a factor of 1.5.

FOR OFFICIAL USE ONLY

BIBLIOGRAPHY

1. Belyayev, V. S., Lyubimtsev, M. M. and Ozmidov, R. V., "Rate of Dissipation of Turbulent Energy and Rate of Evening-Out of Temperature Inhomogeneities in the Ocean," *IZV. AN SSSR: FIZIKA ATMOSFERY I OKEANA* (News of the USSR Academy of Sciences: Physics of the Atmosphere and Ocean), Vol 9, No 11, pp 1179-1185, 1973.
2. Golubev, Yu. Ye., Vasilevskiy, V. V. and Turenko, V. V., "Velocity Sensor for the Flow of Conducting Water," USSR AUTHOR'S CERTIFICATE No 685984, published in *BYULLETEN' IZOBRETENIY* (Inventions Bulletin), No 34, p 195, 1979.
3. Dotsenko, S. V., *TEORETICHESKIYE OSNOVY IZMERENIYA GIDROFIZICHESKIKH POLEY OKEANA* (Theoretical Principles for Measuring Hydrophysical Fields in the Ocean), Leningrad, Gidrometeoizdat, 1974.
4. Monin, A. S. and Ozmidov, R. V., "Ocean Turbulence," *OKEANOLOGIYA. FIZIKA OKEANA* (Oceanology. Ocean Physics), Vol 1, Moscow, Nauka, pp 148-207, 1978.
5. Monin, A. S. and Yaglom, A. M., *STATISTICHESKAYA GIDROMEKHANIKA* (Statistical Hydromechanics), Part 2, Moscow, Nauka, 1967.
6. Paka, V. T., Bubnov, V. A. and Pozdynin, V. D., "Twenty-Fourth Voyage of the Scientific Research Ship 'Dmitriy Mendeleyev'," *OKEANOLOGIYA* (Oceanology), Vol 20, No 5, pp 954-955, 1980.
7. Povkh, I. L., Dunayevskiy, I. G., Korneyev, V. D. and Cheplyukov, V. G., "Metrological Characteristics of Conduction-Type Measurement Converters," *EKSPERIMENTAL'NYYE METODY I APPARATURA DLYA ISSLEDOVANIYA TURBULENTNOSTI* (Experimental Methods and Apparatus for Investigating Turbulence), *TEZISY DOKLADOV II VSE-SOYUZNOGO SOVESHCHANIYA* (Summaries of Reports at the Second All-Union Conference), Novosibirsk, pp 102-105, 1976.
8. Crowford, W. B., "Turbulent Energy Dissipation in the Atlantic Equatorial Undercurrent," Thesis, The University of British Columbia, Canada, 1976.

COPYRIGHT: Izdatel'stvo "Nauka", "Okeanologiya", 1982

5303

USO: 1865/106

FOR OFFICIAL USE ONLY

UDC 502.3:629.78

PHYSICAL ASPECTS OF REMOTE SENSING OF OCEAN-ATMOSPHERE SYSTEM

Moscow FIZICHESKIYE ASPEKTY DISTANTSIONNOGO ZONDIROVANIYA SISTEMY OKEAN-ATMOSFERA  
in Russian 1981 (signed to press 23 Apr 81) pp 2, 212

[Annotation and table of contents from collection of articles "Physical Aspects of Remote Sensing of Ocean-Atmosphere System", M. S. Malkevich, doctor of physical and mathematical sciences, responsible editor, Izdatel'stvo "Nauka", 850 copies, 216 pages]

[Text] Annotation. This collection of articles is devoted to space, aircraft, ship-board and surface investigations of the sea surface and atmosphere for the purpose of remote sensing of the ocean and the atmosphere over the ocean. Much attention is devoted to the transformation of visible and infrared radiation in the atmosphere and analysis of the "ocean-atmosphere" system. The collection is intended for specialists in the field of oceanology, atmospheric physics, meteorology and other specialists using the results of space investigations of the earth.

Contents

Foreword	3
Part 1. Investigation of Thermal Regime of Ocean and Overlying Atmosphere	
Malkevich, M. S. "Status of the Problem of Thermal Sounding of the 'Ocean-Atmosphere' System From Space"	6
Gorodetskiy, A. K., Orlov, A. P. and Petrenko, B. Z. "Determination of Ocean Temperature From Radiation in the Atmospheric Transparency Window 8-12 $\mu$ m"	29
Gorodetskiy, A. K. and Orlov, A. P. "Radiation Regime and Emissivity of the Water Surface in the IR Spectral Range"	36
Badayev, V. V., Gorodetskiy, A. K., Istomina, L. G., Kozlov, Ye. M., Malkevich, M. S. and Orlov, A. P. "Vertical Structure of Atmospheric Transformation of IR Radiation of Ocean"	44
Malkevich, M. S., Shukurova, L. M. and Chavro, A. I. "Anomalous Properties of Atmospheric Transmission in Ozone Band 9.6 $\mu$ m"	57

**FOR OFFICIAL USE ONLY**

Part 2. Aerosol Attenuation of Radiation

- Shukurov, A. Kh. and Chavro, A. I. "Attenuation of Atmospheric Radiation in Windows of the Spectral Range 8-21  $\mu$ m According to Data From Sea and Continental Measurements" 72
- Badayev, V. V., Gorodetskiy, A. K. and Orlov, A. P. "Determination of the Contribution of Water Vapor and Aerosol to Continuum According to Shipboard and Aircraft Measurements of Radiation" 76
- Badayev, V. V., Gorodetskiy, A. K., Kozlov, Ye. M. and Petrenko, B. Z. "Determination of the Characteristics of Transformation of Brightness in Visible and Near-IR Spectral Range" 84
- Malkevich, M. S. and Istomina, L. G. "Spectral Brightness of 'Ocean-Atmosphere' System" 99
- Kozlov, Ye. M. and Badayev, V. V. "Determination of Optical Characteristics of 'Surface-Atmosphere' System in Visible Spectral Range" 137

Part 3. Sensing of Cloud Systems

- Malkevich, M. S., Malkova, V. S. and Syachinov, V. I. "Optical Characteristics of Clouds" 149
- Gorodetskiy, A. K., Orlov, A. P., Syachinov, V. I. and Matveyev, D. T. "Complex Method for Determining Phase State of Water in Clouds" 172
- Gorodetskiy, A. K. and Orlov, A. P. "Radiation Characteristics of Clouds" 178
- Gorodetskiy, A. K., Gol'din, Yu. A. and Malkova, V. S. "Information Yield of Back-scattered Signals in Laser Sounding of Quasihomogeneous Clouds" 191
- Anikin, P. P., Chavro, A. I. and Shukurov, A. Kh. "Complex Optical Apparatus for Investigations of Atmospheric Spectral Transmission on Slant and Horizontal Paths in the Ultraviolet, Visible and IR Spectral Ranges (0.3-25  $\mu$ m)" 200

COPYRIGHT: Izdatel'stvo "Nauka", 1981

5303

CSO: 1865/117

FOR OFFICIAL USE ONLY

UDC 681.883.04

EFFECTIVE RANGE OF HYDROACOUSTIC APPARATUS

Leningrad DAL'NOST' DEYSTVIYA GIDROAKUSTICHESKIKH SREDSTV in Russian 1981  
(signed to press 30 Sep 81) pp 2-4, 205

[Annotation, foreword and table of contents from monograph "Effective Range of Hydroacoustic Apparatus", second edition, revised and supplemented, by Viktor Nikolayevich Matviyenko and Yuriy Fedotovitch Tarasyuk, Izdatel'stvo "Sudostroyeniye", 3500 copies, 206 pages]

[Text] Annotation. The characteristics of the principal parameters of the medium causing a change in the effective range of hydroacoustic apparatus in the seas and oceans are examined. Practical recommendations are given for evaluating their anticipated effective range, taking into account the real characteristics of water masses, the sea surface and floor. In comparison with the first edition (1976), this new edition is supplemented by data on instruments for computing the anticipated range of detection of underwater features. The book is intended for hydroacoustic engineers and oceanologists and will also be useful to shipbuilders and specialists in radio navigation.

Foreword. Hydroacoustic apparatus is the sole means for observation, communication and control in the underwater medium for tens and thousands of kilometers. It is called the "electronic key" to the mastery of knowledge concerning the processes transpiring in the ocean depths. The effectiveness of use of hydroacoustic apparatus (HAA) for observation, communication and control in the ocean is directly dependent on its effective range.

By the term "effective range of hydroacoustic apparatus" is meant that distance at which the probability of correct detection of a feature (signal) is equal to a set value. The probability of correct detection of a feature (signal) is a function of the signal-to-noise ratio. The signal level necessary for obtaining a stipulated probability of correct detection is determined by its characteristic parameters, the spectral-energy characteristics of the noise, the volume and quality of the problems to be solved by the station, its technical capabilities, the degree of professional training of the operator and many other factors.

Each of these factors is the object of study by specialists in different fields, as a result of whose joint efforts it is possible to determine the value of the signal-to-noise ratio corresponding to the required station operating regime.

FOR OFFICIAL USE ONLY

Without diminishing the importance of each individual factor exerting an influence on the effective range of the HAA, it is desirable to emphasize the special significance of the change in signal strength as a function of distance during its propagation in the oceanic medium. It is precisely the peculiarities of this change which are responsible for the level of the hydroacoustic signal (and also many types of noise) at each point in the world ocean at any moment in time.

There are at least three objective circumstances making it possible to consider sound propagation in the ocean to be the most important factor determining the effective range of HAA.

1. The best technically prepared operator of the most modern HAA cannot solve the formulated problem if the sound propagation conditions are such that the signal does not arrive at the station antenna. In such cases -- and they are frequently encountered -- reasonings concerning the importance of other factors simply lose sense. However, it is also possible to detect a signal which arrives at the necessary reception point without complex electronic apparatus.
2. The station operator can control the absolute majority of the processes occurring in the electronic units of the HAA, including assurance of reliability. However, for the time being it is not possible to control the state of the environment. In principle the adaptation of HAA to ambient conditions is possible, but this requires attention first and foremost to the systematic determination of the peculiarities of sound propagation in the neighborhood of station operation. Without a precise knowledge of the laws of spatial-temporal variability of the acoustic field the use of different technical innovations in the HAA channels sometimes does not introduce any effect.
3. The technical improvement of the electronic components of the HAA has attained a level at which an additional signal gain in decibel units can be obtained only by employing complex devices. However, this gain is less than the variability in the conditions for the reception of a direct signal during its propagation in the ocean.

In this connection it is important that shipboard specialists and designers of HAA first of all master practical procedures for determining the hydroacoustic characteristics of the ocean medium and take them into account when using analog-digital computers for constructing the trajectories of acoustic rays and estimating the anticipated effective range of hydroacoustic apparatus.

In the second edition of the book, written by practical workers for practical workers, there has been a continued systematization of data on the hydroacoustic characteristics of the surface, water masses and ocean floor. The peculiarities of sound propagation are examined and new information on measurement apparatus is presented.

The use of the program for computing the acoustic field on widely employed types of digital computers cited in the Appendix will help in finding an answer to many practical questions when precise information is available concerning the vertical distribution of the speed of sound and other ambient parameters.

## FOR OFFICIAL USE ONLY

When working on the manuscript the authors attempted to make full allowance for the comments and wishes of readers expressed at conferences, in published reviews and personal discussions during review of the first edition of the book.

The authors express appreciation to A. S. Potapov, E. F. Aleksandrova, A. M. Vinogradova, V. A. Gavrilov, L. B. Demchenko, L. M. Korneyeva and N. Ye. Cheshun for assistance which they have given in the process of work on and finalization of the manuscript.

Critical comments and desired improvements should be sent to the address: 191065, Leningrad, Ulitsa Gogolya, 8, Izdatel'stvo "Sudostroyeniye."

## Contents

Foreword.....	3
Introduction.....	5
Chapter I. Hydroacoustic Characteristics of Ocean.....	7
#1. Characteristics of water masses.....	7
#2. Speed of sound.....	18
#3. Spatial attenuation.....	36
#4. Volume scattering.....	46
Chapter II. Hydroacoustic Characteristics of Ocean Surface and Floor.....	54
#5. Description of boundaries of medium.....	54
#6. Surface characteristics.....	64
#7. Speed of sound in bottom material.....	73
#8. Hydroacoustic characteristics of bottom.....	81
Chapter III. Hydroacoustic Models.....	94
#9. Wave and ray models.....	94
#10. Focusing factor.....	99
#11. Propagation anomaly.....	110
#12. Reverberation anomaly.....	122
Chapter IV. Peculiarities of Sound Propagation in Ocean.....	130
#13. Hydroacoustic phenomena in ocean.....	130
#14. Acoustic climate and weather.....	141
#15. Determination of sound propagation conditions.....	154
Chapter V. Estimation of Expected Effective Range of Hydroacoustic System.....	163
#16. Measurement of speed of sound in water and bottom material.....	163
#17. Detection zone plotters.....	174
#18. Computations of effective range of hydroacoustic system using digital computer.....	179

FOR OFFICIAL USE ONLY

Summary.....	185
Appendices.....	187
Bibliography.....	201

COPYRIGHT: Izdatel'stvo "Sudostroyeniye", 1981

5303

CSO: 1865/112

FOR OFFICIAL USE ONLY

UDC 55(260)

GEOLOGY OF WORLD OCEAN FLOOR ACCORDING TO DEEP-WATER DRILLING

Moscow VESTNIK AKADEMII NAUK SSSR in Russian No 2, Feb 82 pp 35-40

[Article by A. V. Peyve, academician]

[Text] The deep-water drilling project has an international scope. In addition to the United States, the principal holder of "shares" and the owner of the drilling ship "Glomar Challenger," West Germany, France, Great Britain, Japan and the USSR are participating in the project and are making financial contributions. The "Glomar Challenger" is small, having a displacement of 11 000 tons. Its deck carries more than 7 000 running meters of drilling pipe and it is possible to carry out drilling to approximately this depth, including, to be sure, the water layer.

The "Glomar Challenger" has many unique technical apparatuses for drilling in the ocean. In addition to the fact that for the first time this vessel made use of extremely modern means of navigation, it was outfitted with a system making it possible to hold it in position at a single point during the course of drilling. For this purpose an ultrasonic buoy is lowered to the ocean floor and the hydrophones situated under the ship are directed at this buoy. The data on the vessel's displacement are fed to a computer which then issues a command to four position-control apparatuses situated at the vessel's prow and stern. The ship also has a stabilizing apparatus which safeguards the drilling pipes against rupture during rolling.

From the time of onset of drilling in August 1968 through October 1980, during 75 voyages, a total of 878 boreholes were drilled in 532 regions of the seas and oceans. The maximum penetration into bottom rocks was 1741 m at a place where the ocean depth was 3900 m.

The technical knowledge obtained in the course of implementation of abyssal drilling, the development of drilling techniques and the designing of a variety of instruments in the course of the investigations attained great perfection. Not only standard logging (acoustic, density, induction, neutron, gamma and other types of logging) is carried out in the boreholes, but also different experiments, such as for studying seismic phenomena. The employment of a hydraulic corer, making it possible to extract a 90% largely undisturbed core, attracted the attention not only of geologists, but other specialists as well. It was also found that repeated entry into the borehole shaft is possible and thus it is possible to obtain data over a long period of observations.

## FOR OFFICIAL USE ONLY

Abyssal drilling of the floor of the world ocean and the marginal seas is an important landmark in the history of natural science. Now we can see before us the structure, geological history, history of the life and paleogeography of the time of formation of the upper rock layer of the entire planet, not only its lesser part, represented by the continents. It is understood, to be sure, that modern geological science is experiencing revolutionary changes not only as a result of abyssal drilling. During the post-war years the floor of the world ocean has also been studied by other geophysical and geological methods, in particular, by mapping of the floor by means of deep-water submersible and controllable vehicles, dredging, photography, seismic and magnetic profiling, etc. These studies have been stimulated not only by the interests of science in general, but also by the practical need for studying mineral resources. And the deep drilling project from the very beginning was also directed to a possible general evaluation of the prospects first and foremost of finding petroleum and gas in the world ocean.

As mentioned above, work with abyssal drilling aboard the "Glomar Challenger" began in August 1968, but by the beginning of the 1960's modern concepts relating to the geology, geophysics and geochemistry of the ocean floor, especially the plate tectonics hypothesis, had already begun to form. Accordingly, scientists directed their efforts to finding new reliable facts which could be obtained only by means of drilling.

The most important achievement of the modern earth sciences is the clarification of the fundamental fact that the earth's crust of the oceans is essentially different from the continental crust. The oceanic crust is not only 4-6 times thinner than the continental crust; in its composition the main role is played by basaltoid mafic and ultramafic rocks, whereas the basement of the continental crust for the most part consists of sialic granite gneiss strata which are completely absent in the oceans.

The uppermost layer of the continents, consisting of sedimentary rocks, has been penetrated to the basement by thousands of boreholes, especially in petroleum and gas regions, and the Kola borehole, the deepest in the world, has entered the continental basement to a depth of 10 800 m. The continental granite gneiss crust, due to the fact that its individual parts have been dislocated and have moved relative to one another along faults, has been studied well in its entire depth, or as geologists say, its thickness. It has been established that individual blocks of the continental crust have a very ancient age and were formed 3-4 billion years ago.

Prior to the beginning of abyssal drilling we knew essentially nothing or knew very little concerning the geology of the sedimentary layer of the crust in the seas and oceans, which is determined by use of geophysical data. The scientific results obtained using abyssal drilling in all respects became a true discovery of our times. As already mentioned, as of today a total of 878 boreholes have been drilled in the entire world ocean; some of these have completely passed through the sedimentary layer and have penetrated into the basalt basement to a depth of 600 m in basalts.

Simultaneously by means of dredging and using underwater submersible vehicles studies have been made of basement rocks of the oceanic crust -- ultramafites and mafites, for which the velocities of seismic waves typical for the mantle and the

FOR OFFICIAL USE ONLY

lower part of the oceanic crust are characteristic. The time and geological history of formation of these rocks have still been poorly studied, but as is firmly established, the above-lying basaltic and sedimentary layers of the oceanic crust in all the oceans are not more ancient than 200-230 million years, which is evidence of fundamental differences in the geological history of the crust of the oceans and continents, of the much more ancient age of formation of the crust on the continents.

Now we will discuss briefly some of the fundamental patterns of structure and composition of the sedimentary and basalt layers of the oceans which have been revealed by abyssal drilling.

The sedimentary stratum of the world ocean proved to be extremely favorable for a vertical breakdown of its cross section into layers exceedingly fragmented in time. This became possible because the breakdown of the section was accomplished on the basis of the remains of plankton organisms, such as foraminifera, radiolarians, diatoms, nanoplankton, etc., rapidly evolving and rapidly populating the world ocean, present in the borehole cores. Taking into account the paleomagnetic scale and radiometric determinations, for the first time, as a result of abyssal drilling, it was possible to create a basis for a superdetailed and reliable correlation of the time of appearance of geological phenomena and features over the entire earth.

The study of the global time patterns of geological phenomena and processes in the geological history of the earth, like in the history of life on our planet, is a fundamental problem in natural science. Until now we could carry out only intra-continental, or in the best case, intercontinental correlation of geological phenomena.

It has been demonstrated by drilling and seismic profiling that the sedimentary stratum in the oceans, lying at the top in the vertical section, occurs virtually everywhere. It is absent only locally in the central parts of large oceanic ridges and on underwater volcanic rises. However, its thickness is variable, which is important to know when evaluating the prospects for finding petroleum and gas. Over great areas the thickness of the sedimentary layer does not exceed 1-1.5 km, increasing in the marginal seas on the continental margins to 10 km or more. Here the sedimentary layer contains petroleum and gas. In the internal regions of the oceans there are probably considerable sectors with a great thickness of sediments, to be sure, of a different composition.

According to drilling data, the sedimentary layer in the oceans, except for its narrow margins, everywhere is underlain by basalts. This is the second layer of the oceanic crust. Drilling has demonstrated that the youngest rocks are the basalts of the axial zones of the mid-oceanic ridges, with increasing distance from which the age of the basalts gradually increases. Accordingly, the bottom of the sedimentary layer also becomes more ancient in the direction from the axis of the ridge in the direction of the ocean margins. Thus, the pattern of structure of the ridges in the oceans is directly opposite their structure on the continents where the axial zones of the ridges usually consist of the most ancient rocks.

## FOR OFFICIAL USE ONLY

The sedimentary layer in the oceans with respect to composition of the rocks is variable and diverse. Drilling has revealed many patterns of its structure, among which we will note only one, the most fundamental. The layers of sediments lying above the basalts, it was found, in their character are always relatively more shallow-water than those lying above, which is evidence of uplifting, expressed in the relief at the time of formation of the basaltic crust of the oceans and its subsequent subsidence.

In the Indian Ocean and along the margins of the Atlantic Ocean boreholes have penetrated lagoonal and even terrestrial deposits now submerged to a great depth. It was also found that the basalt layer in its structure is complex and diversified in composition; in addition to the tholeiitic basalts characteristic for the ocean, there is also extensive development of olivine basalts.

Drilling has revealed earlier unknown ore-formation phenomena in ocean ridges. It was found that metal-bearing sediments of the Red Sea type, having increased contents of manganese, iron and some other metals, occur widely in the regions of the East Pacific Ocean Rise; they are also found in the other oceans. They lie locally directly at the base of the sedimentary layer. Rich ores have not yet been encountered by boreholes, but the areas of development of metalliferous sediments and their masses not studied by drilling are enormous.

In 1978, in the East Pacific Ocean Ridge, at a latitude of 21°, American geologists used underwater vehicles to observe the extremely interesting phenomenon of recent sulfide polymetallic ore-formation in the basalt crust. Here at a depth of 2500 m there was found to be a high-yield concentrated hydrothermal ore solution with a temperature of 400°C, under a great pressure escaping from the basalts through fissures. Near the outlets of these sources there is deposition of massive polymetallic sulfide ores that include iron, zinc, lead, copper, silver, gold and platinum. The content of elements is adequate for production if these ores were present on the land.

Data on hydrothermal phenomena in the now-forming oceanic crust are of great importance for learning about the processes of ore formation because in the structure of the continental crust there have been found to be tectonic fragments of the oceanic crust of the geological past. The sea water circulating in the oceanic crust under a pressure of hundreds of atmospheres and being strongly heated is an extremely aggressive medium and leaches out the heavy metals, iron, manganese, nickel, copper, etc., and also lithophylic elements -- potassium, magnesium, and others. The ore solutions forming in this case are a source of formation not only of sulfide ores, but also widely occurring metalliferous sediments.

It is not impossible that the source of metals for complex ores deposited on the floor of the oceans in the form of ferromanganese nodules is hydrotherms of this type. These ores are exceedingly rich. Their reserves are enormous. As is well known, Japanese and American firms have developed methods for their exploitation. In the Pacific Ocean, in particular, these nodules extend over an area of many millions of square kilometers. In each kilometer there are approximately 8 000-10 000 tons of such nodules. In the richest sectors the manganese content in the nodules attains 25%; the content of nickel and cobalt is almost 1.5% and the copper content

## FOR OFFICIAL USE ONLY

is the same. This is enormous wealth which evidently in the near future will begin to be extracted from the ocean floor. In the oceans and seas of the geological past with a melanocratic, basaltoid, ultramafitic crust, characteristic for the present-day oceans, there were also ore processes at work similar to the processes which transpire in the modern oceans and seas. Deposits of the nodule type are known in the Urals and in other regions of the earth. For this reason their comparative study is of great practical interest.

As already mentioned, by the beginning of abyssal drilling a new mobilistic global tectonic concept had already developed. It is now usually called plate tectonics. It is based on a recognition of drift of the continents with the simultaneous formation of a new oceanic crust in the zone of spreading-apart of the lithospheric plates. It has been calculated that the mean rate of crustal drift differs in time and space, varying from 1 to 13 cm per year, and the mean rate of vertical movements of the blocks is from 5 to 10 cm per thousand years. Drilling has yielded indisputable proof of drift and spreading-apart of the continents.

In the Atlantic Ocean, for example, it has been possible to reconstruct, with great detail, the process of spreading-apart of the continental crust and its paleogeography on the basis of synchronous sedimentary rocks which have been drilled through at opposite margins of the continents and which were initially formed in a narrow basin under lagoonal conditions during the initial period of splitting-apart and spreading-apart of the continents.

Abyssal drilling equipment has been used in a detailed investigation of the geological history of the sedimentary layer on the North Atlantic floor. It was found that the onset of spreading-apart was different in different parts. The northern and arctic parts of the ocean began to form later than its southern part.

Already by the beginning of abyssal drilling a partial study had been made of oceanic paleomagnetism. It was established that a special feature of the magnetic field in the oceans is the alternation of zones of normal and reversed polarity of the geomagnetic field. On this basis specialists have developed a paleomagnetic stratigraphic scale. The polarity zones are parallel to the rift zones of the oceanic ridges or are simply parallel to the ridges, which consist of basalts, becoming more ancient with increasing distance from the ridges.

At the time of abyssal drilling the paleomagnetic stratigraphic scale was checked against a detailed biostratigraphic scale. In many cases the boreholes passed through the sedimentary layer and entered the basalt. Determinations of the age of the bottom of the sediments on the basis of biostratigraphic data and the top of the basalts as determined by the potassium-argon method agree very satisfactorily with the age of the paleomagnetic isochronal lines. These data have become the basis of a hypothesis of the spreading-apart and flowing-apart of the floor of the oceans and can be considered a fundamental scientific achievement of abyssal drilling.

In the concept of plate tectonics there has been detailed development of the hypothesis of the mechanism of drift of the continents and formation of the sedimentary and basalt layers of the oceans, especially the problems of crustal subduction and

accretion. The mechanism of movement of masses in the earth's shells nevertheless remains disputable because until now the role and interrelationship of different intraterrestrial and cosmological factors participating in geodynamic processes still have not been interpreted. However, abyssal drilling has confirmed the concept of mobilism, the basis for which is a recognition of the drift of large and small continental and oceanic plates, and this concept must serve as the basis for any geodynamic model.

It can be concluded from this far from complete review of the scientific and practical results of abyssal drilling that this project constitutes a unique attempt at increasing our knowledge concerning the earth, the age, history and processes of development of oceanic basins and seas, and also on the structure and composition of the oceanic crust, its metallogeny and presence of petroleum and gas.

The shortage of time does not make it possible to touch on other serious problems which can be solved by abyssal drilling, such as the interaction of oceanic currents and climate, as well as the evolution of fauna and flora of the geological past.

A unique and invaluable achievement in the deep-water drilling project is the scientific studies which contain the results of core processing. Each voyage of the "Glomar Challenger" is described in one or two books, not to mention numerous other publications in different countries of the world.

Soviet scientists have participated on most of the voyages of the "Glomar Challenger" in all the oceans, first as guests, and after 1974, officially, when the USSR Academy of Sciences began to make a monetary contribution to the drilling project. Forty Soviet scientists, primarily from academic institutes, have participated on the voyages and have processed core material in the laboratories at these institutes. They have honorably and at a high scientific level participated in the common work on the international project and in scientific publications concerning the voyages.

Due to participation in the project the scientists of our country have acquired invaluable experience and knowledge for work on investigation of the geology, geophysics and geochemistry of the world ocean.

Now it is already completely clear that the time has come to turn to the creation of our own modern technical means for studying the geology and mineral resources of the oceans. But prior to solution of this complex problem it is necessary to continue to participate in the international abyssal drilling project.

\*\*\*

Academician A. V. Sidorenko, vice president, USSR Academy of Sciences, spoke after the scientific conference. He stated that the results of abyssal drilling examined at the session of the Presidium, USSR Academy of Sciences, dealt with a problem of the greatest significance. A very great amount of work has been done and highly interesting material has been obtained which is not only of fundamental importance for understanding the geological development of our planet, but also of enormous

**FOR OFFICIAL USE ONLY**

practical value, affording prospects for using the world ocean as a source of mineral raw materials. Accordingly, A. V. Sidorenko noted the importance of further participation of Soviet scientists in work under the international abyssal drilling project and also the need for creating our own technical means for abyssal drilling in the world ocean. Work on study of the world ocean merits special attention, he emphasized, and it is necessary to ensure organizational and material possibilities for carrying out this work in a full volume.

Academician A. P. Aleksandrov, president, USSR Academy of Sciences, pointed out the importance of the considerations expressed at the session concerning our own technical means for abyssal drilling in the world ocean and expressed appreciation to the speaker for an interesting communication.

COPYRIGHT: Izdatel'stvo "Nauka", "Vestnik Akademii nauk SSSR", 1982

5303

CSO: 1865/122

FOR OFFICIAL USE ONLY

UDC 551.46

STUDY OF CARIBBEAN-GULF OF MEXICO BASIN

Moscow VESTNIK AKADEMII NAUK SSSR in Russian No 2, Feb 82 pp 98-102

[Article by V. A. Gorbanev]

[Text] The geographical position of the Central American Basin -- the Caribbean Sea, Gulf of Mexico and adjacent regions of the Atlantic, its already exploited and considerable potential mineral, energy and food resources, and key importance for solution of a number of fundamental problems in oceanology all account for the close attention which scientists of different countries are devoting to this region at the present time.

There are enormous reserves of petroleum and gas on the shelves of the United States, Mexico, Venezuela, Colombia, Trinidad and Tobago. Suffice it to mention that only the Maracaibo petroleum and gas basin, situated in the southern part of the Caribbean Sea, among the sea basins occupies second place in the world with respect to the volume of petroleum production: its output here exceeds 100 million tons. In this region the basis of fishing is menhaden, which accounts for about 40% of the total catch. In addition, fishermen here also take sardines, tuna, shrimp and squid. The total annual production in the basin is about 2 million tons of living resources, which is only 20% of the catch which could be allowed.

One of the tasks of USSR participation in the joint investigations of the basin is study of its hydrodynamic and hydrometeorological regimes exerting an influence on the weather and climate of our country. The computations made by Soviet specialists on the basis of a numerical model of interaction between the atmosphere and ocean, developed under the direction of Academician G. I. Marchuk, demonstrated that the region of the western Atlantic is one of the most important energy-active regions of the world ocean, where processes of transfer of heat and moisture from one medium to another occur most intensively. As a result of these processes macroscale anomalies of temperature and atmospheric pressure arise in the ocean and atmosphere, which in turn causes an anomalous transport of heat and moisture by air masses for tens of thousands of kilometers to the east in the direction of Eurasia. Thus, the hydrodynamic regime of the Caribbean-Mexican region in many respects determines the weather over Western Europe and the European USSR and can serve as an indicator for its long-range forecasting.

In the Caribbean-Mexican basin Soviet scientists are studying the geological structure of the ocean floor for the purpose of developing a global theory of tectonics of the lithosphere and are investigating the biological structure and the living

FOR OFFICIAL USE ONLY

**FOR OFFICIAL USE ONLY**

resources in the ocean. It must be emphasized that the investigation of living resources, the same as practical investigations in the field of the geology of the shelves, is carried out primarily in the interests of the developing countries of the region in rendering them selfless assistance in the mastery of modern methods of marine research, in the training of national cadres and in setting right their own marine economy.

Being guided by these humane goals, the USSR has actively supported the proposal of the Netherlands concerning the formulation of an international program within the framework of the Intergovernmental Oceanographic Commission (IOC) of UNESCO -- "Joint Investigations of the Caribbean Sea and Adjacent Regions."\*

The resolution on creation of this program for "Joint Investigations of the Caribbean Sea and Adjacent Regions" was adopted by the IOC Assembly in 1967. At the same time an international coordination group was established in order to coordinate the efforts of the IOC member states participating in this program. The Institute of Oceanology imeni P. P. Shirshov, USSR Academy of Sciences over the course of a number of years was the key institute in the country in implementing the program. One of the first voyages of the scientific research flagship of this institute, the "Akademik Kurchatov," was an expedition to the Caribbean-Gulf of Mexico region. This expedition, having a biological orientation, left a considerable trace in the history of joint investigations of the Caribbean Sea and the Gulf of Mexico.

In addition to the biological studies, the Institute of Oceanology carried out large-scale hydrological investigations and also investigations in the field of the geology and dynamics of the sea shores of a number of countries, especially the Republic of Cuba.

In addition to the USSR Academy of Sciences, major investigations in the Caribbean-Gulf of Mexico region were carried out by the Ukrainian Academy of Sciences by the personnel of the Marine Hydrophysical Institute and the Institute of Geological Sciences. In the Caribbean Sea and in the Gulf of Mexico the Marine Hydrophysical Institute carried out considerable hydrological surveys, refining the system of currents in this basin and its influence on the formation of the Gulf Stream. The Institute of Geological Sciences has carried out much work for studying the geology of the floor of the Caribbean-Gulf of Mexico Basin and sedimentation processes.

Important fishery investigations in the region have been carried out by the specialists of the Atlantic Scientific Research Institute of Fishing and Oceanography of the USSR Ministry of the Fish Industry. In particular, major studies were carried out by these specialists in collaboration with Cuban scientists. Systematic hydrophysical observations in the Caribbean Sea and the Gulf of Mexico were carried out by scientists and specialists on the ships of the USSR Hydrographic Service.

Our country has made a major contribution to study of the Caribbean-Gulf of Mexico Basin during the lifetime of the program "Joint Investigations of the Caribbean Sea and Adjacent Regions." This was evidenced, in particular, by a review symposium

\* In Russian: SIKAR -- Sovmestnyye Issledovaniya Karibskogo Morya i Prilegayushchikh Rayonov -- Joint Investigations of the Caribbean Sea and Adjacent Regions.

## FOR OFFICIAL USE ONLY

held in Caracas in 1976 where the conferees summarized the results of work under the program "Joint Investigations of the Caribbean Sea and Adjacent Regions" during the period 1967-1976. The reports of the Soviet scientists were characterized by breadth in formulation of the problems, depth of their development and validation by a considerable volume of data.

Considerable progress in study of the Caribbean-Gulf of Mexico Basin during the lifetime of the program "Joint Investigations of the Caribbean Sea and Adjacent Regions" was noted at the symposium. The collected data have created a good scientific basis for further investigation of the region of joint efforts of the IOC member countries.

At the last, VIIIth Session of the International Coordination Group on the Program "Joint Investigations of the Caribbean Sea and Adjacent Regions" (1976) a resolution was adopted on the creation, on an interim basis, of an IOC Association on the Caribbean Basin and Adjacent Regions.\* The task of the association included the development and coordination of joint scientific programs, the collection, processing and dissemination of the collected data, as well as assistance and furnishing of experience to the developing countries of the region. A regional secretariat was created within the framework of the association whose task was the carrying out of routine activity during the period between sessions of the association.

Twenty-one countries are members of the association. Its president at the present time is Manuel Murillo (Costa Rica) and its regional secretary is Robert Lankford (United States). The Marine Hydrophysical Institute, Ukrainian Academy of Sciences, became the key USSR organization under the association.

The Soviet Union is taking an active part in implementing the joint programs. During the period 1978-1980 alone several expeditions were carried out in the Caribbean-Gulf of Mexico Basin, including aboard the ship "Mikhail Lomonosov." During this voyage multisided oceanological investigations were carried out in the central and eastern parts of the Caribbean Sea. New data were collected making it possible to refine the conclusions drawn earlier concerning the thermohaline, dynamic, hydrochemical and hydrobiological structures of the water masses and also the hydrooptical characteristics of the water and to advance new scientific hypotheses. In particular, it was demonstrated that there are anticyclonic meanders over the Colombian Basin on the basis of factual data for the autumn and spring periods. The direction of movement of deep North Atlantic waters was determined. During the course of the entire voyage depths were measured and as a result 30 points with new depths were measured. The measurements of the strait between Pedro and Rosalind Banks were determined with a higher accuracy; it is through this strait that the principal water exchange occurs between the Yucatan and Colombian Basins. The results of measurement of currents in the Grenada region indicated that the vertical dynamic structure here is considerably more complex than was assumed.

Hydrobiological data are of special interest from the point of view of study of the formation of the productivity of waters. At the same time, these data to a considerable degree made it possible to refine the conclusions drawn concerning the

\* In Russian: MOKARIB -- IOC Association on the Caribbean Basin and Adjacent Regions.

## FOR OFFICIAL USE ONLY

structure and dynamics of water masses. Data were obtained for the first time on the internal waves in the region. They are based both on instrumental measurements of temperature and current velocity fluctuations, but also on the results of computations of hydrological parameters.

All the materials collected during the voyage of the scientific research ship "Mikhail Lomonosov" have been fed into the international data exchange system through World Data Center B (Moscow) and thus they can be used by any IOC member countries, including member countries of the IOC Association on the Caribbean Basin and Adjacent Regions.

The results of investigations by Soviet scientists in 1978-1980 in the Caribbean-Gulf of Mexico region were reported at the third session of the association, which transpired in December 1980 at Cancun (Mexico). During this period, on the basis of all available data, a study was made of the spatial-temporal variability of temperature, salinity, water density and oxygen content of water. In addition, a study was made of the exchange of water masses through the principal straits between the Greater and Lesser Antilles; a hydrodynamic model of the Caribbean-Gulf of Mexico Basin was constructed. The enumerated results obtained on the hydrology and dynamics of waters in the Caribbean Sea and Gulf of Mexico are set forth in a recently published monograph\*.

At the same time a detailed study was made of the dynamics of vertical movements of water masses as an extremely important factor determining the bioproductivity of waters. Interesting data were obtained as a result of an analysis of the processes of formation of the radioactivity fields and also on geophysics and hydrobiology.

Particular attention was devoted to the fishery aspects of oceanography of the Caribbean Basin, including investigations of the ecological basis of rational use of bottom ichthyofauna of the Gulf of Mexico. Extensive fishery investigations were made in different parts of the Caribbean-Gulf of Mexico Basin and adjacent regions of the Atlantic. They were carried out simultaneously both within the framework of the association and in conformity to bilateral agreements between the Soviet Union and Cuba, Jamaica, Nicaragua and Grenada. In particular, during 1979-1980 alone there were two joint Soviet-Jamaican expeditions in which scientists of both countries participated. The collected data made it possible to obtain the pattern of distribution of the principal concentrations of bottom species of fish on the Jamaican shelf and Pedro Bank and also to estimate the biomass of the predominant fish species. The collected data on the biology of these species are enabling specialists to make the first estimate of the volumes of their possible commercial catch. The total biomass of bottom species of fish on the Jamaican and Pedro Bank shelves during July-August 1979 was 49 400 tons, whereas in December 1979-January 1980 it was 34 800 tons.

During the period April-September 1980 there was an expedition in the waters of Grenada and Nicaragua in collaboration with specialists of these countries for studying the distribution of the principal concentrations and biomass of bottom and pelagic species of fish on the shelves. Data were also obtained on the biology

\* See GIDROLOGIYA KARIBSKOGO MORYA I MEKSIKANSKOGO ZALIVA (Hydrology of the Caribbean Sea and Gulf of Mexico), Leningrad, Gidrometeoizdat, 1981.

## FOR OFFICIAL USE ONLY

of these species and the biomass of the predominant species of fish was estimated. The material collected during the expedition served as a basis for developing a model of the dynamics of populations of commercial fish and in predicting their reserves.

During geomorphological and geophysical work specialists collected and generalized an enormous amount of material relating to relief, magnetic and gravitational fields in the Caribbean Sea. New information was obtained on the structure and thickness of the sedimentary layer and the earth's crust. New highly precise gravimetric charts and maps of the bottom relief of the Caribbean Sea floor were compiled, as well as diagrams of tectonic structures. All these maps and diagrams are of enormous practical importance and can be used as a scientific basis in the search for petroleum and gas.

In addition to carrying out joint expeditions for clarifying the presence of regions which are promising for fishing, the Soviet Union is systematically providing places for foreign trainees on board its ships carrying out different investigations. For example, the "Mikhail Lomonosov," carrying out hydrophysical investigations, carried six specialists from different countries in the region. During work in the eastern part of the Caribbean Sea three specialists from Grenada underwent training aboard this ship.

An important role in the professional training of specialists from the developing countries was played by a scientific-academic seminar held aboard the "Akademik Vernadskiy" during its call at the port of Nassau (Bahamas). The seminar was attended by scientists from different member countries of the association.

At the third session of the association held in December 1980 there was a detailed analysis of the association's activity during the elapsed four years. Despite the successes attained, in general the results of the joint investigations, in the opinion of Soviet scientists, have not yet justified those hopes which it was thought that the association would realize. The regional character of the association led to a predominance of small narrowly specialized projects formulated by the association and being of interest for only an insignificant part of the developing countries of the region. At the same time, the carrying out of wide-scale fundamental or practical investigations not formally approved by the association, and this under conditions under which all the countries of the region have declared 200-mile economic zones in which the carrying out of any scientific investigations requires the permission of the corresponding coastal state with the imposing of a whole series of preliminary conditions, involves considerable organizational difficulties. As a result, there is a marked decrease in the flow of data entering into the international data exchange system.

Evidently these same factors in large part explain why the session adopted a resolution on transforming the association into the IOC Subcommittee on the Caribbean Basin and Adjacent Regions. Nevertheless, the orientation on small local projects persisted. At the present time only two projects have really been developed: "Scientific Programs in Support of Fishing in the Lesser Antilles" and "Program for Monitoring Sea Contamination." The remaining projects -- "Program for Studying Lobsters in the Central American Basin," "Program for Studying Sea Turtles in the Western Regions of the Central Atlantic," "Program on the Geology

**FOR OFFICIAL USE ONLY**

of the Gulf of Paria" and "Program on Oceanic Dynamics" are only in the stage of formulation.

Soviet scientists also intend to pursue further the idea that it is necessary to carry out large-scale global programs for investigating the Caribbean-Gulf of Mexico region by the personnel of IOC member countries. Only on the basis of such major fundamental investigations will it be possible to proceed to serious practical projects related to the possible presence of petroleum and gas in the basin and biological resources. As promising directions the Soviet Union proposes several principal approaches for future fundamental and practical investigations which in turn can serve as a basis for solving special local problems of interest to one or more developing countries in the region.

An extremely timely problem is that of detecting the frequency of recurrence of formation of large thermal anomalies in the basin and adjacent regions of the Atlantic for evaluating their influence on the corresponding long-period variations of weather in Europe and the creation of modern numerical methods for long-range weather forecasting.

It is also necessary to carry out a further study of the structure and circulation of water masses and mapping of vertical movement, the determining abiotic factor exerting an influence on the formation and movement of regions with a high bioproductivity.

Investigations must be continued for studying the variability of hydrophysical and hydrochemical fields for the purpose of ascertaining the laws of influence of these factors on basin bioproductivity.

The problem of further improvement of the hydrodynamic model of the Caribbean Basin is of extremely great importance for describing the variability of oceanological fields at different spatial-temporal scales. A serious problem which still has not been solved is that of creating a hydrobiological model of the Caribbean-Gulf of Mexico Basin.

Such are the principal scientific tasks which await solution in the Central American Basin. Soviet scientists and specialists hope that the existing difficulties are of a temporary character and international cooperation in study of the nature of the Caribbean Sea, the Gulf of Mexico and adjacent regions will rise to a qualitatively new stage and will become a more powerful lever by means of which it will be possible to carry out scientific research freely for the good of the present and future.

COPYRIGHT: Izdatel'stvo "Nauka", "Vestnik Akademii nauk SSSR", 1982

5303

CSO: 1865/122

FOR OFFICIAL USE ONLY

UDC 551.46

## NEW MONOGRAPH ON OCEANIC TURBULENCE

Leningrad OKEANSKAYA TURBULENTNOST' in Russian 1981 (signed to press 5 Feb 81)  
pp 2, 320

[Annotation and table of contents from monograph "Oceanic Turbulence", by Andrey Sergeyevich Monin and Rostislav Vsevolodovich Ozmidov, Gidrometeoizdat, 1630 copies, 320 pages]

[Text]. Annotation. This book gives a review of turbulence theory in stratified flows, examines the mechanisms of generation of turbulence and summarizes data on microscale turbulence. Information is given on the statistical parameters of turbulent fluctuations and their dependence on background hydrological conditions. The rates and dissipation of turbulent energy are analyzed and the characteristics of intermittence of turbulent fields in the ocean are presented. The theory of macroscale, quasi-two-dimensional oceanic turbulence is set forth and the "negative viscosity" effects associated with it are analyzed. Information pertinent to recently discovered synoptic eddies is given. The book is intended for oceanologists, geophysicists and students at the appropriate institutions of higher education.

## Contents

Foreword.....	3
Chapter 1. Theory of Turbulence in Stratified Flows	
1. Definition of turbulence.....	8
2. Equations of dynamics of turbulent flows.....	26
3. Mechanisms of generation of oceanic turbulence.....	39
4. Influence of stratification on turbulence.....	56
5. Theory of turbulence spectrum.....	76
6. Microscale structure of turbulence.....	97
Chapter 2. Microscale Turbulence	
7. Apparatus for investigating microscale turbulence. Measurement method.....	113
8. Statistical characteristics of turbulence.....	132
9. Velocity fluctuations.....	150
Mean square values.....	150
Correlation and spectral functions.....	155
Dependence on local background conditions.....	163
Spectra of intensity of fluctuations and energy dissipation.....	170
Rate of dissipation of turbulent energy.....	172
Climatology of microscale turbulence.....	180

FOR OFFICIAL USE ONLY

FOR OFFICIAL USE ONLY

10. Temperature fluctuations.....	185
Indirect method for evaluating temperature fluctuations.....	185
Local temperature gradients in ocean.....	186
Variability of fine-structured temperature profiles.....	190
Direct measurements of high-frequency temperature fluctuations.....	200
Turbulent heat flows.....	201
Spectra of high-frequency temperature fluctuations.....	202
Spectral characteristics of variability of temperature field in ocean.....	205
Rate of evening-out of temperature inhomogeneities.....	209
11. Conductivity and salinity fluctuations.....	213
General principles.....	213
Local C and S gradients.....	214
Spectral characteristics.....	220
Dependence on local background conditions.....	222
Intermittence of conductivity fluctuations.....	231
Data from deep measurements.....	235
Determination of salinity fluctuations.....	236
Density fluctuations and turbulent flows of mass.....	237
Climatology of turbulence in conductivity field.....	240
Chapter 3. Macroscale Horizontal Turbulence.....	246
12. Macroturbulence and negative viscosity.....	246
13. Theory of two-dimensional turbulence.....	261
14. Spectrum of horizontal turbulence.....	284
Bibliography.....	299

COPYRIGHT: Gidrometeoizdat, 1981

5303

CSO: 1865/116

FOR OFFICIAL USE ONLY

UDC 551.596.1:551.55

PROPAGATION OF INTERNAL WAVES IN STRATIFIED MEDIUM WITH FLOW VELOCITY SHEAR

Moscow IZVESTIYA AKADEMII NAUK SSSR: FIZIKA ATMOSFERY I OKEANA in Russian  
Vol 18, No 2, Feb 82 (manuscript received 3 Mar 81) pp 145-152

[Article by V. Yu. Tseytlin, Institute of Atmospheric Physics, USSR Academy of Sciences]

[Text]            Abstract: It is shown that solution of the two-dimensional problem of the propagation of internal waves in a medium with arbitrary velocity and density profiles can be reduced to the scattering problem for the Schrödinger equation. Also examined is the velocity profile in the form of a hyperbolic tangent and it is shown that there is a region of the values of the parameters with which the corresponding potential has a nontrivial structure. One of the results of this is the existence of a horizontal waveguide for adequately long waves. The limits of applicability of the geometrical approach are determined and the necessary boundary value conditions are discussed.

1. In this article a study is made of the propagation of internal waves (IW) in a nonviscous stratified fluid which moves with a velocity changing with height. The importance of this problem is attributable to the fact that internal waves play an appreciable role in the energy balance of the upper layers of the atmosphere (for example, see [1] and the literature cited there), but during propagation they usually pass through regions of a marked change in wind velocity and density which may be either local, caused by surface temperature inversions, or global, caused by more or less macroscale synoptic formations. The coefficients of reflection and propagation of IW through such layers determine the corresponding energy fluxes and thus the contribution of IW to the energy balance.

The simplest method for examining the effects of reflection and refraction of waves is geometrical, when the region of a sharp change in the parameters of the medium is replaced by an interface at which the parameters and/or their derivatives experience a discontinuity. By "splicing" the solutions on both

FOR OFFICIAL USE ONLY

## FOR OFFICIAL USE ONLY

sides of the discontinuity by means of the appropriate boundary conditions, it is possible to obtain the corresponding Fresnel formulas, and thus solve the problem in a particular approximation. An excellent review of such an approach for a density discontinuity and/or its derivative can be found in [2]\*. Without discussing the density discontinuities in detail and assuming that density is a smooth function of the vertical coordinate, we will investigate flow velocity shears. It is also possible to attempt to consider the latter geometrically, assuming velocity to be constant above and below the discontinuity and having a jump at this level, but this description is not self-consistent because such a velocity profile is unstable. In actuality, the flow stability criterion is the condition  $R > 1/4$ , where  $R$  is the global Richardson number [3, 4], which qualitatively denotes a quite smooth transition from one asymptotic form of flow velocity to another. Thus, we arrive at the need for a more rigorous examination of the problem. The latter, nevertheless, does not mean that the geometrical approach must be discarded. A more precise examination will make it possible to refine the boundary conditions at the discontinuity and the framework of its applicability.

2. The object of investigation is only IW and therefore it is desirable from the very beginning to exclude the effects of compressibility and the acoustic waves caused by them. The continuity equation is used in the form

$$(\partial_t + \mathbf{U} \cdot \nabla) \rho = 0, \quad \nabla \cdot \mathbf{U} = 0, \quad (1)$$

where  $\rho$  is density,  $\mathbf{U}$  is fluid velocity, that is, density is invariable along the trajectory of a fluid particle (quasicompressibility).

The equations of hydrodynamics in the investigated case have the form

$$\rho(\partial_t + \mathbf{U} \cdot \nabla) \mathbf{U} + \nabla p + \rho \mathbf{g} = 0. \quad (2)$$

Then as a simplification we will examine a two-dimensional case, where  $x, y$  are the horizontal and vertical coordinates. We will assume that the flow moves only in the horizontal direction. Then in accordance with the problem formulated above, the flow parameters in the zero approximation have the form:

$$\rho_0 = \rho_0(y), \quad p_0 = p_0(y), \quad \mathbf{U}_0 = (u_0(y), 0). \quad (3)$$

The zero subscript denotes background parameters on the basis of which wave disturbances are propagated, that is

$$\rho = \rho_0 + \rho, \quad p = p_0 + p, \quad \mathbf{U} = \mathbf{U}_0 + \mathbf{U}, \quad \mathbf{U} = (v_x, v_y) \quad (4)$$

(below the parameters without a zero subscript correspond to a disturbance of the principal state).

With an accuracy to the second order of magnitude we have the following system of linear equations:

\* The reflection of internal waves from solid obstacles has been described in detail in [10, 11].

## FOR OFFICIAL USE ONLY

$$\begin{aligned} \rho_0 D v_x + \partial_x p + \rho_0 u_0' v_y &= 0, \quad \rho_0 D v_y + \partial_y p + \rho g = 0, \\ D \rho + v_y \rho_0' &= 0, \quad \partial_x v_x + \partial_y v_y = 0, \quad D = \partial_t + u_0 \partial_x, \end{aligned} \quad (5)$$

where the derivatives of the background values are denoted by a prime.

The introduction of the stream function  $\psi(x, y)$ :

$$v_x = \partial_y \psi, \quad v_y = -\partial_x \psi \quad (6)$$

makes possible a substantial simplification of system (5). Differentiating the first equation for  $x$  and the second for  $y$  and subtracting them one from the other, we exclude  $p$ . Then applying the operator  $D$  to the derived equation and adding it to the third equation, multiplied by  $g$ , we exclude  $\rho$ . Finally we have:

$$D^2 (\partial_x^2 + \partial_y^2) \psi + \frac{\rho_0'}{\rho_0} D^2 \partial_y \psi - \frac{(\rho_0 u_0')'}{\rho_0} D \partial_x \psi - g \frac{\rho_0'}{\rho_0} \partial_x^2 \psi = 0. \quad (7)$$

Since the background over which the disturbances propagate is uniform relative to  $x$ , it is natural to seek a solution of equation (7) by separating the variables in the following way:

$$\psi = \tilde{\varphi}(y) \exp [i(k_x x - \omega t)]. \quad (8)$$

Introducing the  $x$ -component of phase velocity  $c_x = \omega/k_x$ , we obtain an equation for  $\tilde{\varphi}(y)$ :

$$\tilde{\varphi}'' + \frac{\rho_0'}{\rho_0} \tilde{\varphi}' - \left[ k_x^2 + \frac{u_0''}{(u_0 - c_x)} + g \frac{\rho_0'}{\rho_0} \frac{1}{(u_0 - c_x)^2} + \frac{\rho_0'}{\rho_0} \frac{u_0'}{(u_0 - c_x)} \right] \tilde{\varphi} = 0. \quad (9)$$

Equation (9) was discussed in the literature [3-5] in relation to the problem of the stability of currents with a shear, but in this article it is interpreted in a different context. Eliminating the term with the first derivative by means of the standard replacement

$$\tilde{\varphi} = \rho_0^{-1/2} \varphi, \quad (10)$$

we arrive at the equation

$$\begin{aligned} \varphi'' + \left\{ -k_x^2 - \left[ \frac{1}{2} \rho_0^{-1} \rho_0'' - \frac{1}{4} \rho_0^{-2} (\rho_0')^2 + (u_0 - c_x)^{-1} u_0'' + \right. \right. \\ \left. \left. + g \rho_0^{-1} \rho_0' (u_0 - c_x)^{-2} + \rho_0^{-1} \rho_0' (u_0 - c_x)^{-1} u_0' \right] \right\} \varphi = 0, \end{aligned} \quad (11)$$

which will serve as a basis for further examination. It is similar to the stationary Schrödinger equation, where the role of energy is played by the value  $k_x^2$ , whereas the role of potential  $V(y)$  is the remaining expression in brackets. Even before the choice of a specific velocity profile it is possible to draw some conclusions concerning the properties of solution of such an equation. If  $V(y)$  has the constant asymptotic forms  $V(-\infty)$  and  $V(+\infty)$  (an adequate condition for this in the case of an exponential stratification, which will also

## FOR OFFICIAL USE ONLY

be considered, is evidently the presence of constant asymptotic forms of the velocity field (here  $V(\pm\infty) < 0$ ); the solution asymptotically has the form of a plane wave with the wave number

$$k_y^{\pm} = (-k_x^2 - V(\pm\infty))^{\frac{1}{2}} \quad (12)$$

A characteristic feature of potential  $V(y)$  is its dependence on  $c_x$ , that is, waves with different phase velocities  $c_x$  are scattered at different potentials. In the asymptotic form this leads to a dependence of  $k_y$  on  $k_x$  and  $c_x$ , that is, as is easily confirmed, using (12) this leads to a standard dispersion relationship for IW [6], taking flow velocity into account:

$$k_x^2 + k_y^2 + \frac{\beta^2}{4} = \frac{g\beta k_x^2}{\sigma^2}, \quad (13)$$

where it is assumed that

$$\begin{aligned} \sigma &= \omega - k_x u_0(\pm\infty), \\ \rho_0 &\sim \exp(-\beta y). \end{aligned} \quad (14)$$

It is clear from (13) that with a stipulated  $u_0$  and  $c_x$  there will be a threshold value  $k_x = k_{thr}^{\pm}$ , corresponding to  $k_y = 0$ . IW with  $k_x > k_{thr}$  cannot propagate in the medium. On the other hand, with stipulated  $k_x$  there is a threshold value  $c = c_{thr}$ , such that with  $c > c_{thr}$  waves are impossible.

Below we will examine those waves for which  $u_0 - c_x$  nowhere becomes equal to zero (the critical levels where  $u_0 = c_x$  correspond to the singular potential in (11), which destroys waves arriving from infinity). Then, continuing a general examination of equation (11), we note that in accordance with the spectrum of the operator  $-d^2/dy^2 + V(y)$  in the problem there are scattering states (continuous spectrum) and related states (discrete spectrum). In the first case, if  $k_x > k_{thr}^{\pm}$  ( $k_x > k_{thr}^+$ ), there is no wave asymptotic form with  $y = +\infty$  ( $y = -\infty$ ) and, accordingly, there is a complete reflection of the wave arriving from the lower (upper) half-plane. If there are states of the discrete spectrum, then these are normalized (localized with respect to  $y$ ) solutions which if they attenuate more rapidly than  $\exp(-\beta y/2)$  with  $y \rightarrow \infty$  (see (10), (14)), correspond to a waveguide.

Now we will proceed to an investigation of equation (11) for a specific velocity profile.

3. As a smooth approximation of velocity shear we select

$$u_0(y) = v \operatorname{th}(y/h), \quad (15)$$

where  $h$  is the characteristic transition region from  $u_0(-\infty) = -v$  to  $u_0(+\infty) = +v$ . The stratification is taken in the form (14). Converting in (11) to dimensionless variables, with (14) and (15) taken into account we obtain

$$\varphi''(y/h) + [E - V(z)]\varphi(y/h) = 0, \quad (16)$$

## FOR OFFICIAL USE ONLY

where

$$E = -(k_x^2 + \beta^2/4)h^2, z = th(y/h), \quad (17)$$

$$V(z) = -\left\{ \frac{2z(1-z^2)}{(z-C)^2} + \frac{R}{(z-C)^2} + \frac{L(1-z^2)}{(z-C)} \right\}.$$

Here

$$R = g\beta h^2/\nu^2, C = c_x/\nu, L = \beta h, \quad (18)$$

R is the global Richardson number of the particular base flow. Henceforth we will adopt the standard simplification in such cases [3, 4], assuming  $\beta \ll h^{-1}$ ,  $L \rightarrow 0$ ,  $E \rightarrow -k_x^2 h^2$ , which corresponds to the real distributions (we note that the term with L in V(z) exerts no influence on the asymptotic form and its contribution to scattering is easily restored). Despite the simplifications made, the resulting potential

$$V(z) = -\left\{ \frac{2z(1-z^2)}{(z-C)^2} + \frac{R}{(z-C)^2} \right\} \quad (17a)$$

is quite complex and is dependent on two parameters. We will immediately cite the limitations on the R and C parameters. The requirements of stability of flow [3, 4] and the absence of critical levels give:

$$R > 1/4, |C| > 1. \quad (19)$$

The results of investigation of the potential V(z) are as follows:

1) asymptotic forms

$$V(+\infty) = -\frac{R}{(1-C)^2}, \quad V(-\infty) = -\frac{R}{(1+C)^2}, \quad (20)$$

which, as was already noted, leads to a standard dispersion relationship for IW with  $y/h \rightarrow \pm \infty$ ;

2) evenness: V(z) is invariant relative to the replacement  $y \rightarrow -y$ ,  $C \rightarrow -C$ , which makes it easy to obtain solutions for waves with opposite  $c_x$  or  $\nu$ ;

3) extrema: with  $R > C^2$  the potential does not have local extrema and smoothly interpolates the asymptotic form; with  $R \leq C^2$  there is a local minimum and a local maximum (Fig. 1). This peculiarity leads to a number of important effects (see below);

4) dependence on parameters: dependence of asymptotic forms on the parameters is obvious (see (20)). The difference

$$V(+\infty) - V(-\infty) = 4RC/(C^2 - 1)^2 \quad (20a)$$

decreases monotonically with an increase in C and increases with R. In the case  $R \leq C^2$  (a) with fixed R  $V_{\max}$  with an increase in C first increases, attains a maximum, and then drops off to zero,  $V_{\min}$  increases monotonically, remaining

## FOR OFFICIAL USE ONLY

negative and asymptotically approaching zero (we note that with  $C \rightarrow \infty$   $V(z) \rightarrow 0$ ); b) with fixed  $C$   $V_{\max}$  with an increase in  $R$  decreases monotonically, passing through zero;  $V_{\min}$  also decreases monotonically, remaining negative.

The relative change in the amplitude of the  $V(z)$  change in the transitional region  $(|V_{\max}| - |V_{\min}|) / (|V(+\infty)| - |V(-\infty)|)$  increases with an increase in  $C$  with a fixed  $R$  and decreases with an increase in  $R$  with fixed  $C$ . With stipulated  $R$  the right asymptote (see (20)) increases with an increase in  $C$  more rapidly than  $V_{\min}$  (both parameters are negative); therefore, for any  $R \leq C^2$  we find such a  $C_{cr}$  that with  $C \geq C_{cr}$   $V_{\min} < V(+\infty) < V(-\infty)$ , that is

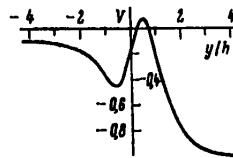


Fig. 1. "Potential" in case  $R < C^2$ ,  $R = g\beta h^2/v^2 = 1$ ,

$$C = \frac{\omega \lambda_x}{2\pi v} = 2$$

there is a possibility of appearance of a discrete spectrum. In the remaining cases the spectrum is evidently continuous.

Returning to the initial problem of the reflection and propagation of IW through a region of sharp change in flow velocity, we see that it is reduced to the problem of scattering for the potential investigated above. The standard formulation of the scattering problem is as follows (for example, see [7]): with  $y/h \rightarrow -\infty$  there is an incident wave of a unit amplitude, which, scattering on the potential, is broken down into transmitted and reflected waves, and it is necessary to find such a solution of equation (16) which has the asymptotic forms (we will consider waves arriving from the region where their phase velocity  $c_x$  is opposite the flow velocity):

$$\begin{aligned} \varphi(-\infty) &= \exp(ik_y y) + a \exp(-ik_y y), \\ \varphi(+\infty) &= b \exp(ik_y y). \end{aligned} \quad (21)$$

The latter play the role of boundary conditions for the corresponding boundary-value problem. The  $a$  and  $b$  parameters are the amplitudes of the reflected and transmitted waves. In this case  $r = aa^*$  and  $t = (k_y^+/k_y)bb^*$  are the coefficients of reflection and transmission which are related to one another by the condition

$$r + t = 1, \quad (22)$$

following from the nondependence of the Wronskian  $W(\varphi, \bar{\varphi})$  on  $y$ .

Unfortunately, the analytical solution of equation (16) with the potential (17) is inadmissible (in this connection see [3]). Accordingly, for solving the formulated boundary-value problem, relying on a preliminary qualitative investigation, we apply the numerical integration method.

## FOR OFFICIAL USE ONLY

4. First we will examine the simpler situation when  $R > C^2$ . Assuming that the potential rather rapidly arrives at an asymptotic form (the characteristic width of the transient region is  $\sim 3$ ), in this case it can be expected that the precise solution differs little from that obtained as a result of a rectangular approximation of potential (step):

$$V \rightarrow \varphi = \begin{cases} V(+\infty), & y > 0, \\ V(-\infty), & y < 0, \end{cases} \quad (23)$$

where  $V(\pm\infty)$  are given by formula (20). Applying the latter, however, it is necessary to refine the boundary conditions at the discontinuity.

In quantum mechanics in such cases the requirement of continuity of the function and its first derivative is imposed. In hydrodynamics, however, as a rule use is made of the condition of continuity of the velocity component normal to the discontinuity and pressure variation [8]. Using formulas (5), (6) and (8) it is easy to confirm that with a continuous velocity profile these two pairs of boundary conditions are identical\*. The formulas for  $r$  and  $t$  in the case of the potential (23) have the form

$$r = \left( \frac{k^+ - k^-}{k^+ + k^-} \right)^2 = aa^*, \quad (24)$$

$$t = \frac{4k^+k^-}{(k^+ + k^-)^2} = \frac{k^+}{k^-} bb^*,$$

where  $k_{\pm}^{\pm}$  were determined in (12). A comparison of the  $|b|^4$  values given by numerical integration and formula (24) is given in Fig. 2. It can be seen that the geometrical approach, involving a replacement of the potential in accordance with formula (23) and use of the continuity conditions  $\varphi$  and  $\varphi'$  at the discontinuity, is a good approximation. This approximation is the better the steeper the step in (23), that is, the smaller the  $C$  value and the greater the  $R$  value (see (20a)). The dependence of the  $|b|^2$  and  $t$  values on  $C$  with fixed  $k_x$  is shown in Fig. 3, a. The presence of a maximum on the  $|b(C)|^2$  graph is of interest. The transmission coefficient with a decrease in  $C$  from the threshold value ( $C_{thr} = 6.07$  in this case) rapidly attains unity. This means that in this situation there is a sharp transition (in the interval of change  $\Delta C = 0.5$ ) from the total reflection to total propagation of IW.

Now we will proceed to an examination of the more interesting situation when  $R \leq C^2$ . In this case due to the nontrivial structure of potential in the transitional region (see Fig. 1) it is possible to expect a strong difference from the solution stipulated by the rectangular approximation. In actuality, here we meet with the pattern of scattering in a quasistationary or bound (for adequately large  $C$ , see above) state well known in quantum mechanics [7, 9]. Unfortunately, the region of change of  $E$  in equation (16) is limited

$$V(-\infty) < E < 0 \quad (25)$$

\* It is also easy to confirm that the use of a discontinuous velocity profile -- a naive geometrical approach -- leads to an incompatibility of the boundary conditions if  $\rho_0$  and  $\rho_0'$  are continuous.

## FOR OFFICIAL USE ONLY

and cannot be traced completely for the scattering states and fine effects of resonance scattering. However, even simple semiquantitative reasonings based on the replacement of the potential (17) by the rectangular potential well and the barrier following it indicate a considerable increase, at least for small  $C$ , in the transmission coefficient in comparison with that obtained from (24). The results of numerical integration confirm this conclusion (Fig. 4).

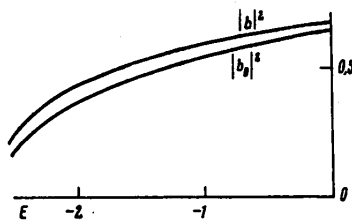


Fig. 2. Dependence of square of amplitude of transmitted wave  $|b|^2$  on  $E = 4\pi^2 h^2 / \lambda_x^2$  with fixed  $C$  and  $R > C^2$  in comparison with result of geometrical approach  $|b_0|^2$ ;  $R = 100$ ,  $C = 5$ .

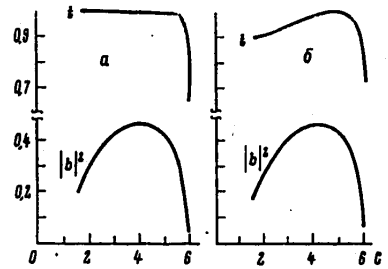


Fig. 3. Dependence of square of amplitude of transmitted wave and reflection coefficient on  $C$  with fixed  $E$  in the case  $R > C^2$ ,  $R = 100$ ,  $E = -2$  (a) and  $R < C^2$ ,  $R = 1$ ,  $E = -0.2$  (b).

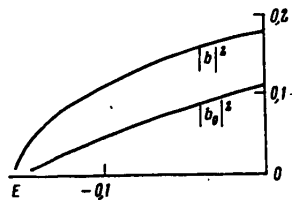


Fig. 4. Dependence of square of amplitude of transmitted wave  $|b|^2$  on  $E$  with fixed  $C$  with  $R < C^2$  in comparison with result of geometrical approach  $|b_0|^2$ . It can be seen that  $|b_0|^2$  is reduced by a factor of  $\sim 2$ ;  $R = 1$ ,  $C = 1.5$ .

The dependence of  $|b|^2$  and  $t$  on  $C$  is shown in Fig. 3, b and is similar to that shown in Fig. 3, a. The change in  $t$  (and  $|b|^2$ ) consists of two effects: with an increase in  $C$  the asymptotic forms of potential approach one another (see (20)), which leads to an increase in  $t$  ( $|b|^2$ ), but on the other hand,  $C$  simultaneously approaches the threshold value, which decreases  $t$  (and  $|b|^2$ ).

In contrast to the case  $R > C^2$ , when there are solutions corresponding to 1) scattering -- in the  $E$  range stipulated by (25), 2) total reflection with  $V(+\infty) < E < V(-\infty)$ , with  $R \leq C^2$  and sufficiently large  $C$  there are additional solutions for  $V_{\min} < E < V(+\infty)$ . For small  $R$   $V_{\min}$  already becomes less than  $V(+\infty)$  with quite small  $C$ .

## FOR OFFICIAL USE ONLY

However, it is known [9] that in the case  $V(-\infty) \neq V(+\infty)$  for the appearance of bound states in the potential well there must be satisfaction of special conditions related to its depth.\* Since in all the considered cases the well is small, the bound state appears when  $V(-\infty) \approx V(+\infty)$ , that is, for  $R = 0.5$  with  $C$  of the order of several tens, as indicated by numerical calculations. In this case the corresponding  $k_*$  is close to zero and the waveguide is feasible only for very long (in comparison with  $h$ ) internal waves.

5. In conclusion we will cite an example based on the real parameters of wind velocity shear and internal waves in the atmosphere. For this we use the characteristics of the wind profile cited in [8, Chapter 1, #5] and the results of experiments for detecting internal waves [12]. The mean data on the wind parameters indicate that during the summer there is a sharp shear of horizontal wind velocity with altitude. At a latitude  $30^\circ$   $v \approx 5$  m/sec,  $h \approx 3$  km and  $H = \beta^{-1} = 6.5$  km (notations as before). Then  $R \approx 540$ ,  $L \approx 0.46$ . The parameters of the observed internal waves are as follows:  $c_x = 20$ -100 m/sec,  $k_x^{-1} \approx 12$ -60 km,  $\rightarrow E \approx - (0.08-0.14)$ ,  $C = 4$ -20. Thus, for the observed internal waves we have a situation similar to that shown in Figures 1, 3, 4, a:  $R > C^2$ ,  $R$  is large and accordingly a geometrical approach gives a correct result. The  $E$  and  $C$  parameters for the experimentally observed waves are far from the threshold values (for these wavelengths  $C_{thr} \approx 60$ ) and therefore  $t \approx 1$ . These conclusions are confirmed by precise computations whose results with  $E = -0.1$  are:

$C$	5	10	15	20
$ b ^2$	0,67	0,82	0,87	0,90

For all  $C$   $t = 1$  with an accuracy to the fourth place. Accordingly, waves with the observed parameters transmit the described wind shear virtually without reflection. A detailed investigation of the other observed wind distributions requires separate examination.

In conclusion, I express deep appreciation to A. M. Obukhov for formulating the problem and stimulating discussions. I thank Ye. P. Chunchuzov and N. N. Romanov for discussions and O. A. Gel'fond for assistance in carrying out numerical computations.

## BIBLIOGRAPHY

1. Chunchuzov, Ye. P., "Contribution of Traveling Gravitational Waves to the Energy Balance of the Atmosphere at the Mesopause Level," IZV. AN SSSR: FAO (News of the USSR Academy of Sciences: Physics of the Atmosphere and Ocean), Vol 15, No 10, pp 1087-1091, 1979.
2. Tolstoy, I., "The Theory of Waves in Stratified Fluids Including the Effects of Gravity and Rotation," REV. MOD. PHYS., Vol 35, No 1, pp 207-230, 1963.
3. Drazin, P. G., "The Stability of a Shear Layer in an Unbounded Heterogeneous Inviscid Fluid," J. FLUID MECH., Vol 4, No 2, pp 214-224, 1958.

\* It is well known that when  $V(-\infty) = V(+\infty)$  in a one-dimensional case there is always at least one bound state when  $V_{min} < V(\infty)$ .

FOR OFFICIAL USE ONLY

4. Miles, J. W., "On the Stability of Heterogeneous Shear Flows, Part II," J. FLUID MECH., Vol 16, No 2, pp 209-227, 1963.
5. Yi Chua-shun, "Wave Movements in Stratified Fluids," Nelineynyie Volny (Nonlinear Waves), Moscow, Mir, pp 271-296, 1977.
6. Uizem, Dzh., Lineynyie i nelineynyie Volny (Linear and Nonlinear Waves), Moscow, Mir, 1977, 622 pages.
7. Messia, A., Kvantovaya Mekhanika (Quantum Mechanics), Part 1, Moscow, Nauka, 1979, 478 pages.
8. Gossard, E. and Khuk, U., Volny v atmosfere (Atmospheric Waves), Moscow, Mir, 1978, 532 pages.
9. Davydov, A. S., Kvantovaya Mekhanika (Quantum Mechanics), Moscow, Nauka, 1973, 703 pages.
10. Brekhovskikh, L. M., Goncharov, V. V., Naugol'nykh, K. A. and Rybak, S. A., "Oceanic Waves," Izv. VUZov. Radiofizika (News of Institutions of Higher Education. Radiophysics), Vol 19, No 5-6, pp 842-863, 1976.
11. Golitsyn, G. S., "Reflection of Atmospheric Waves From Solid Obstacles," Akust. Zh. (Acoustics Journal), Vol 11, No 3, pp 313-317, 1965.
12. Kazankov, A. M. and Portnyagin, Yu. I., "Some Results of Investigation of Traveling Gravitational Waves According to Data From Radiometeor Observations," Izv. AN SSSR: FAO, Vol 17, No 1, pp 95-98, 1981.

COPYRIGHT: Izdatel'stvo "Nauka", "Izvestiya AN SSSR, Fizika atmosfery i okeana", 1982

5303

CSO: 1865/114

FOR OFFICIAL USE ONLY

UDC 551.465.41

EFFECT OF THERMAL STRUCTURE OF UPPER OCEAN LAYER ON TURBULENCE DEVELOPMENT

Moscow IZVESTIYA AKADEMII NAUK SSSR: FIZIKA ATMOSFERY I OKEANA in Russian  
Vol 18, No 2, Feb 82 (manuscript received 17 Dec 80) pp 178-184

[Article by V. T. Paka and K. N. Fedorov, Institute of Oceanology, USSR Academy of Sciences]

[Text]

Abstract: A comparison of the results of measurements of turbulent fluctuations of velocity in the upper layer of the equatorial part of the Pacific Ocean with the diurnal variability of the vertical temperature profiles in this same layer indicated that with moderate winds (up to 5-6 m/sec) a stable thermal stratification arising as a result of daytime heating of the surface layer effectively suppresses turbulence in the upper quasihomogeneous layer of the ocean (UQL). The intensity of turbulence in this case thus experiences a well-expressed diurnal variation, despite the constantly available kinetic energy of velocity shear, which in this region of the ocean is especially great in the lower part of the UQL.

It has already been noted in the literature [1, 2] that in the evolution of the upper quasihomogeneous layer of the ocean (UQL) there are periods when the temporal attenuation of the wind (such as the Trades) or the daytime heating of the thin surface layer leads to the rapid and intensive destruction of the quasihomogeneous layer from below. Figure 1, taken from [1], shows two vertical temperature profiles, obtained in the morning (at 0900 LT) and after midday (at 1600 LT) at station 450, 7th voyage of the scientific research vessel "Dmitriy Mendeleev" on 13 February 1972 near the equator in the Indian Ocean. Under the influence of the wind (3-5 m/sec) and nighttime convection an UQL of moderate thickness by 0900 hours acquired an ideal homogeneity with a very clearly expressed temperature jump layer at the horizon 40 m. Daytime heating led to the formation of a warm layer in the upper part of the UQL

51  
FOR OFFICIAL USE ONLY

FOR OFFICIAL USE ONLY

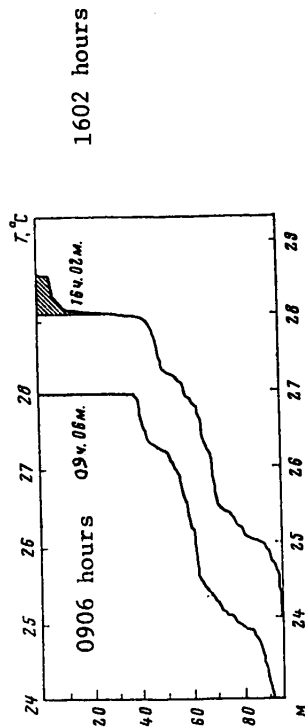


Fig. 1. Vertical temperature profiles in upper layer of ocean at station 450 near equator in Indian Ocean on 13 February 1972 at 0900 and 1600 hours local solar time.

Time of Day and Mean Wind Velocity at Stations on Section Across Equator					
No of station	Time of day	Wind, m/sec	No of station	Time of day	Wind, m/sec
2001	0100-0200	4.5	2007	1300-1400	7.0
2002	0700-1000	3.9	2008	1800-2100	4.9
2003	1400-1600	4.0	2009	0000-0100	6.4
2004	2000-2300	4.1	2010	0600-1000	7.6
2005	0200-0300	4.7	2011	1400-1600	6.9
2006	0600-0900	6.5			

FOR OFFICIAL USE ONLY

## FOR OFFICIAL USE ONLY

whose thickness by 1600 hours had attained 10 m. At this time the lower boundary of the UQL began to be considerably blurred. Usually the process ceases and the lower boundary of the quasihomogeneous layer is again accentuated immediately after the next intensification of the wind or destruction of the heated layer, even if the UQL has a greater thickness, as was the case, for example, in the polygon in the tropical Atlantic [2].

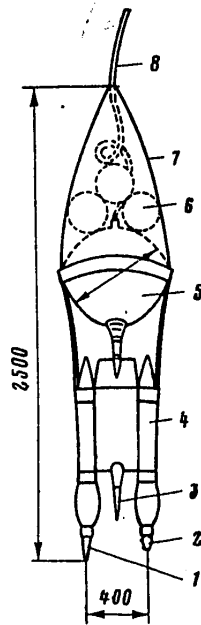


Fig. 2. Diagram of design of "Baklan" sonde. 1) sensor of velocity fluctuations  $u'$ ; 2) conductivity sensor; 3) temperature sensor; 4) cylindrical sealed containers; 5) spherical sealed container; 6) balls; 7) fabric fairing; 8) cable

sources of turbulent energy in the UQL, it is also possible to expect additional turbulence due to strong velocity shear at the upper boundary of the equatorial subsurface countercurrent [5-7]. On the other hand, in this case there is intensive solar heating creating a clearly expressed thermal stratification near the ocean surface during the daytime.

Measurement methods and instrumentation. The measurements were made with the "Baklan" microstructural sonde developed at the Atlantic Division, Institute of Oceanology imeni P. P. Shirshov, USSR Academy of Sciences. The "Baklan" sonde has a cable connection with the ship, but due to the fact that the cable in the process of submergence of the probe is cast overboard with a velocity exceeding the rate of submergence the "Baklan" sonde can be classified as a

Analogies with known laboratory experiments [3] suggest that the reason for the blurring of the lower sharp boundary of the UQL in all probability is the attenuation of turbulence in the UQL, which can be associated with the thermal stratification of the UQL from above. Whereas turbulence in the upper quasihomogeneous layer has a predominantly wind-wave origin, the development of a hydrostatically stable stratification in its upper part can effectively suppress turbulent velocity fluctuations near the surface and thus create a "blocking" effect ending the energy influx from the wind to turbulence remaining in the UQL. In this case turbulence rapidly attenuates without energy receipts.

The in situ checking of this hypothesis has now become possible due to the successful development of methods for direct measurements of microturbulent fluctuations in the ocean by means of freely falling sondes. Such checking was undertaken on the 24th voyage of the scientific research ship "Dmitriy Mendeleev" on runs along 163 and 167°W through the equatorial part of the Pacific Ocean [4]. In the equatorial zone, in addition to ordinary wind-wave

## FOR OFFICIAL USE ONLY

freely falling probe. Such a method was used successfully earlier by Gallagher [8]. The presence of a solid cable simplifies the requirements on the submergible sonde and makes it possible to work in series, not in individual soundings. This feature advantageously distinguishes the "Baklan" probe and the Gallagher sonde from the completely autonomous (self-contained) Gregg [5] and Crawford-Osborn [6] sondes.

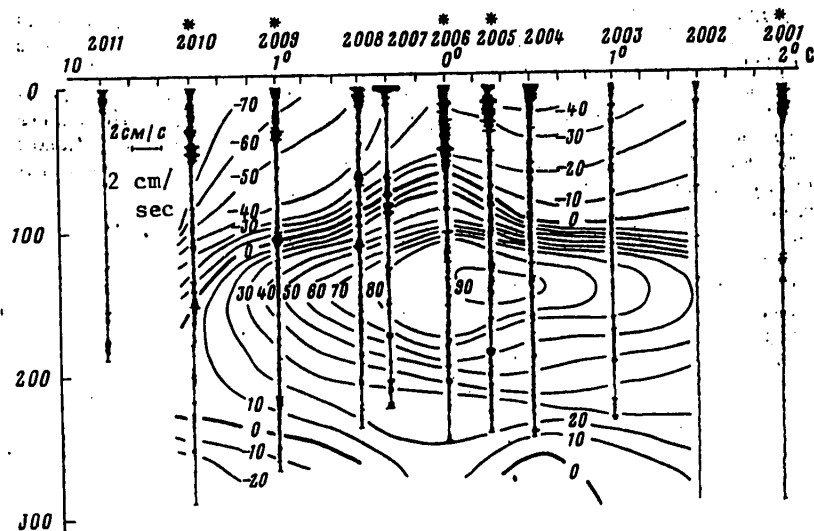


Fig. 3. Vertical profiles of turbulent velocity fluctuations  $u'$  against background of distribution of zonal component of current velocity on section across equator in Pacific Ocean along  $163^{\circ}15'W$ . The "-" symbol denotes velocities (in cm/sec) of a current directed to the west. The scale of turbulent velocity fluctuations is indicated in the upper left corner of the section. The asterisk "\*" designates the numbers of the stations occupied during the nighttime and morning hours.

The sensors of the "Baklan" sonde include:

- 1) the sensor of the longitudinal component is of the conduction and magneto-hydrodynamic type (the sensing element is a pair of point platinum electrodes in the field of a strong permanent magnet), not sensitive to the influence of medium stratification, linear in the range of amplitudes  $0.07-20 \text{ cm}\cdot\text{sec}^{-1}$  and frequencies of fluctuations 4-64 Hz with an averaging scale 2 cm;
- 2) temperature sensor constructed by the Atlantic Division, Institute of Oceanology, on the basis of a thermoresistor of the MMT-6 type, time constant 0.3 sec, measurement range  $0-30^{\circ}\text{C}$ , output slightly nonlinear, stability of characteristic in range  $0.2^{\circ}\text{C}$ ;
- 3) depth sensor -- standard vibrofrequency instrument for measuring pressure, type DDV, measurement range  $0-50 \text{ kg}\cdot\text{cm}^{-2}$ , error about 1.5 m, frequency output slightly nonlinear.

## FOR OFFICIAL USE ONLY

In addition, on the sonde there is a sensor for investigating the fine structure and microstructure of conductivity, but its readings were not used in this study.

With respect to design the sonde consists of three principal components: a two-section coupled container ("catamaran"), the frontal part of which carries the sensors; a spherical container ( $\phi 450$  mm) with power source batteries and the fairing of the spherical container, constituting a framework of convex thin rods over which a dense fabric is stretched. The empty spherical container has a buoyancy of about 50 kg, but it was inadequate for slowing the movement of the sonde. For this reason polyethylene balls were placed under the fairing. Each of the 3 or 4 balls had a buoyancy of about 3 kg. By means of these balls the rate of free sinking of the sonde was reduced to 1 m/sec  $\pm 10\%$ . The limiting pressure which the balls withstand corresponds to the 400-m horizon, which limits the depth of sounding. The cable has a length of 500 m, but due to drift and a deep current the depth of submergence usually is within the range 250-300 m. The external configuration of the sonde is shown in Fig. 2, where its principal dimensions are shown. The weight of the sonde in the air is about 70 kg. The tensile strength of the cable is 300 kg (a cable of the type KGZ-3-70 is used). The cable is usually attached at the upper point, which was dictated by convenience in drawing the sonde to the surface. However, under conditions of strong drift it is desirable to move the point of attachment of the cable closer to the sensors for the purpose of maintaining a zero angle of inclination of the sonde during submergence. The rolling of the ship does not cause disturbances in movement of the sonde and therefore it can be regarded as an all-weather instrument, which broadens the possibility of its use. The requirements on deck equipment for work with the "Baklan" sonde are simple: it is entirely possible to use a rotating loading boom, but it is considerably more convenient and productive to employ a cable winch.

Investigations of turbulence in the upper layer were accompanied by measurements of currents at buoy and drift stations and also standard hydrology. Meteorological observations were made regularly at intervals of one hour. Thus, the investigations had a multisided and systematic character, which considerably facilitated the interpretation of observations for the purpose of clarifying the cause-and-effect relationships between the intensity and distribution of turbulence and the thermal stratification of the upper layer.

Measurement results. In accordance with the tasks of the 24th voyage of the scientific research ship "Dmitriy Mendeleev," most of the data were obtained in the equatorial polygon. The measurements were made on two sections across the equator: a section along  $163^{\circ}15'W$  -- run 4 times, and a section along  $167^{\circ}W$  -- run once. On each section the stations were situated at 11 points from  $2^{\circ}N$  to  $2^{\circ}S$ . Five of these were situated near automatic anchored buoy stations which were used as reference points for determining drift during current measurements from shipboard.

An attempt to represent microturbulence measurements in the form of sections was without results: no apparent pattern in the meridional distribution of turbulence intensity was detected despite a priori ideas based on the conclusions of Crawford and Osborn [6]. Figure 3 shows one of the sections of the zonal current velocity component constructed by V. A. Bubnov and V. D. Yegorikhin with profiles of the intensity of turbulent velocity fluctuations obtained with the "Baklan" sonde.

## FOR OFFICIAL USE ONLY

The section clearly shows the nucleus of the subsurface Cromwell countercurrent with velocities attaining almost 2 knots. The nucleus is situated at the horizon 150 m and is somewhat displaced northward relative to the equator. It can also be seen that the intensity of turbulence as a whole in this region is rather high. Other sections constructed on the basis of the measurements made in this region have a similar form. At four stations on the cited section the thickness of the constantly turbulent layer falls in the range from 30 to 60 m. In addition to these "intensively turbulent" profiles and alternately with them there are profiles with shallow penetration of turbulence, and also with very weak turbulence (stations 2002 and 2003), although at all stations the weather conditions were virtually identical (see table).

The isotachs shown in the section (Fig. 3) clearly show the maximum shear region. Its positioning, however, is difficult to relate to the features of distribution of turbulence in the section. For example, at stations 2009 and 2003 the shear values are approximately identical but the vertical profiles of turbulence intensity are completely different.

The patterns in this picture begin to appear if we compare the profiles of turbulence intensity with the vertical temperature profiles (Fig. 4), taking into account the time of day for each station (see table). It appears that the minimum development of turbulence (stations 2002-2004, 2007, 2011) correspond to temperature profiles with a clearly expressed heated surface layer with a thickness of 10-20 m. On the other hand, the maximum development of turbulence corresponds to poorly stratified temperature profiles (2001, 2005, 2006, 2009, 2010). In turn, profiles with a heated surface layer are usually observed during the daytime hours when there is radiation heating. During the nighttime and early morning hours the vertical temperature profiles in the upper layer are most homogeneous since by this time nighttime convection can destroy traces of heating of the preceding day. The day-long station 2012 was occupied in order to confirm this pattern in the development of turbulence and its correlation with the diurnal thermal cycle. In general it revealed the same correlation. However, the wind at this station attained 8 m/sec, which stirred the forming surface heated layer.

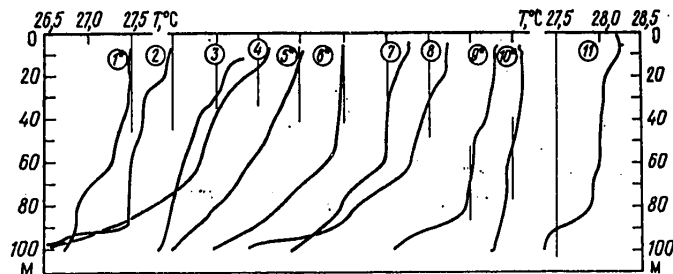


Fig. 4. Vertical temperature profiles in upper layer of ocean at stations of section represented in Fig. 3. The numbering of the profiles from 1 to 11 corresponds to the numbers of stations 2001 through 2011. The temperature scales are given for the first and last profiles. All the profiles have been successively displaced to

## FOR OFFICIAL USE ONLY

the right relative to one another by 0.5°C. The 27.5°C values are marked for each profile by a thin vertical line.

The existence of a diurnal cycle in the variability of the vertical thermal structure of the upper layer in the ocean has been repeatedly noted in the literature (for example, see [9]). It was again investigated in detail using the "Bumerang" thermobathysonde on the 27th voyage of the scientific research ship "Akademik Kurchatov" (the materials are being processed), and was also studied on this same voyage by other means in connection with the so-called "calm weather thermal inhomogeneities" [10].

Discussion of results. The development of turbulence in any layer of the ocean should be related primarily to the energy sources which maintain it, but secondly to the degree of hydrostatic stability of stratification in this layer, exerting an extinguishing effect on turbulence. Two energy sources: 1) wind-wave movement and 2) a high vertical velocity gradient at the upper boundary of the Cromwell Current are invariably present in the upper layer of the considered region of the ocean, virtually not experiencing any diurnal variation. The kinetic energy introduced by convection into the upper quasihomogeneous layer is proportional to the potential energy set free as a result of cooling through the free surface in the layer from 0 to the depth of thermal compensation [11, 12]. The quantity of this energy usually begins to increase in the evening hours and attains a maximum prior to sunrise, decreasing to a minimum close to zero in the afternoon hours. The energy of this convection becomes minimum when the sole factor counteracting turbulence -- the Archimedes forces of thermal stratification -- attains a maximum at about 1600 hours local solar time. At that time, according to observations made by the authors on the 27th voyage of the scientific research ship "Akademik Kurchatov" in the Sargasso Sea, the Brunt-Väisälä frequency in the upper temperature-stratified meter layer of the ocean can attain  $(2-3) \cdot 10^{-2} \text{sec}^{-1}$ . Thus, the nighttime and early morning hours are the most favorable for the development of turbulence and the least favorable are the daytime and evening hours. The stations occupied during the nighttime and early morning hours have been marked on the section (Fig. 3) by asterisks. Precisely they are characterized by the profiles with the best developed turbulence.

Turbulence of wind-wave origin, when it is observed, during the nighttime intensifies convective turbulence fed by the kinetic energy of velocity shear, penetrating, as indicated by the profile for station 2006, by the early morning hours to depths of 60-80 m. Thereafter the energy influx from above ceases as a result of attenuation of surface turbulence in the developing daytime thermocline at depths of about 10-20 m. Turbulence in the thickness of the upper quasihomogeneous layer (UQL) also attenuates, although far more slowly. In the interval from 30 to 80 m thick quasihomogeneous layers persist up to midday (stations 2002, 2007) in which, however, turbulence is virtually not sensed, at least by the "Baklan" sonde. However, the vertical shear is evidently inadequate for maintaining active microturbulence at the same level to which it is usually developed in the surface quasihomogeneous layers when there is a wind of about 5 m/sec (stations 2001, 2004, 2007, 2011). It is not impossible that the above-mentioned quasihomogeneous layers within the limits 30-80 m in the daytime are in a dynamic state, being boundary layers between turbulent and laminar movement and somehow similar to the unstable state of

## FOR OFFICIAL USE ONLY

the supercooled fluid. With a thickness of about 30-50 m and a current velocity of 20-40 cm/sec these layers should be characterized by Reynolds numbers in the range  $10^6$ - $10^7$ . The introduction of a very small disturbance into these layers (for example, with a local increase in shear or with penetration of convective instability from above) should lead to them becoming turbulent rapidly. Evidently this also explains the restoration of a sharp lower boundary of the UQL after disappearance of the surface heated layer or during an intensification of the wind noted in [1, 2]. Judging from the profiles for stations 2004-2006 (Fig. 3), which are situated close to one another, only 5-6 hours are required in order for the lower boundary of the turbulent layer to drop from 15 to 60-70 m. It is not impossible that this occurs even considerably more rapidly.

The detection of a diurnal variation of turbulence in the UQL in the equatorial zone, that is, where its latitude dependence on the change in the characteristics of velocity shear at the upper boundary of the Cromwell Current was expected, is unquestionably a new result meriting attention. Scarcely anywhere else in the world ocean is it possible to encounter such high values of vertical velocity shear in the lower part of the UQL. It therefore follows that under conditions of a moderate wind and in the absence of heavy precipitation the turbulence of the UQL should experience a well-expressed diurnal variation virtually everywhere except for the region of the high latitudes. The "blocking" role of thermal stratification in the surface layer of the ocean in this case is fully revealed and it can be extrapolated easily to any anomalous conditions when intensive heating is accumulated during a synoptic period (for example, in the case of freshening of the surface layer by precipitation [13]) and in the surface layer creates a stable thermocline which is not overcome by nighttime convection over the course of several days (usually to the next storm).

On the other hand, the direct "blocking" role of precipitation falling on the ocean surface may be as equally important as the role of thermal stratification [13]. The freshened layer, forming at the ocean surface after the falling of rain, according to our observations has at its lower boundary a stable density jump characterized by a Brunt-Väisälä frequency  $N$  of the order of  $2 \cdot 10^{-2} \text{ sec}^{-1}$  or more. Such a sharp stratification should extinguish the turbulence in the thickness of the UQL when there are moderate winds (up to 5-6 m/sec) as effectively as daytime heating. Precipitation, however, in contrast to insolation, does not have a clearly expressed diurnal variation in most climatic zones.

## BIBLIOGRAPHY

1. Monin, A. S. and Fedorov, K. N., "Fine Structure of the Upper Layer of the Ocean," *IZV. AN SSSR: FAO (News of the USSR Academy of Sciences: Physics of the Atmosphere and Ocean)*, Vol 9, No 4, pp 442-444, 1973.
2. Fedorov, K. N., Plakhin, Ye. A., Prokhorov, V. I. and Sedov, V. G., "Features of Thermohaline Stratification in a Polygon Region in the Tropical Atlantic," *ATLANTICHESKIY GIDROFIZICHESKIY POLIGON-70 (Atlantic Hydrophysical Polygon-70)*, Moscow, Nauka, pp 236-282, 1974.
3. Rouse, N. and Dodu, J., "Diffusion Turbulent a Travers Une Discontinuité de Densité," *LA HOUILLE BLANCHE*, No 4, pp 522-532, 1955.

FOR OFFICIAL USE ONLY

4. Paka, V. T., Bubnov, V. A. and Pozdynin, V. D., "24th Voyage of the Scientific Research Ship 'Dmitriy Mendeleyev'," OKEANOLOGIYA (Oceanology), Vol 20, No 5, pp 954-957, 1980.
5. Gregg, M. C., "Temperature and Salinity Microstructure in the Pacific Equatorial Undercurrent," J. GEOPHYS. RES., Vol 81, No 6, pp 1180-1196, 1976.
6. Crawford, W. R. and Osborn, T. R., "Microstructure Measurements in the Atlantic Equatorial Undercurrent During GATE," DEEP-SEA RES., Suppl. II to Vol 26, GATE, Vol 2, pp 309-324, 1980.
7. Paka, V. T., Vasilenko, V. M., Osadchiy, A. S. and Shkurenko, V. I., "Turbulence, Internal Waves and Thermohaline Microstructure in a Polygon in the Equatorial Atlantic According to the Results of the First Voyage of the Scientific Research Ship 'Professor Shtokman'," IZMENCHIVOST' TROPICHESKOY ATLANTIKI V PERIOD PGEP (Variability of the Tropical Atlantic During the FGGE Period), 1981 (in press).
8. Gallagher, B., "Vertical Profiles of Temperature and Fine-Scale Velocity Structure in the Thermocline," J. GEOPHYS. RES., Vol 81, No 6, pp 1201-1206, 1976.
9. Fedorov, K. N., "On the Summer Daily Heating and Diurnal Heat Budget of the Upper Ocean Layer," STUDI IN ONORE DI GIUSEPPINA ALIVERTI, Napoli, pp 27-40, 1972.
10. Fedorov, K. N., Ginzburg, A. I. and Piterbarg, L. I., "Physical Nature of the 'Calm Weather Inhomogeneity' in the Temperature Field of the Ocean," OKEANOLOGIYA, Vol 21, No 2, pp 203-210, 1981.
11. Solov'yev, A. V., "Fine Thermal Structure of the Ocean Surface Layer in the POLYMODE-77 Region," IZV. AN SSSR: FAO, Vol 15, No 7, pp 750-757, 1979.
12. Woods, J. D., "Diurnal and Seasonal Variation of Convection in the Wind-Mixed Layer of the Ocean," Q. J. ROY. METEOR. SOC., Vol 106, No 449, pp 379-394, 1980.
13. Ginzburg, A. I., Zatsepin, A. G., Sklyarov, V. Ye. and Fedorov, K. N., "Effects of Precipitation in the Ocean Surface Layer," OKEANOLOGIYA, Vol 20, No 5, pp 828-836, 1980.

COPYRIGHT: Izdatel'stvo "Nauka", "Izvestiya AN SSSR, Fizika atmosfery i okeana", 1982

5303

CSO: 1865/114

FOR OFFICIAL USE ONLY

SPECTRAL DEPENDENCES OF LIGHT SCATTERING BY SEA WATER

Moscow IZVESTIYA AKADEMII NAUK SSSR: FIZIKA ATMOSFERY I OKEANA in Russian  
Vol 18, No 2, Feb 82 (manuscript received 19 Feb 81) pp 185-190

[Article by V. I. Burenkov, B. F. Kel'balikhanov and L. A. Stefantsev, Institute of Oceanology, USSR Academy of Sciences]

[Text]                      Abstract: The article gives the results of measurements and computations of the spectra for the scattering coefficient at different angles. The measured spectral dependences can have a maximum for small scattering angles. The elongation of the scattering coefficient increases with an increase in the wavelength. The computations indicate that a model of two fractions of suspension makes possible a satisfactory description of the principal patterns of the measured scattering spectra.

In investigations of the scattering properties of sea water it is customary to measure the angular dependence of the scattering coefficient in some direction  $\sigma(\gamma)$  at a definite wavelength  $\lambda$ . Far less attention is being devoted to measurements of the spectral dependences  $\sigma(\gamma, \lambda)$  and until now few actual data have been obtained on the scattering spectra in sea water. The same applies to theoretical computations. Available light scattering tables, including tables of light scattering by models of sea water [1], contain data only on the scattering functions.

This article gives the results of measurements of the spectral dependences  $\sigma(\gamma, \lambda)$  for different scattering angles and also data on the corresponding theoretical computations. The  $\sigma(\gamma, \lambda)$  spectra were measured using a submersible nephelometer in which a diffraction grating was used as the dispersing element. Scanning in wavelength was accomplished continuously, which made it possible to carry out quite precise spectral measurements in the wavelength range 400-700 nm. The spectral resolution of the instrument is 2.5 nm. Measurements of  $\sigma(\gamma, \lambda)$  were made in the range of angles 3-165° with an angular resolution of 1°.

1. The principal experimental data on the spectral dependences  $\sigma(\gamma, \lambda)$  were obtained in the equatorial Atlantic; a number of measurements were made in other regions of the world ocean.

60  
FOR OFFICIAL USE ONLY

## FOR OFFICIAL USE ONLY

Figure 1 shows the most characteristic  $\sigma(\gamma, \lambda)$  curves for different scattering angles measured in the surface waters of the central part of the Atlantic Ocean (all the curves were matched at  $\lambda = 420$  nm). A common property of the reduced curves, the same as all the other experimental dependences, is an increase in the steepness of the dropoff of  $\sigma(\gamma, \lambda)$  with a transition from small to large scattering angles. This is attributable to the fact that in sea water scattering at large angles is determined to a considerable degree by small particles [2] scattering light more selectively than large particles and also by molecular scattering. For all measurements at large angles the scattering index  $\sigma(\gamma, \lambda)$  decreases monotonically with an increase in  $\lambda$ ; for a particular angle the scatter of spectral curves is relatively small. Far greater variations are characteristic for the spectral dependences for small-angle scattering. Here there are two types of spectral curves. Curves of the first type drop off monotonically with transition into the red part of the spectrum (Fig. 1,a); curves of the second type have a maximum at wavelengths 460-480 nm (Fig. 1,b). The presence of a nonmonotonic behavior of the spectral dependences of small-angle scattering is the most interesting and unexpected result of the measurements made because it is usually assumed that for polydisperse systems the peculiarities of the angular and spectral scattering distributions are smoothed.

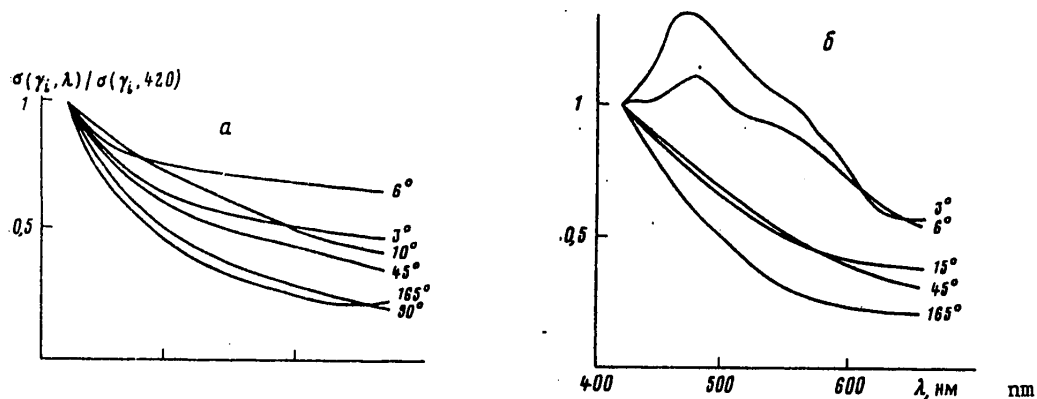


Fig. 1. Spectral dependences of index of scattering at different angles measured at station 2832 (a), (0, 0°) and station 2838 (b), (0°, 23°30'W). Scientific research ship "Akademik Kurchatov."

The collected experimental data can be used in an investigation of change in the shape of the scattering function in the spectrum. In general, as follows from Fig. 1, the elongation of the scattering function increases with transition into the red region. This is also illustrated by Fig. 2, which shows the spectral dependences of the parameters characterizing elongation of the scattering function. As such parameters we used the ratio  $\sigma(\gamma_1)/\sigma(\gamma_2)$ , where the  $\gamma_1$  angle corresponds to small scattering angles and  $\gamma_2$  corresponds to large scattering angles. The  $\sigma(\gamma_1)/\sigma(\gamma_2)$  value with  $\lambda = 420$  nm was arbitrarily assigned the value unity. The figure shows that the function elongation increases most significantly in the blue-green part of spectrum; after  $\lambda \approx 600$  nm it changes insignificantly. It is usually assumed that

## FOR OFFICIAL USE ONLY

the change in the shape of the scattering function is associated with an increase in the contribution of molecular scattering with a decrease in wavelength [3]. These measurements indicate that solely on the basis of this effect it is impossible to explain the behavior of the spectral dependences  $\sigma(\gamma, \lambda)$ . In actuality, it follows from Fig. 1 that the shape of the scattering function can change considerably also in the range of angles ( $\gamma \leq 30-45^\circ$ ), where the contribution of molecular scattering is known to be small. Below it will be demonstrated that the features of the  $\sigma(\gamma, \lambda)$  experimental curves can be related to scattering on suspended particles.

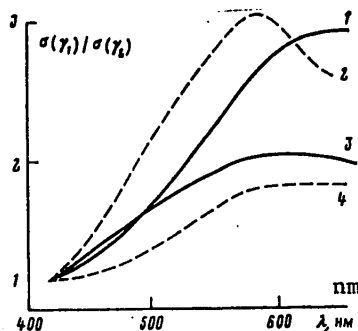


Fig. 2. Dependence of ratio  $\sigma(\gamma_1)/\sigma(\gamma_2)$  on  $\lambda$ :  $\gamma_2 = 165^\circ$ ,  $\gamma_1 = 6^\circ$  (1, 2),  $16^\circ$  (3),  $10^\circ$  (4) for station 2838 (1, 3) and station 2832 (2, 4).

2. Computations of the spectral dependences of light scattering in sea water were made on the basis of a model according to which the suspended matter consists of two fractions: large measuring  $r \geq 1 \mu\text{m}$  and refractive index  $m \sim 1.02$  and fine measuring  $r \leq 1 \mu\text{m}$  and a refractive index  $m \sim 1.15$  [2]. The large particles determine scattering at small angles, whereas fine particles determine scattering at large angles. The size distribution of both fractions is close to the Junge distribution  $f(r) = Ar^{-\nu}$ . This model has been used repeatedly for an analysis of data on the angular dependences of the scattering index  $\sigma(\gamma)$ , but it was not compared with data on the  $\sigma(\gamma, \lambda)$  spectra.

Computations of the spectral dependences  $\sigma(\gamma, \lambda)$  were made using both the Mie formulas and using the approximate formulas. Before proceeding to an analysis of the results of the computations, we will examine the limiting dependences  $\sigma(\gamma, \lambda)$  on wavelength within the framework of different approximations. For large spherical particles scattering at small angles is described by the formula [4]:

$$[d\phi/d\phi = \text{dif}(\text{fraction})] \quad I(\gamma, r, \lambda) = I_0 4 |K(i\delta)|^2 \frac{r^3}{\lambda^2} J_1^2(\rho\gamma) = I_{\text{dif}} 4 |K(i\delta)|^2, \quad (1)$$

where

$$\rho = 2\pi r / \lambda, \quad K(w) = \frac{1}{2} + e^{-w} / w + (e^{-w} - 1) / w^2; \quad w = i\delta; \quad \delta = 2\rho |m - 1|.$$

$J_1(x)$  is a first-order Bessel function of the first kind. The factor  $I_{\text{dif}}$  in (1) describes diffraction in a circular aperture. It is simple to obtain limiting spectral dependences for it. With  $\rho\gamma \ll 1$   $J_1(\rho\gamma) \approx \rho\gamma$  and  $I_{\text{dif}} \sim \lambda^{-2}$ . In the case  $\rho\gamma \gg 1$   $J_1(x) \sim x^{-1/2} \cos x$  and  $I_{\text{dif}} \sim \lambda$  (the rapidly oscillating factor  $\cos^2(\rho\gamma)$  can be assumed equal to 1/2). Scattering by large particles at great angles is described by the formulas of geometrical optics and the dependence of the intensity of scattering on wavelength

## FOR OFFICIAL USE ONLY

in this case is absent (it is assumed that the dispersion of particulate matter is small). The factor  $4|K(i\delta)|^2$  with  $\delta = 2\rho|m-1| \gg 1$  is not dependent on  $\lambda$ , but with  $\delta \ll 1$  is proportional to  $\lambda^{-2}$ .

For the fine fraction of suspended matter the Rayleigh-Gans approximation is correct [5]:

$$I(\gamma, r, \lambda) = \frac{2}{9} \rho^2 r^2 (m-1)^2 R^2(\gamma, \rho) (1 + \cos^2 \gamma), \quad (2)$$

where

$$R(u) = \frac{3}{u^3} (\sin u - u \cos u); \quad u = 2\rho \sin \frac{\gamma}{2}.$$

With  $\rho\gamma \ll 1$  we have  $R(u) \approx 1$  and  $I(\gamma, r, \lambda) \sim \lambda^{-4}$ . In the case  $\rho\gamma \gg 1$   $R^2(u) \sim \cos^2 u/u^4$  and  $I(\gamma, r, \lambda)$  is not dependent on  $\lambda$  ( $\cos^2 \approx 1/2$ ).

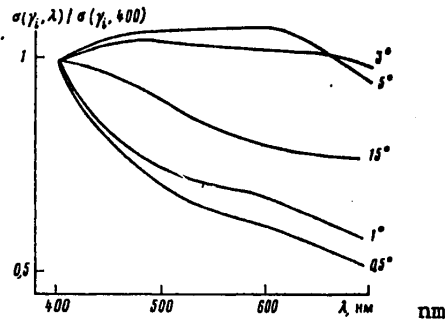


Fig. 3. Computed spectral dependences of scattering by large suspended particles for one of variants of parameters.

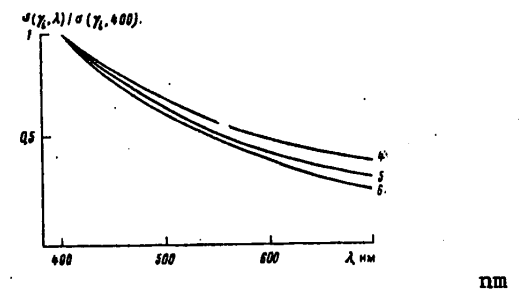


Fig. 4. Computed spectral dependences of scattering by fine suspended particles for angles 15-180° (the figures on the curves are the values of the  $\nu$  parameter).

The approximate limiting spectral dependences  $I(\gamma, r, \lambda)$  are correct for a definite combination of particle sizes and scattering angles and are realized for the considered model of sea suspended matter only in rare cases. In particular, they do not make it possible to explain the presence of a maximum on the spectral curves at small scattering angles. For monodisperse suspended matter this peculiarity can be explained qualitatively on the basis of the form of the functions entering into (1). First we will examine only the function  $J_1^2(\rho\gamma)$ , having, as is well known, an oscillating character. For particles with a radius of several microns and not very small scattering angles (if the  $\gamma$  angle is so small that  $\rho\gamma \ll 1$ , there will be a limiting dependence  $I(\gamma, r, \lambda) \sim \lambda^{-2}$ ) a change in wavelength here by a factor of 1.5-2 (which corresponds to a change in  $\lambda$  in the visible spectral range) leads to a change in the argument  $\rho\gamma$  by several units. For example, with  $r = 5 \mu\text{m}$   $\gamma = 3^\circ$ ,  $\lambda = 400-700 \text{ nm}$   $x = \rho\gamma$  changes in the range 4-2.5. Since the period of the function  $J_1^2(x)$  with not very large  $x$  is equal to approximately 5 (the term period is used here arbitrarily because the amplitude of the oscillations of this function

## FOR OFFICIAL USE ONLY

decreases with an increase in  $x$ ), with such a change in the argument  $J_1^2(x)$  and accordingly  $I(\gamma, \lambda)$  can increase, decrease, have a minimum or maximum. Superposed on these changes is a spectral dependence of the factor  $4 |K(i\delta)|^2$ , also having an oscillating character. Thus, depending on the combination of particle sizes the refractive index and the scattering index there can be diverse spectral dependences  $I(\gamma, r, \lambda)$ . It is more difficult to explain the behavior of scattering spectra for polydisperse systems; here it is necessary to use numerical computations. However, it can be postulated that if the particle sizes vary in a not very broad range, the oscillations of the functions entering into (1) will be smoothed incompletely and the behavior of the spectral curves can resemble the spectral dependences for monodisperse suspended matter. The experimentally observed fine structure of the scattering function [6] is also possibly related to an incomplete smoothing of the functions entering into (1), (2). We note that the appearance of different peculiarities in the behavior of the  $I(\gamma, r, \lambda)$  spectra is more probable precisely at small scattering angles because at large angles the oscillations of the  $R^2(\gamma, \rho)$  function entering into (2) are superposed on the monotonic dependence  $\lambda^{-4}$ .

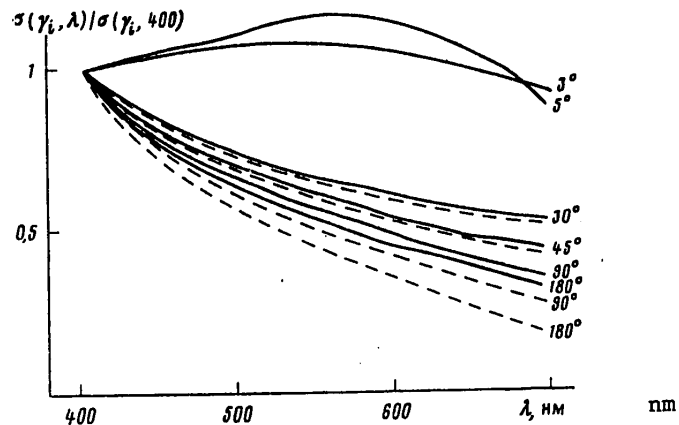


Fig. 5. Computed spectral dependences of scattering by large and small suspended particles without (solid curve) and with allowance (dashed curve) for molecular scattering by water. Explanations in text.

Numerical computations of the spectral dependences  $I(\gamma, \lambda)$  were carried out separately for the large and small fractions of suspended matter. For the large fraction of suspended material we used the following values of the Junge distribution parameters:  $f(r) = Ar^{-\nu}$ ,  $r_1 \leq r \leq r_2$ ,  $r_1 = 1 \mu m$ ,  $r_2 = 5, 7, 10 \mu m$ ,  $\nu = 2, 3, 4$ ; the refractive index  $m = 1.02, 1.03, 1.05$ . The wavelength varied from  $0.4$  to  $0.7 \mu m$ . The computations were made using the Mie formulas. Figure 3 shows the spectral dependences of scattering at different angles for one of the variants of the used parameters (all the curves are matched at  $\lambda = 0.4 \mu m$ ). A common property of all the computed dependences is a dropoff of  $I(\gamma, \lambda)$  with an increase in  $\lambda$  for the smallest scattering angles  $0.5$  and  $1^\circ$ , which is attributable to the limiting dependence

## FOR OFFICIAL USE ONLY

of the factor  $I_{\text{dif}}(\gamma, \lambda) \sim \lambda^{-2}$  in (1). The influence of the factor  $4|K(i\delta)|^2$  is that the computed curves, depending on the used parameters, drop off with an increase in  $\lambda$  either more strongly or more weakly than  $\lambda^{-2}$ . We note that we made no measurements for such small angles. The shape of the spectral curves for greater scattering angles ( $3-5^\circ$ ) is essentially dependent on the computed parameters. For the determined variants there are spectral dependences close to those obtained in the experiment. In particular, the computed curves (Fig. 3), like the experimental curves (Fig. 1,b), have a maximum (its wavelength position is not constant and is dependent on the computed parameters). In other variants the spectral curves can drop off with an increase in wavelength (like the experimental curves in Fig. 1,a) or have a more complex shape. It is characteristic that the features of the computed spectral curves are situated in the same range of angles ( $3-6^\circ$ ) as for the experimental curves. As indicated above, the most probable reason for this is an incomplete smoothing of oscillations of the functions entering into (1) with values  $\rho\gamma \sim 1$ . The considerable dependence of the shape of the spectral curves on the initial parameters in the indicated range of angles can be useful in solving the inverse problem -- determination of the spectrum of sizes of suspended particles from their scattering properties.

With a further increase in the angle scattering by the large suspended particles becomes increasingly less selective and for  $\gamma \geq 45^\circ$  is virtually not dependent on wavelength.

For the fine fraction of suspended matter we used a Junge distribution with the following values of the parameters:  $r_1 = 0.01 \mu\text{m}$ ,  $r_2 = 1 \mu\text{m}$ ,  $\nu = 4, 5, 6$ ,  $m = 1.15$ . The computations reveal that the spectral dependences of scattering by the fine suspended matter always decrease monotonically with an increase in wavelength. The steepness of the dropoff is appreciably greater than for the spectra for the scattering by large suspended particles. This result agrees with data from measurements of the spectra of scattering at large angles. With an increase in the  $\nu$  parameter the spectral dependences become more selective (Fig. 4). The results of the computations show that with fixed  $\nu$  the spectral curves for different angles ( $15-180^\circ$ ) do not differ from one another. The latter does not agree with the results of measurements since the experimental curves are characterized by an increase in slope with transition to large angles (from  $15$  to  $165^\circ$ ). The observed effect can be attributed, on the one hand, to the influence of molecular scattering by water, and on the other hand, to the contribution of large particles to scattering at large angles. The latter is attributable to the fact that the elongation of the scattering function for large suspended particles is greater than for small particles. Accordingly, with an increase in the angle the fraction of nonselective scattering of large particles decreases and the spectral curves become steeper. In our case such a situation is extremely probable because the region of measurements is situated far from the sources of terrigenous suspended matter and the production of phytoplankton here is rather great.

We made computations of the spectral dependences for the complete functions, which were computed as the sum of the functions of the large and small suspended particles and molecular scattering by water. In the computations we varied the relationship between scattering by the above-mentioned components. Figure 5 shows curves computed for a case when the large and small fractions of suspended matter

## FOR OFFICIAL USE ONLY

scatter light at an angle  $45^\circ$  in the proportion 1:2 (in this case molecular scattering is not taken into account). The dashed curve in Fig. 5 represents dependences computed taking molecular scattering into account (it is assumed that it constitutes 40% of the total scattering for  $\gamma = 90^\circ$ ). The figure shows that the selectivity of scattering increases with transition to large angles, which agrees with the experimental data. In this case this effect to an equal degree is related to both the above-mentioned factors. The influence of molecular scattering is evidently most substantial in the most transparent waters where its contribution can attain 30-50% for angles  $\gamma \geq 90^\circ$ .

Thus, the computations made indicate that the model of two fractions of suspension makes possible a satisfactory description of the principal patterns of the measured spectral dependences of light scattering in sea water. The greatest peculiarities are characteristic of the scattering spectra in the range of angles  $3-6^\circ$ , which agrees with the experimental data. The selectivity of scattering at large angles is expressed more clearly than at small angles. With definite assumptions the steepness of the spectral curves, as in the experiment, increases with a transition to greater angles.

We note in conclusion that we made the measurements in relatively transparent ocean waters. Further investigations will make it possible to clarify how general the mentioned patterns of sea water scattering spectra may be.

## BIBLIOGRAPHY

1. Shifrin, K. S. and Salganik, I. N., RASSEYANIYE SVETA MODEL'YAMI MORSKOY VODY. TABLITSY PO SVETORASSEYANIYU (Light Scattering by Sea Water Models. Light Scattering Tables), Vol 5, Leningrad, Gidrometeoizdat, 1973, 218 pages.
2. Shifrin, K. S., Kopelevich, O. V., Burenkov, V. I. and Mashtakov, Yu. L., "Light Scattering Functions and the Structure of Suspended Matter in Sea Waters," IZV. AN SSSR: FAO (News of the USSR Academy of Sciences: Physics of the Atmosphere and Ocean), Vol 10, No 1, p 25, 1974.
3. OKEANOLOGIYA. FIZIKA OKEANA (Oceanology. Oceanic Physics), T 1. GIDROFIZIKA (HYDROPHYSICS) (Chapter: "Ocean Optics"), Moscow, "Nauka," 1968, 340 pages.
4. Burenkov, V. I., Kopelevich, O. V. and Shifrin, K. S., "Light Scattering by Large Particles With a Refractive Index Close to Unity," IZV. AN SSSR: FAO (News of the USSR Academy of Sciences: Physics of the Ocean and Atmosphere), Vol 2, No 8, p 828, 1975.
5. Van de Hulst, H., RASSEYANIYE SVETA MALYMI CHASTITSAMI (Light Scattering by Small Particles), Moscow, Izd. Inostr. Lit., 1957, 536 pages.
6. Man'kovskiy, V. I., "Fine Structure of the Light Scattering Function in Sea and Ocean Waters," MORSKIYE GIDROFIZICHESKIYE ISSLEDOVANIYA (Marine Hydro-physical Investigations), No 2(58), p 126, 1972.

COPYRIGHT: Izdatel'stvo "Nauka", "Izvestiya AN SSSR, Fizika atmosfery i okeana", 1982

5303  
CSO: 1865/114

FOR OFFICIAL USE ONLY

UDC 551.466.1

RADAR OBSERVATIONS OF WIND WAVES AT SEA

Moscow IZVESTIYA AKADEMII NAUK SSSR: FIZIKA ATMOSFERY I OKEANA in Russian  
Vol 18, No 2, Feb 82 (manuscript received 25 Mar 80, after revision 13 Oct  
80) pp 211-215

[Article by K. V. Konyayev and A. D. Rozenberg, Acoustics Institute]

[Text] The intensity of pulsed radar signals reflected from the wave-covered sea surface at glancing angles of elevation for the most part is dependent on the local angles of slope of surface sectors situated along the radar ray. This makes it possible to employ a radar for noncontact measurement of the parameters of wind waves [1]. However, the study is usually limited only to a spatial or only a temporal analysis of the signals, whereas a more complete idea concerning waves can be obtained by a spatial-temporal analysis. The dependence of the intensity of the received signals on the surface slopes is nonlinear and is superposed on a number of other dependences -- on the intensity of ripples, which changes within the limits of a long wave, on the presence of foam and spray, etc. Nonlinearity leads to the appearance of difference frequencies in the signal corresponding to the envelope of wind waves and also carrying information on waves. The article discusses the spatial-temporal processing of radar signals obtained during moderate and strong waves with a determination of the parameters of the principal waves on the basis of the radar image of these waves and their envelope.

The observations were made in the summer of 1978 (methodological measurements in 1977) in the Caspian Sea from a pile base with a local depth of 40 m. A shipboard "Don" radar station was installed on a mast at a height of 35 m above sea level. The length of the radio wave was 3 cm, the pulse power of the transmitter was 75 KW, the width of the antenna directional diagram in the azimuthal plane was 1°, pulse duration was 0.1  $\mu$  sec (range resolution 15 m), pulse repetition rate was 1.6 KHz. The signal from the output of the amplitude detector is fed through a range gating stage, controlled by the generator of a scanning strobe pulse, to a peak detector which discriminates the pulse envelope. After the detector the signal is registered on a brightness indicator-automatic recorder (electrothermal paper tape) with range scanning, controlled by the

67  
FOR OFFICIAL USE ONLY

## FOR OFFICIAL USE ONLY

strobe pulse generator, with a uniform movement of the tape in time or on a magnetic recorder after measurement on a digital voltmeter. The strobe pulse moves in range from 300 to 1300 m with a velocity of about 2 km/sec and with a frequency of 1 cycle per second. The brightness indicator has a small dynamic range; the signal level at its output is set by manual regulation of the amplification factor with visual control of the brightness pattern. The voltmeter makes 50 readings from three significant digits per second; there is virtually no signal limitation.

The moving strobe shapes the signal as a function of the range corresponding to the profile of waves along the radar ray. A series of range scans forms a two-dimensional pattern of change in signal intensity in space (along the radar ray) and in time. In the course of the experiment the radar ray is set at different azimuthal angles to the direction of movement of the waves (an angle of  $0^\circ$  corresponds to the direction of the ray along the movement of the principal waves and  $180^\circ$  toward them). At the same time the waves are measured by a wire wave recorder lowered from the base.

Figure 1 shows the radio image of a sector of the sea surface obtained in the course of 18 minutes on 14 August 1977 [2]. The angle  $\theta$  between the direction of irradiation and the main direction of wave movement is  $225^\circ$ , wave height is class 4, wind velocity is 12 m/sec, wave height is 1-1.5 m. The intensity of the scattered signal as a function of range and time has a characteristic banded structure: in some sectors it is easy to discriminate lines corresponding to the spatial-temporal trajectories of sectors of energy-carrying waves with large local slopes. The distance between range lines determines the projection of the wave vector onto the direction of irradiation  $k_1 = k \cos \theta$ , where  $k$  is the modulus of the wave vector, the distance along the time axis is the period of these waves; the slope of the lines to the range axis determines the phase velocity of the principal waves along the ray  $v_1 = v / \cos \theta$ , where  $v$  is the phase velocity of the waves. In some places the lines form clear spots elongated at an angle to the range axis. The spots correspond to groups of waves; the dimensions of the spots determine the extent and duration of the groups, the slope of the spots to the range axis determines the group velocity of the waves along the radar ray.

Figure 2 is a schematic representation of a sector of the surface (Fig. 1, dashed line) [figure not reproduced here] with an extent of 275 m and a duration of 80 sec. The figure shows that the length and period of the waves are equal to 70 m and 6.5 sec respectively, the group consists of three waves in space and six waves in time. The group velocity is equal to half the phase velocity and accordingly the envelope of the observed waves is formed for the most part by waves differing with respect to the modulus of space frequency, not with respect to direction.

These parameters of waves are easily transmitted in a two-dimensional space-time spectrum which has the form of a compact region of high values situated on the dispersion curve. At low frequencies there is a small spectral peak corresponding to the wave envelope [2].

FOR OFFICIAL USE ONLY

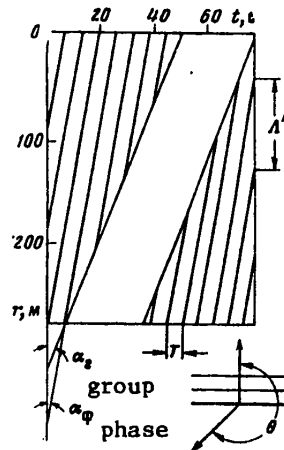


Fig. 2.

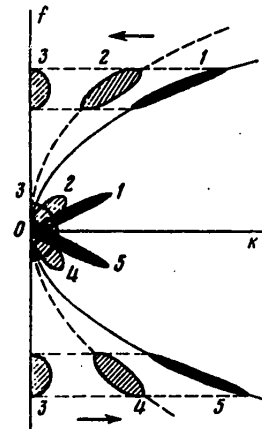


Fig. 4.

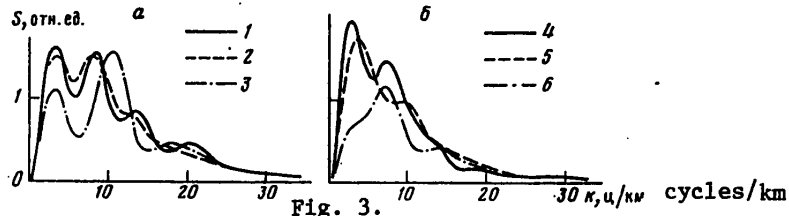
relative  
units

Fig. 3.

Fig. 2. Schematic representation of sector of surface defined by dashed line in Fig. 1.

Fig. 3. Spatial spectra of signal in cases of irradiation toward (a) and across (b) wave movement. The  $\theta$  angle is equal to: 1) 180, 2) 150, 3) 180, 4) 270, 5) 240, 6) 300°. The spectra 3, 4, 6 correspond to the two-dimensional spectra in Fig. 5.

Fig. 4. Change in wave spectrum and envelope of these waves with change in angle: 1) 180, 2) 120, 3) 90, 4) 60, 5) 0°.

The observations of 1 July 1978 were made under the conditions of a developing storm with a wind constant in direction whose velocity varied from 6 m/sec in the morning up to 13.5 m/sec at nighttime. At the height of the storm waves with collapsing crests attained 3 m in height. Judging from the available data of the wave recorder, the spectral maximum was at a frequency of 0.24 Hz (wavelength 30 m) at 1000 hours at a frequency of 0.14 Hz (wavelength 80 m) at 2400 hours. A spectral analysis was carried out for the records of signals obtained in the second half of the day (1700-2200 hours).

The spatial spectra of the signals were computed from 60 profiles each with a length of 256 m, following each other each 1 sec. The constant component was separated from each profile and therefore the spectrum at the zero frequency is equal to zero and an artificial low-frequency peak arises at the adjacent frequency. The adjacent spatial profiles were correlated. With a correlation time of about 10 sec the number of degrees of freedom in evaluating the spectrum is close to 10.

FOR OFFICIAL USE ONLY

## FOR OFFICIAL USE ONLY

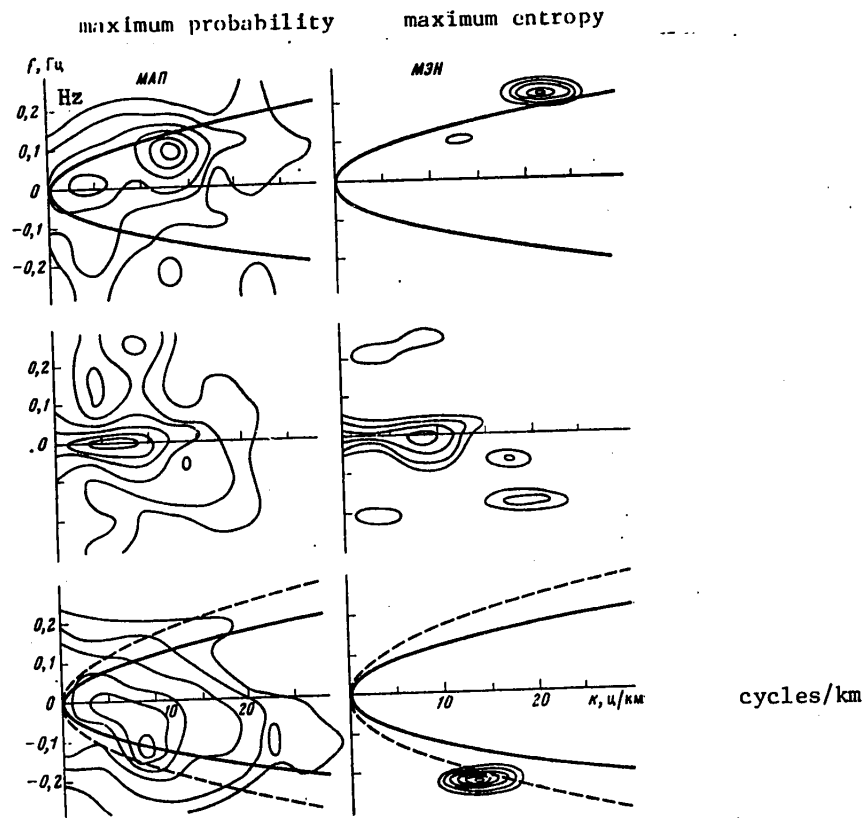


Fig. 5. Two-dimensional spectra of signals with  $\theta$  angles: 180, 270 and 300° (top to bottom). At left -- evaluations of maximum probability, at right -- evaluations of entropy. The solid curve is the dispersion curve, the dashed curve is the same curve for the projection of the wave vector onto the direction of the ray.

The principal feature of the spatial spectra is an overwhelming predominance of the low-frequency components absent in the wave spectrum (Fig. 3). These variations belong to the envelope of waves to one degree or another distorted with a nonlinear conversion from the wave profile to the intensity of the reflected signals. The spectra are combined into two groups: the radar ray is directed approximately toward the movement of the waves ( $\theta = 180, 180, 150^\circ$ ) and across the movement of waves ( $\theta = 240, 270, 300^\circ$ ). In the first case the spectra drop off with great oscillations; in the second -- more smoothly. The spectral peaks in the first group, at 8-11 cycles/km, corresponds to swell. The wind waves, whose frequency is greater, do not give significant peaks in the spatial spectra, which is possibly associated with the unstable position of sectors with a large slope within the limits of wind waves with steep crests. The equivalent width of the spectra is equal to approximately 10 cycles/km. This value should reflect the width of a spatial spectrum of waves approximately equal to 100 m; the width of the angular spectrum (with a wave length of 70 m) is equal to 0.7 rad ( $40^\circ$ ).

## FOR OFFICIAL USE ONLY

Proceeding to a two-dimensional analysis, we will examine the change in the configuration of the projection of the total spectrum of waves onto the plane  $k_1, f$ , where  $k_1$  is the wave vector component along the ray, with a change in the azimuthal angle  $\theta$  in a case when the total spectrum of waves has the form of a compact spot on the dispersion surface (Fig. 4). With  $\theta = 180^\circ$  (the ray is directed toward the movement of the waves) virtually the entire projection of the spectrum is concentrated in the dispersion curve segment. With a decrease in the  $\theta$  angle the space frequencies of the fluctuations decrease and the time spectra remain unchanged. The projection of the spot is gradually displaced toward the axis of time frequency and is broadened with respect to space frequency. With  $\theta = 90^\circ$  the projection reaches the time frequency axis, having a relatively isotropic form. With a further decrease in the  $\theta$  angle the projection of the spot, moving into the lower half-plane (the waves withdraw along the ray), moves in the direction of the lower branch of the dispersion curve and reaches it at  $\theta = 0^\circ$ . In the latter position the spot is again concentrated in a segment of the dispersion curve. The envelope spectrum in the first approximation duplicates the projection of the wave spectrum, transferred to the zero frequency. In the initial position, with  $\theta = 180^\circ$ , the envelope spectrum is drawn out in a zone parallel to the discriminated part of the dispersion curve. With broadening of the spot the envelope spectrum is drawn toward the origin of coordinates, becoming relatively isotropic when observing waves along their crests ( $\theta = 90^\circ$ ). With  $\theta = 0^\circ$  the envelope spectrum again is drawn out toward the pole, parallel to the lower branch of the dispersion curve.

The two-dimensional spectra of the radar signals are computed using 10 successive records with an extent of 256 m and a duration of 6 sec (32 x 6 points) without frequency averaging. With respect to time frequency the analysis is made using the maximum probability algorithm and the maximum entropy algorithm, ensuring a higher frequency resolution. With respect to space frequency, use is made of linear analysis algorithms. The maximum probability evaluation is ensured by approximately two degrees of freedom; the maximum entropy evaluation is considerably more variable.

On the average the two-dimensional spectra drop off with respect to time and space frequencies (Fig. 5). Due to the centering of data along several profiles the spectrum at the origin of coordinates was considerably suppressed, which creates a fictitious peak at a low frequency at which the remnants of the wave envelope spectrum are situated. These remnants are displaced considerably from the origin of coordinates along the time and space frequency axes with irradiation of the surface along the direction of wave movement. With irradiation across the wave movement they fall at the zero time frequency and are pressed to the limit toward the low space frequencies. This agrees with the diagram of change in the spectrum envelope represented in Fig. 4. Using the  $f$ - and  $k_1$ -coordinates of the envelope spectrum remnants it is possible to estimate the group velocity along the ray: with movement of the waves along the ray the group velocity is equal to 3.5 m/sec. Waves with a length of 32 m and a period of 4.5 sec have such a group velocity; this is somewhat less than the parameters measured with a wave recorder. In the case of azimuthal angles of  $180^\circ$  and  $300^\circ$  in the two-dimensional spectra it is easy to discriminate a peak at relatively low time and space frequencies. This peak falls fairly well on the dispersion curve and evidently corresponds to swell waves with a length of about 80 m moving in the same direction as the wind waves. The wind waves themselves do not

FOR OFFICIAL USE ONLY

create an appreciable peak in the spectrum (maximum probability evaluations) for the reason indicated above. The maximum entropy evaluations emphasize the acute peaks at the high frequencies, evidently belonging to the main wind waves. Sometimes these peaks fall fairly well on the dispersion curve (in the case of irradiation of the surface along the direction of wave movement), but in many cases several wider scattered peaks appear due to the considerable variability of the evaluation.

The registry of radar signals reflected from the wave-covered sea surface in the case of moderate waves and wind makes it possible to determine the parameters of the main waves -- length, period, phase and group velocity, number of waves in the space and time groups, width of the angular spectrum; in the case of intensive waves and a strong wind using the wave envelope it is possible to determine the group velocity and indirectly the frequency of the main wind waves.

Despite the dependence of the properties of the radar as an apparatus for measuring waves on many factors, which complicates the interpretation of data, evidently only radar observations can give reliable mass data on the space-time structure of waves on the sea.

The authors express appreciation to I. A. Leykin for assistance in the measurements and V. I. Men'shikov and G. I. Merinova for participation in data processing.

BIBLIOGRAPHY

1. Bass, F. G., et al., "Radiophysical Investigations of Sea Roughness (Radio-oceanography) at the Ukrainian Academy of Sciences," TRANS. IEEE, AP-25, No 1, pp 43-52, 1977.
2. Lomeyko, A. I. and Rozenberg, A. D., "Space-Time Structure of the Radar Image of the Sea Surface," TR. XII KONFERENTSII PO RASPROSTRANENIYU RADIOVOLN (Transactions of the Twelfth Conference on Radio Wave Propagation), Tomsk, Part II, pp 197-198, 1978.

COPYRIGHT: Izdatel'stvo "Nauka", "Izvestiya AN SSSR, Fizika atmosfery i okeana", 1982

5303

CSO: 1865/114

UDC 551.463:551.46.07/08

DETERMINATION OF SPECTRUM OF SEA WAVES BY SPECTRAL ANALYSIS OF  
AERIAL PHOTOGRAPHS\*

Moscow IZVESTIYA AKADEMII NAUK SSSR: FIZIKA ATMOSFERY I OKEANA in Russian  
Vol 18, No 2, Feb 82 (manuscript received 10 Mar 80, after revision 13 Oct 80)  
pp 215-216

[Article by V. I. Titov, Institute of Applied Physics, USSR Academy of Sciences]

[Text] As is well known [1,2], the method for determining the spectrum of waves by spectral analysis of photographs of the sea surface has recently become very popular. This method is based on the assumption of the existence of a linear dependence (under definite illumination conditions: clear sky, absence of solar reflections) between the slopes and the brightness of the sea surface, which leads to a linear correlation between the energy spectrum of the photograph and the spectrum of waves.

In this article we propose a model of formation of the image of a sea surface, taking into account nonlinearity in the brightness distribution over the sky, which made it possible to evaluate the contribution of nonlinear effects to the spectrum of the sea surface image.

Assuming the surface slopes to be small, we will expand the surface brightness  $I$  into series in powers of the surface gradient  $\eta$  and we will limit ourselves to second-order terms

$$I \approx I(\eta=0) + \hat{\nabla}_\eta^T I(\eta=0) \hat{\eta} + \frac{1}{2} \hat{\eta}^T \hat{\Delta}_\eta I(\eta=0) \hat{\eta},$$

where we used a matrix form of writing:

$$\hat{\eta} = \begin{pmatrix} \eta_1 \\ \eta_2 \end{pmatrix}$$

is a matrix column ( $\eta_1$  and  $\eta_2$  are the  $\eta$  coordinates in a Cartesian coordinate system at the mean sea surface),

$$\hat{\nabla}_\eta = \begin{pmatrix} \partial/\partial\eta_1 \\ \partial/\partial\eta_2 \end{pmatrix}, \quad \hat{\nabla}_\eta = \hat{\nabla}_\eta^T \hat{\nabla}_\eta^T.$$

\* Full article deposited at the All-Union Institute of Scientific and Technical Information, No 4324-81. Deposited 3 September 1981.

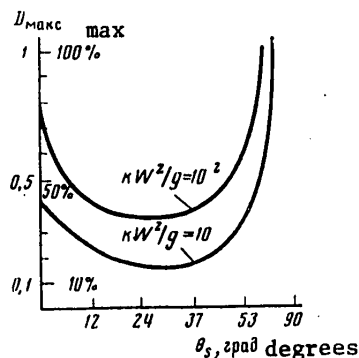
## FOR OFFICIAL USE ONLY

The gradients and second derivatives of brightness  $I$  are determined from the known angular dependences of sky brightness and the reflection formulas of geometrical optics.

Then it can be shown that the statistical mean square modulus of the two-dimensional Fourier spectrum  $G_k$  of the photograph (or the energy spectrum of the photograph [3]) will be determined by the formula:

$$G_k(k) \sim G_1(k) (\nabla_n I/k)^2 + \frac{1}{2} \int G_1 \left( k' + \frac{k}{2} \right) \times \\ \times G_1 \left( k' - \frac{k}{2} \right) \left[ \left( \hat{k}'^r + \frac{\hat{k}^r}{2} \right) \times \right. \\ \left. \times \hat{\Delta}_n I \left( \hat{k}' - \frac{\hat{k}}{2} \right) \right]^2 dk',$$

where  $k$  is the space frequency.



In this expression the first term is proportional to the product of the sought-for energy spectrum of rises in the sea surface  $G_\xi(k)$  (or the spectrum of waves) and the function  $(\nabla_n I/k)^2$ . It is obvious that the contribution of the linear term to the spectrum of the photograph will be maximum when  $k \parallel \nabla_n I$  and the linear term is transformed to zero when  $k \perp \nabla_n I$ .

The second term, caused by the nonlinearity in the angular distribution of sky brightness, is the contraction of the spectra of rises and can be regarded as noise or nonlinear distortions of the spectrum obtained in this way  $G_\xi(k)$ .

We will determine the coefficient of nonlinear distortions  $D(k)$  as the ratio of the nonlinear term to the linear term in the formula for  $G_k$ . In the case of isotropic waves it is possible to obtain the following approximate formula for an upward evaluation of the  $D(k)$  values:

$$[MAKS = \max] \quad D(k) \leq D_{max} = \frac{4 \cdot 10^{-3} (Sp^2 \hat{\Delta}_n I - 2 \hat{\Delta}_n I) k^2 \ln(kW^2/2g)}{2(\nabla_n I/k)^2},$$

where  $W$  is wind velocity. The figure shows the dependence  $D_{max}$  on the angular solar altitude  $\theta_s$  for the case of a photosurvey at the nadir and  $k \parallel \nabla_n I$ . The angular dependence of sky brightness was described by the Pokrovskiy function [1]. Evidently,  $D$  increases with an increase in frequency  $k$  and wind velocity  $W$  (there is an increase in the  $kW^2/g$  ratio), and also with an increase in the angle between the direction  $k$  and the brightness gradient  $\nabla_n I$ . In this case the minimum nonlinear distortions of the spectra will be observed with some optimum solar altitude  $\theta_s \sim 30^\circ$ . If  $\theta_s \rightarrow 0$  or  $\theta_s \rightarrow 90^\circ$  the distortions increase due to the relative decrease in the brightness gradient since when  $\theta_s \rightarrow 0$  the solar point of the sky corresponding to the brightness minimum approaches the zenith, whereas with  $\theta_s \rightarrow 90^\circ$ , when the sun approaches the zenith, the sky brightness increases and becomes an essentially nonlinear function.

FOR OFFICIAL USE ONLY

The author expresses appreciation to L. S. Dolin and A. G. Luchinin for assistance in the work, a number of useful comments and advice.

BIBLIOGRAPHY

1. Kasevich, R. S., "Directional Wave Spectra From Daylight Scattering," J. GEOPHYS. RES., Vol 80, No 33, pp 4535-4541, 1975.
2. Zagorodnikov, A. A. and Chelyshev, K. B., "Use of Optical Processing in Measurements of Waves by Remote Methods," TRUDY GOIN (Transactions of the State Oceanographic Institute), No 117, pp 25-34, 1973.
3. Konyayev, K. V., SPEKTRAL'NYY ANALIZ SLUCHAYNYKH PROTSESSOV I POLEY (Spectral Analysis of Random Processes and Fields), Moscow, Nauka, 1973.

COPYRIGHT: Izdatel'stvo "Nauka", "Izvestiya AN SSSR, Fizika atmosfery i okeana", 1982

5303

CSO: 1865/114

75  
FOR OFFICIAL USE ONLY

FOR OFFICIAL USE ONLY

UDC 551.465.553

INVESTIGATION OF SURFACE WIND CURRENT ON SEA

Moscow IZVESTIYA AKADEMII NAUK SSSR: FIZIKA ATMOSFERY I OKEANA in Russian  
Vol 18, No 2, Feb 82 (manuscript received 23 Apr 79, after revision 19 Feb 80)  
pp 217-220

[Article by O. V. Perepelitsyn and V. V. Chernyavets]

[Text] During recent years increasing attention has been devoted to study of the movement of the surface layer of water occurring under the influence of a local wind. A knowledge of this is necessary both for investigation of the structure of waves and for solution of many practical problems, including allowance for the influence of movement of the surface layer of water on the spectrum of a signal reflected from the sea surface in the case of a low height of objects. In this article we have obtained an experimental dependence of the velocity of the surface layer of water on the velocity and direction of the local wind during tests of a Doppler instrument for measuring velocity. The testing method is examined and the results of tests and processing of the collected data are given.

The orbital motion of reflecting particles of the water surface exerts the main influence on the displacement of the frequency of a signal reflected from the sea surface relative to the computed value [1]. As is well known, during wave movement the water particles in a deep sea in the case of steady waves move in orbits close to circles (Fig. 1). These circles lie in planes perpendicular to the wave crests. The velocity of motion of a particle in orbit  $V_{orb}$  with a wave period  $T_w$  and with a wave height  $H_w$  is

$$V_{orb} = \pi H_w / T_w.$$

The orbital motion of particles leads to a frequency modulation of the reflected signal and a broadening of the spectrum if the reflection from different parts of the wave is identical. However, experience shows that the reflection is maximum from the parts of the wave situated in the neighborhood of its crest. In the case of high waves the crests are broken and spray and foam are formed, which can also lead to an increase in the level of the signal reflected from the sectors near the crests. Since reflection from these sectors predominates, the frequency of the reflected signal is displaced by a value close to the corresponding orbital velocity values, as occurs in the presence of a current. This fictitious current is arbitrarily called an orbital current [2]

76  
FOR OFFICIAL USE ONLY

## FOR OFFICIAL USE ONLY

and its velocity during wind waves is dependent on wind velocity, increasing with its increase.



Fig. 1. Profile of sea wave and trajectory of reflecting particles during wave movement: 1) wave; 2) water particle; 3) orbit of movement of water particle.

This reasoning is correct during flights of an aircraft with Doppler apparatus at great altitudes when the area irradiated by the antenna is considerably greater than the length of the sea wave and the power of the reflected signal is determined for the most part by the sectors situated in the region of the crests of sea waves, that is, the frequency of the reflected signal is displaced by a value corresponding to the orbital velocity at the wave crest. In the case of a low flight altitude, when the area irradiated by the antenna is considerably less than the length of the sea wave, the influence of movement of sea waves on the operation of the Doppler apparatus changes considerably. The value of the displacement of the Doppler spectrum in this case will be determined by the mean velocity of the surface current.

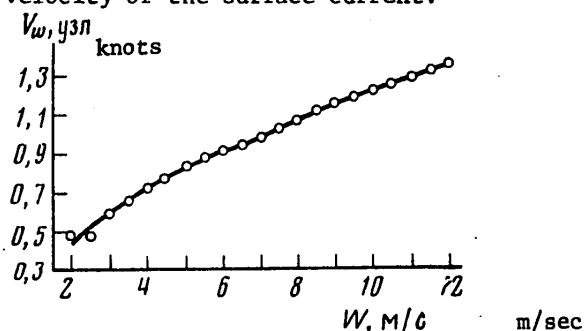


Fig. 2. Dependence of velocity of wind movement of surface current on wind velocity: W -- wind velocity,  $V_w$  -- velocity of surface current.

In order to obtain the dependence of the velocity of the surface layer of water on velocity and direction of the local wind, in 1973-1977 specialists carried out experimental investigations in the waters of the Baltic Sea. Special Doppler apparatus was installed on the ship (similar to airborne instruments for measuring velocity), making it possible to carry out measurements with a high accuracy at low heights of about 3-10 m.

The velocity of movement of the surface water layer was determined from the difference in the values of the longitudinal component of the ship's speed, which was obtained using the Doppler apparatus, and the standard velocity (with allowance for current intensity), determined on a radiotheodolite

## FOR OFFICIAL USE ONLY

measurement line using the following method. During the ship's movement on the measurement line five determinations of the ship's positions were made at the beginning and end of the measurement sector (run) at equal time intervals by means of theodolites by command from the ship. The results of the measurements were processed using an overlay with isolines of the bearings. An overlay at a scale of 1:5000 ensured determination of the rate of movement of the ship on the run as the mean velocity values, determined from five segments of the distances covered with an accuracy not less than 0.035 knot.

Synchronously with measurements of the standard velocity we measured the ship's speed using a Doppler measurement instrument and a standard hydrodynamic log, and the hydrometeorological factors were also registered (wind velocity and direction, sea waves in units, etc.). Wind direction and velocity were measured at a height of 3-8 m above the sea level. The error in the Doppler system was no worse than 0.06 knot.

Table 1

Wind velocity W, m/sec	2.0	2.5	3.0	3.5	4.0	4.5	5.0	5.5	6.0	6.5	7.0
Intensity of surface wind current $V_w$ , knots	0.48	0.49	0.61	0.66	0.72	0.77	0.81	0.86	0.9	0.94	0.98
Wind velocity W, m/sec	7.5	8.0	8.5	9.0	9.5	10.0	10.5	11.0	11.5	12.0	
Intensity of surface wind current $V_w$ , knots	1.02	1.05	1.09	1.13	1.16	1.2	1.23	1.28	1.33	1.38	

The statistical material obtained as a result of the investigations was processed using the following formulas:

$$\Delta V_{wx} = |V_{xi}^D - V_{xi}^{st}| - V_{cur}, \quad V_w = \Delta V_{wx} \frac{1}{|\cos(k_w - k_k)|};$$

where  $\Delta V_{wx}$  is the velocity change due to the wind surface current along the diametral plane of the ship,  $V_w$  is the velocity of the wind movement of the surface film,

$$V_{cur} = \frac{1}{n} \sum_{i=1}^n |V_x^{log} - V_x^{st}|$$

is current velocity,  $k_w$  is wind direction,  $k_k$  is the ship's course,  $n$  is the number of measurements,  $V_x^{log}$  is velocity according to the standard hydrodynamic log,  $V_x^{st}$  is standard velocity,  $V_x^D$  is velocity according to the Doppler measuring instrument.

As a result of the measurements it was possible to construct a graph of the dependence of the velocity of wind movement of the surface current on wind velocity (Fig. 2)

$$V_w = f(W).$$

## FOR OFFICIAL USE ONLY

For an approximation of the functional dependence we selected an exponential function in the form (taking into account that  $V_w = 0$  with  $W = 0$ )

$$V_w = AW^b,$$

where  $A$  and  $b$  are coefficients. Putting this into the logarithmic form  $\lg V_w = \lg A + b \lg W$  and introducing the notations  $\lg V_w = y$ ,  $\lg A = a$ ,  $\lg W = x$ , we have  $y = a + bx$ .

For finding the coefficients  $a$  and  $b$  by a linear function it is possible to use the least squares method [3], that is, the  $a$  and  $b$  values at the minimum must turn to the value

$$\theta_w = \sum_{i=1}^n (y_i - a - bx_i)^2.$$

For this it is necessary that

$$a = \bar{y} - b\bar{x}, \quad b = \frac{\sum_{i=1}^n (y_i - \bar{y})(x_i - \bar{x})}{\sum_{i=1}^n (x_i - \bar{x})^2},$$

where

$$\bar{x} = \frac{1}{n} \sum_{i=1}^n x_i, \quad \bar{y} = \frac{1}{n} \sum_{i=1}^n y_i$$

are the mathematical expectations of the random values.

Table 2

Wind velocity $w$	Wind course angles $K_w$ , degrees							
	0—20	20—40	40—60	60—80	100—120	120—140	140—160	160—180
1	0,35	0,3	0,2	0,1	0,1	0,2	0,3	0,35
2	0,5	0,4	0,3	0,1	0,3	0,3	0,4	0,5
3	0,7	0,6	0,5	0,2	0,2	0,5	0,6	0,7
4	0,9	0,8	0,7	0,3	0,3	0,7	0,8	0,9
5	1,1	0,9	0,9	0,4	0,4	0,9	0,9	1,1
6	1,3	1,2	1,0	0,5	0,5	1,0	1,2	1,3
7	1,6	1,3	1,1	0,6	0,6	1,1	1,3	1,6
	180—200	200—220	220—240	240—260	280—300	300—320	320—340	340—360
1	0,35	0,2	0,2	0,1	0,1	0,2	0,3	0,35
2	0,5	0,4	0,3	0,1	0,1	0,3	0,4	0,5
3	0,7	0,6	0,5	0,2	0,2	0,5	0,6	0,7
4	0,9	0,8	0,7	0,3	0,3	0,7	0,8	0,9
5	1,1	0,9	0,9	0,4	0,4	0,9	0,9	1,1
6	1,3	1,2	1,0	0,5	0,5	1,0	1,2	1,3
7	1,6	1,3	1,1	0,6	0,6	1,1	1,3	1,6

Making the computations, under the condition that  $V_w$  is expressed in knots,  $W$  in m/sec, we find  $b = 0.558$ ,  $a = -0.483$ ,  $A = 0.329$ , and we finally have  $V_w \pm \Delta W^{0.56}$ ,  $A = 0.329$ , with  $V_w$  expressed in knots;  $A = 0.17$  -- with  $V_w$  expressed in m/sec.

FOR OFFICIAL USE ONLY

Computations on the basis of experimental data show that in accordance with the Student-t distribution the coefficients A and b of the approximating curve with a confidence coefficient 0.9 fall in the interval  $A = 280-0.386$ ,  $b = 0.56 \pm 0.08$ . The evaluation of the empirical standard deviation  $V_w$  from the resulting curve, under the condition that the dispersion is not dependent on wind intensity, is equal to  $S_w = 0.06$  knot.

The final result is given in Table 1.

The statistical material was processed on a BESM-4M electronic computer. Table 2 was developed on the basis of the derived dependence. This shows the velocity of the surface wind current on wind velocity and direction (simplified variant).

It was confirmed as a result of these investigations that the direction of the surface wind current coincides with the wind direction. It was also found that there is a dependence of the velocity of the surface current on wind velocity and direction. An evaluation of this dependence was made and with the derived dependence taken into account, a table was constructed showing the velocity of the surface wind current as a function of wind direction and velocity.

BIBLIOGRAPHY

1. Shuleykin, V. V., KRATKIY KURS FIZIKI MORYA (Concise Course in Marine Physics), Leningrad, Gidrometeoizdat, 1959, 478 pages.
2. Kolchinskiy, B. Ye., Mandurovskiy, I. A. and Konstantinovskiy, M. I., DOPLEROVSKIYE USTROYSTVA I SISTEMY NAVIGATSII (Doppler Apparatus and Navigation Systems), Moscow, Sovetskoye Radio, 1975, 432 pages.
3. Venttsel', Ye. S., TEORIYA VEROYATNOSTEY (Theory of Probabilities), Moscow, Nauka, 1964, 576 pages.

COPYRIGHT: Izdatel'stvo "Nauka", "Izvestiya AN SSSR, Fizika atmosfery i okeana", 1982

5303

CSO: 1865/114

## FOR OFFICIAL USE ONLY

UDC 551.565.41

UDC 551.466.2:551.466.81

## ADIABATIC INTERACTION OF SURFACE AND INTERNAL WAVES

Moscow IZVESTIYA AKADEMII NAUK SSSR: FIZIKA ATMOSFERY I OKEANA in Russian  
Vol 18, No 2, Feb 82 (manuscript received 20 May 80, after revision 25 Aug 80)  
pp 220-223

[Article by A. Ya. Basovich, Institute of Applied Physics, USSR Academy of Sciences]

[Text] The interaction of surface and internal waves has been examined in many studies in which the authors have determined changes both in the characteristics of surface waves [1-4] and the parameters of internal waves [5,6]. However, earlier such an interaction was investigated without taking into account the reflection and capture of surface waves in the field of an internal wave as a result of the blocking effect [2, 4]. As will be demonstrated, this effect can be important in the case of intensive internal waves.

We will assume that in a fluid with a two-layer stratification of the depth  $h_1 + h_2$ , where  $h_1$  is the depth of the pycnocline\*, an internal wave develops at the time  $t = 0$ . We will assume that with  $t < 0$  there were surface waves with a statistically and spatially homogeneous energy spectrum  $W_0 = W_0(k)$ . As a simplification we will assume that the wave vectors of the surface waves are parallel to one another and to the direction of internal wave propagation. The equations of the problem can be written in the form

$$\frac{\partial N_k}{\partial t} + \dot{x} \frac{\partial N_k}{\partial x} + k \frac{\partial N_k}{\partial k} = 0, \quad (1)$$

$$\frac{\partial U}{\partial t} + C_1 \left( 1 - \frac{3}{2} \frac{h_1 - h_2}{h^2 C_1} U \right) \frac{\partial U}{\partial x} + \frac{C_1}{\theta} h_1 h_2 \frac{\partial^3 U}{\partial x^3} = -\alpha \frac{\partial}{\partial x} \int_k N_k dk, \quad (2)$$

where  $N_k(x, k, t) = W(x, k, t) / \sqrt{gk}$  is the density of wave action,  $k$  is the wave number of the surface waves,  $U$  is the velocity of the current created at the surface of the internal wave,  $C_1 [gh_1 h_2 \delta \rho / \rho (h_1 + h_2)]^{1/2}$  is the velocity of internal waves of a low amplitude,  $\rho$  and  $\delta \rho$  are the density of the fluid and its change at the pycnocline, and  $\alpha = C_1 h_2 / 2 \rho h_1 (h_1 + h_2)$ . Equation (1) is correct if the influence of the wind and the nonlinearity of the surface waves is small during the characteristic time of the considered processes [4]. The conditions of applicability of this approximation are defined below. Equation (2) can be derived with the use of the results in [7] and differs from that cited in [7] by allowance for the characteristic nonlinearity

\* A two-layer stratification is examined to simplify computations. Similarly a case of an arbitrary stratification can be considered.

## FOR OFFICIAL USE ONLY

of internal waves. The length of the internal wave is assumed to be much greater than the depth of the fluid.

The change in the parameters of the surface waves and the internal wave can be found in an adiabatic approximation with satisfaction of the condition  $|\tau/\tau_L| \ll 1$ . Here  $\tau$  is the characteristic time of the change in the spectrum of surface waves [4],  $\tau$  is the decrement (increment) of the internal wave during interaction with surface waves in a case when the changes in the spectrum of the latter can be considered small. With satisfaction of this condition the interaction of the waves can be considered in two stages: first it is necessary to find a change in the spectrum of waves in the stipulated field of the internal wave and then its parameters\*. The first part of the problem was examined in detail in [4]. Accordingly, in this study we analyze the direct behavior of the internal wave.

2. The change in the parameters of the internal wave is described by equation (2). There can be both a periodic and single internal waves (solitons) of a negative ( $U < 0$ ) and a positive polarity ( $U > 0$ ). The polarity of the soliton is determined by the sign on the nonlinear term in (2), that is, by the relationship of  $h_1$  and  $h_2$ .

First we will examine a periodic internal wave, neglecting its characteristic nonlinearity. In this case it is possible to neglect the weak dispersion and equation (2) assumes the form:

$$\frac{\partial U}{\partial t} + C_1 \frac{\partial U}{\partial x} = -\alpha \frac{\partial}{\partial x} \int k N_k dk. \quad (3)$$

We will seek its solution in the form  $U = U_0(t) \cos q \tilde{x}$ , where  $U_0(t)$  is the slowly changing amplitude of the wave,  $q$  is its wave number,  $\tilde{x} = x - C_1 t$ . Multiplying equation (3) by  $U$ , integrating for  $x$  in the period of the internal wave, and from the right in parts, we obtain the relationship:

$$\frac{d}{dt} \left( \frac{1}{2} \int_{2\pi/q} U^2 d\tilde{x} \right) = -\alpha \int_{2\pi/q} \int k N_k \frac{\partial U}{\partial \tilde{x}} d\tilde{x} dk \quad (4)$$

Equation (4) can be simplified if we use one of the equations of motion of wave packets of surface waves

$$\frac{\partial U}{\partial \tilde{x}} = -\frac{1}{k} \frac{\partial k}{\partial t} \quad (5)$$

and the retention of  $N_k$  along the trajectories of their movement in space  $\tilde{x}$ ,  $k$  [4]. Proceeding in (4) from integration for  $\tilde{x}$ ,  $k$  to integration for  $x_0$ ,  $k_0$ , corresponding to the initial position of the wave packets with ( $t = 0$ ), using (5) and with retention of  $N_k$ , we obtain the expression

$$\frac{d}{dt} \left( \frac{U_0^2}{4\alpha} + \frac{q}{2\pi} \int_{2\pi/q} \int k N_k d\tilde{x} dk \right) = 0, \quad (6)$$

expressing the law of conservation of momentum in the internal wave - surface

\* For the first time such an approach was used in investigating the interaction of a wave and particles in plasma [8]. Applicable to the interaction of waves it was developed in [9].

## FOR OFFICIAL USE ONLY

wave system. With relatively small changes in the wave numbers of surface waves under the influence of an internal wave  $k = k - k_*$ , where  $k_* = g/4C_1^2$  is the wave number of the surface waves with a group velocity equal to  $C_1$ , equation (6) with an accuracy to the notations corresponds to the law of conservation of momentum in the wave-particle system [10]. Accordingly, its solution can be immediately written:

$$\gamma(t) = \left( \frac{dU_0}{dt} \right) / U_0 = \gamma_L P(t),$$

where

$$\gamma_L = \frac{2gk_*^2 h_2}{\rho h_1 (h_1 + h_2)} \left( \frac{\partial N_k}{\partial k} \right)_{k=k_*}$$

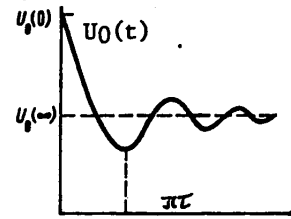


Fig. 1. Temporal change in amplitude of sinusoidal internal wave.

and the expression for  $P(t)$  [8] is not cited due to its unwieldiness. The behavior of  $U_0(t)$  with  $(\partial N_k / \partial k)_{k=k_*} < 0$  is indicated qualitatively in the figure. It represents aperiodic oscillations with the characteristic time  $\pi\tau$ ; as a result of the asynchronicity of movement of the wave packets along the trajectories in the space  $\tilde{x}$ ,  $k$  the change in the spectrum of surface waves occurs in such a way that their effect on the internal wave decreases with the course of time and the oscillations of the amplitude  $U_0$  disappear. The amplitude of the wave changes substantially differently than in the absence of capture of surface waves (exponential dropoff or increase) and with an increase in time tends to the value  $U_0(\infty)$ , differing from  $U_0(0)$  by a value of the order of  $\gamma_L U_0(0)\tau$ .

Now we will examine the change in the solitons of internal waves under the influence of surface waves. Assuming the change in the amplitude to be quite slow, so that there is satisfaction of the condition of retention of the form of the soliton [11], we will seek solution of equation (2) in the form

$$U = U_0(t) \operatorname{ch}^{-1} \left( \frac{\tilde{x}}{\Delta(t)} \right), \quad U_0(t) \Delta^2(t) = - \frac{4C_1 h_1 h_2^2}{3(h_1 - h_2)},$$

where  $\tilde{x} = x - Ct$ ,  $C$  is the velocity of the soliton. Adhering to [9], we obtain the law of conservation of momentum for a soliton and surface waves, similar to (4):

$$\frac{d}{dt} \left( \int_{-\infty}^{\infty} \frac{U^2}{2} d\tilde{x} \right) = \alpha \int_{-\infty}^{\infty} \int_k k N_k \frac{\partial U}{\partial \tilde{x}} d\tilde{x} dk. \quad (7)$$

The behavior of the amplitude of the soliton is dependent on its polarity. With  $t \gg \tau$ , where  $\tau_0$  is the characteristic time of movement of the wave packets in the field of the soliton, we have the following equation for  $U_0(t)$ :

$$\frac{d|U_0|}{dt} = \frac{4\alpha k_*^2}{C_1 h_2} \left[ \frac{3(h_1 - h_2)}{C_1 h_1} \right]^{1/2} \left( \frac{\partial N_k}{\partial k} \right)_{k=k_*} |U_0|^{1/2}. \quad (8)$$

## FOR OFFICIAL USE ONLY

From (8) we have the law of change in amplitude of the soliton

$$U_0(t) = U_0(0) (1+t/t_0)^{-1}, \quad (9)$$

where

$$t_0 = - \left\{ \frac{2\alpha k_*^3}{C_1 h_2} \left[ \frac{3(h_1 - h_2)}{C_1 h_1} |U_0(0)| \right]^{1/2} \left( \frac{\partial N_k}{\partial k} \right)_{k=k_*} \right\}^{-1}.$$

The amplitude of the solitone of negative polarity decreases monotonically with  $(\partial N_k / \partial k)_{k=k_*} < 0$ . With an opposite sign of the inequality the amplitude of the solitons will increase. The change in amplitude (and accordingly  $\Delta(t)$  and  $C(t)$ ) is monotonic since a soliton with  $U_0 < 0$  does not capture surface waves but only reflects them.

The capture of surface waves arises with  $U_0 > 0$  ( $h_1 < h_2$ ). As a result of the movement of wave packets of surface waves in closed trajectories the behavior of amplitude is qualitatively close to that cited in the figure. The change in amplitude during the time  $\pi\tau_0$ , corresponding to half the "turns" of the packets along the trajectory, can be estimated roughly using formula (9), assuming that  $t \sim \pi\tau_0$ . As in the case of periodic waves, the change in the amplitude of the soliton with  $U_0 > 0$  ceases with the course of time.

3. We will cite some estimates determining the limits of the region of applicability of our examination. As the undisturbed wave spectrum we will select the Rolle-Fisher spectrum [12] (in a one-dimensional modification):

$$n_k(k) = Ak^{-3} \exp(-2g/kv^2),$$

where  $A = 2.5 \cdot 10^{-2}$ ,  $v$  is wind velocity. The  $N_k$  and  $n_k$  values are related by the expression  $N_k = \rho gh_k / \sqrt{gk}$ . Then the condition of applicability of the adiabatic method has the following form ( $\tau\gamma_L \ll 1$ ):

$$512 \left[ \frac{AC_1^2 h_2}{h_1(h_1 + h_2)g} \left( 7 - \frac{16C_1^2}{v^2} \right) \right]^2 \exp \left( - \frac{16C_1^2}{v^2} \right) \ll \beta_0, \quad (10)$$

where  $\tau = T_i / \pi \sqrt{2\beta_0}$ ,  $T_i$  is the period of the internal wave,  $\beta_0 = U_0 / C_1$ .

Allowance for the nonlinearity of surface waves leads to the appearance of the collision term  $st(N_k)$  in equation (1) corresponding to the transfer in the spectrum of the energy obtained by waves from the wind. The neglecting of the term  $st(N_k)$  is possible under the condition of the smallness of the characteristic time of the considered processes ( $\sim \tau$ ) in comparison with the time of energy pumping in the spectrum [13]:

$$\tau_{st}^{-1} \sim \frac{st(N_k)}{N_k} \sim \left[ \frac{(V_k n_k k)^2}{\gamma g k} \right]_{k=k_*}^{-1},$$

where  $V_k \sim \sqrt{gk^5}$  is a matrix element of the interaction of surface waves [14]. By comparing  $\tau$  and  $\tau_{st}$  we obtain the inequality:

$$T_i / \pi \sqrt{2\beta_0} \ll [\gamma g k (n_k k^2)^2]_{k=k_*}^{-1},$$

or

$$\left[ \frac{gA^2 \exp(-16C_1^2/v^2)}{\sqrt{2} q C_1^2} \right]^2 \leq \beta_0. \quad (11)$$

For an evaluation in accordance with the inequalities (10) and (11) we select  $C_1 = 0.5-1$  m/sec,  $2\pi/q \sim 200$  m,  $h_1 \sim 20$  m. We will assume that  $h_2 > h_1$ ; in this case the  $h_2$  value does not change the order of magnitude of the evaluation (10). We will assume that there are surface waves which are in synchronism with the internal wave, for which with the selected model of the spectrum it is necessary that  $3v^2 \geq 8C_1^2$ . For the cited parameters it is inequality (11) which is decisive, from which it follows that:  $(3.2 \cdot 10^{-1} - 2 \cdot 10^{-2}) \exp(-32C_1^2/v^2) \leq \beta_0$ . This inequality shows that the model of adiabatic interaction is applicable in the case of adequately intensive internal waves.

In the future it will be of interest to examine the influence of surface waves in the train of internal waves within the framework of the model proposed above.

The author expresses appreciation to V. I. Talanov for constant interest in the work and useful comments.

#### BIBLIOGRAPHY

1. Gargett, A. E. and Hughes, B. A., "On the Interaction of Surface and Internal Waves," J. FLUID MECH., Vol 52, No 1, pp 179-191, 1972.
2. Phillips, O. M., "Interaction of Internal and Surface Waves," IZV. AN SSSR: FAO (News of the USSR Academy of Sciences: Physics of the Atmosphere and Ocean), Vol 9, No 9, pp 954-961, 1973.
3. Hughes, V. A., "The Effect of Internal Waves on Surface Wind Waves," J. GEOPHYS. RES., Vol 3, No 41, pp 455-465, 1978.
4. Basovich, A. Ya., "Transformation of the Spectrum of Surface Waves Under the Influence of an Internal Wave," IZV. AN SSSR: FAO, Vol 15, No 6, pp 655-661, 1979.
5. Petrov, V. V., "Interaction Between Internal Waves and Microscale Surface Turbulence in the Ocean," IZV. AN SSSR: FAO, Vol 14, No 3, pp 342-347, 1978.
6. Yermakov, S. A. and Pelinovskiy, Ye. N., "Role of Nonlinear Interactions in the Formation of Mean Fields," IZV. AN SSSR: FAO, Vol 13, No 5, pp 537-542, 1977.
7. Petrov, V. V., "Dynamics of Nonlinear Surface Waves in a Stratified Ocean," IZV. AN SSSR: FAO, Vol 15, No 7, pp 740-749, 1979.
8. O'Neil, T., "Collisionless Damping of Nonlinear Plasma Oscillations," PHYS. FLUIDS, Vol 8, No 12, pp 2255-2262, 1965.

FOR OFFICIAL USE ONLY

9. Basovich, A. Ya. and Gromov, Ye. M., "Adiabatic Interaction of Ionosonic and Langmuir Waves," FIZIKA PLAZMY (Plasma Physics), Vol 5, No 4, pp 833-839, 1979.
10. Shapiro, V. D. and Shevchenko, V. I., "Wave - Particle Interaction of Non-equilibrium Media," IZV. VUZov: RADIOFIZIKA (News of Institutes of Higher Education: Radiophysics), Vol XIX, No 5-6, pp 767-791, 1976.
11. Karpman, V. N. and Maslov, Ye. M., "Theory of Perturbations for Solitons," ZhETF (Journal of Experimental and Theoretical Physics), Vol 73, No 2(8), pp 537-559, 1977.
12. Lugovskiy, V. V., DINAMIKA MORYA (Sea Dynamics), Leningrad, Sudostroyeniye, pp 162-178, 1976.
13. Galeev, A. A. and Sagdeyev, R. Z., "Nonlinear Theory of Plasma," VOPROSY TEORII PLAZMY (Problems in the Theory of Plasma), Moscow, Atomizdat, No 7, pp 7-145, 1973.
14. Phillips, O. M., "Theoretical and Experimental Investigations of Interactions of Gravitational Waves," NELINEYNAYA TEORIYA RASPROSTRANENIYA VOLN (Nonlinear Theory of Wave Propagation), Moscow, Mir, pp 141-160, 1970.

COPYRIGHT: Izdatel'stvo "Nauka", "Izvestiya AN SSSR, Fizika atmosfery i okeana", 1982

5303

CSO: 1865/114

UDC 681.325.5-181.4

ORGANIZATION OF COMPUTER-INSTRUMENT INTERACTION IN SYSTEMS FOR AUTOMATION OF  
SCIENTIFIC RESEARCH WITH VARIABLE STRUCTURE

Riga AVTOMATIKA I VYCHISLITEL'NAYA TEKHNIKA in Russian No 3, May-Jun 81  
(manuscript received 18 Jun 80) pp 81-91

[Article by S. N. Domaratskiy, O. S. Zudin and O. Vaynio]

[Text] A characteristic feature of recent years is the widespread introduction of distributed computer networks into the practice of operation of industrial and scientific organizations. Networks unite centers consisting of several computers that interact with each other and exchange data with the network through a common processor [1]. These centers may be in fixed locations or even on mobile platforms, for example, on ships intended for oceanic research. Radio and space communications may be used to include these centers in the network. Single-center computer networks located on scientific research ships (NIS) of the USSR AN [Academy of Sciences = AS] unite laboratory systems for automation of scientific research (SANI), automatic navigation facilities, meteosynoptic data acquisition systems and data acquisition and processing centers. Laboratory scientific research automation systems [LSRAS] contain computers; data input, output and display devices; and a substantial number of scientific instruments. A feature of the functioning of the majority of LSRAS in ship systems is the variable composition of equipment and the need for frequent and rapid reconfigurations of the system in the process of operating with orientation to various experiments. This article is aimed at generalizing the experience of organization of computer-instrument interaction in LSRAS with a variable structure gained in the process of a joint effort by Soviet and Finnish specialists on developing the Integrated Scientific Research Automation System for the USSR AS scientific research ship, "Akademik Mstislav Keldysh," at the shipyard of the "Khollming" AO [joint-stock company] in Rauma (Finland).

In the most general form, any experiment can be reduced to sending some set (in the particular case, an empty set) of stimulating actions to the object of study and determining (measuring) object responses to these actions.

By analogy to the concept of the computing process ([2], p 25), one can introduce the concept of the process of performing an automated experiment that covers sending the stimulating actions, measuring object response to them, interaction with the human operator, processing of the quantitative indicators of object response according to specified algorithms and presentation of the data obtained in a convenient form, and exchange of information with other center systems.

87  
FOR OFFICIAL USE ONLY

## FOR OFFICIAL USE ONLY

From here on, the measuring process should be understood as the sending of actions to an object and the measuring of its responses, and let us consider the experiment program an isomorphic mapping of the algorithm for performing the experiment onto the set of hardware.

The process of performing an automated experiment may be represented in the form of a set of computing (VP) [CP] and measuring (IP) [MP] processes. Irrespective of the experiment complexity and the quantity of apparatus taking part in it, the predominant role in the process of performing an automated experiment is played by one of the CP. All MP and other CP are subordinate. As a rule, the processes making up the automated experiment flow in standalone hardware modules: computers and various scientific instruments. Therefore, in developing scientific research automation systems, much importance is attached to the proper choice of procedures for interaction between the processes and apparatus which are implemented at the functional-logic, electrotechnical and mechanical levels. The first level extends to the formats of protocols and algorithms for exchange of data and commands, the second to the electrical characteristics of the physical data media and data transmission lines, and the third ensures the mechanical compatibility of the inputs and outputs for the various instruments.

Let us call an interface the set of hardware and software that permits effecting the interaction of the component computing and measuring processes in an automated experiment.

The same scientific research automation system may include both instruments capable of only the simplest interaction and very complex instruments built on the basis of microprocessors in which CP flow along with MP. The interface system must enable the organization of interaction at all levels of instruments of varying complexity both between each other and with one or more computers, in which the main and subordinate CP of the automated experiment flow. A natural condition in doing so is the orientation to existing standards.

Two standard interfaces for LSRAS that meet the requirements listed have now received broad international recognition: the CAMAC system [3-5] and the Interface for Programmable Instruments of the International Electrotechnical Commission [IEC] [6], known as the IEC Bus or the GPIB (General Purposes Interface Bus). Both standards describe buses (set of communication lines) for data exchange and determine the interaction of apparatus. The main difference between them is in throughput and the length of the communication lines. The CAMAC standards also impose more severe restrictions on the mechanical level of interaction (including restrictions on apparatus sizes), and the IEC bus on protocols [7]. The areas for application of these standards are discussed in [8].

Both of these standards have been used in the LSRAS for the single-center computer network on the "Akademik Mstislav Keldysh" scientific research ship to automate various types of research. Additional capabilities are realized with joint use of the CAMAC system and IEC bus in the process of performing the same automated experiment. For this purpose, modules that match up the buses are included in the CAMAC crates and the appropriate software has been developed. Thus, the IEC bus is used practically in all the LSRAS on the ship and is a major means for automating experimental research.

## FOR OFFICIAL USE ONLY

Let us go into more detail on the organization of interaction of processes in systems based on the IEC bus. The IEC bus is a set of 24 communication lines: 8 are informational when transferring data and multiline commands, 3 are used for establishing correspondence of the states of the processes of receiving and sending the next portion (byte) of data, 5 are used to send commands for general management of interaction of the processes making up the experiment, and 8 are used to organize interaction at the electrotechnical level. An example of the interaction of the instruments joined by the IEC bus and the name and function of the bus lines are shown in fig. 1. In any of the processes shown in the figure, three groups of functions, conventionally depicted in fig. 2 by using sections  $S_1$ ,  $S_2$ ,  $S_3$  and  $S_4$ ,

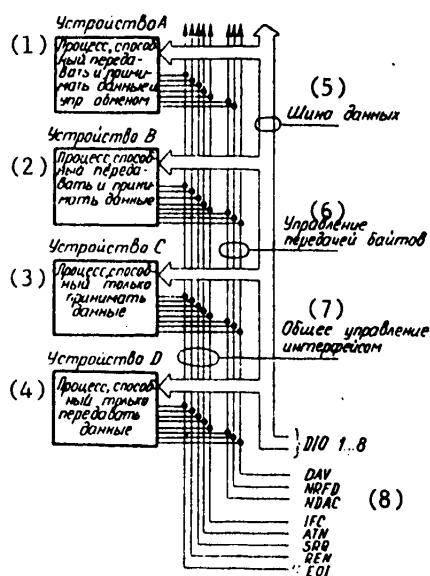


Fig. 1. IEC bus structure and capabilities

Key:

1. device A; process able to talk, listen and control
2. device B; process able to listen and talk
3. device C; process able only to listen
4. device D; process able only to talk
5. data bus
6. byte transfer control

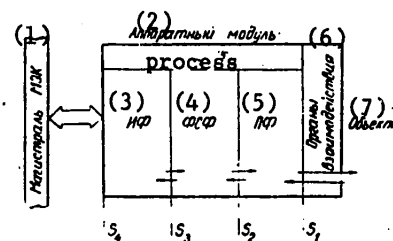


Fig. 2. Structure of processes interacting by means of IEC bus

Key:

1. IEC Bus
2. hardware module
3. IF [interface functions]
4. FSF [data format matching functions]
5. PF [instrument functions]
6. organs of interaction
7. object

## FOR OFFICIAL USE ONLY

can be distinguished. The functions are described by algorithms or diagrams of states and transfers effected by using external commands and actions. At any given time, the meaning of a process function should be understood as its state and set of commands and actions being sent in the process. Instrument functions realize the basic purpose of an instrument, for example, sending some known action or measuring a physical quantity. Instrument functions (PF) provide for interaction with the object of the experiment and the researcher. Interface functions (IF) effect interaction of a given process with other processes in the automated experiment when commands and data are exchanged. The functions enclosed between sections  $S_2$  and  $S_3$  (FSF) match formats of data received or generated by instrument functions with the protocols adopted in the system in accordance with the restrictions of the standard [7].

Table of Interface Functions Described by IEC Standard

Symbol	Designation	Number of Possible Versions (Subsets)	Number of Subsets Simultaneously Realizable
SH	source handshake	1	1
AH	acceptor handshake	1	1
T(TE)	talker or (extended talker)	8 each	1
L(LE)	listener or (extended listener)	4 each	1
C	controller-instrument	28	5 (no more)
SR	service request	1	1
RL	remote local control	2	1
PP	parallel poll	2	1
DC	device clear	2	1
DT	device trigger	1	1

The IEC standard describes 10 interface functions, each of which has several possible versions of interpretation. The name and purpose of the functions are given in the table above. The predominant computing process in systems organized on the basis of the IEC bus flows in the system controller, and the subordinate CP for control of the experiment (if any) flow in other controllers. A small or medium-size computer is most often used as the controller. Processes flowing in controllers have the capability of issuing single- and multiline commands to subordinate processes and of transferring control to each other. The system controller, and it alone, has the capability of terminating interaction of all processes at any given time and assuming system control itself. The only interface function mandatory for all instruments is "acceptor handshake" (AH) which permits processes flowing in the instrument to receive multiline commands and data. The other functions may be contained in instruments in any combination. When data is exchanged, each process must be addressed in advance by the controller controlling the bus at the time as the data acceptor or source. Only one addressed data source with several addressed acceptors is possible on the bus at any given time. Addressing of the processes is two-byte: by the primary and secondary address. Under conditions of interaction at the electrotechnical level, the number of instruments joined by the

## FOR OFFICIAL USE ONLY

bus must not exceed 15 with multiformity of primary addresses for acceptors (31) and for sources (31). Several acceptors may have identical addresses. Each of the primary processes may additionally activate by secondary addresses up to 31 processes. Data exchange over the bus is possible with or without the participation of the controller. Manual addressing of instruments is provided for operation in the simplest scientific research automation systems without a controller. The rate of data exchange over the bus is determined by the slowest of the interacting processes. It is preferable to use the seven-bit ASCII code (KOI-7) in the system.

Over two hundred different instruments that are capable of interacting in systems based on the IEC bus are now produced in the world. However, in developing scientific research automation systems, instruments have to be used that were developed prior to propagation of the standard or are not compatible with the IEC bus for some other reason. To ensure compatibility of the processes flowing in these instruments with the experiment, they have to be equipped with FSF and IF [format match and interface functions]. These functions with realization of compatibility of the processes can be interpreted by both the hardware (by using electronic components) and the software (or microprogram) method. In doing so, the task of ensuring compatibility at the electrotechnical and mechanical levels is solved in all cases uniformly. In instruments based on microprocessors, a large share of the interface functions can be interpreted by the software method [9], but this slows execution of the instrument functions and increases response time to control actions of the bus. Some change to the instrument electrical circuits is also required, which under laboratory conditions is not always convenient, and for ship systems is often impermissible. Therefore, for these instruments and for instruments that realize their basic functions on a base of analog and digital electronic components, it is advisable to use separate standalone modules that realize the functions of process matching.

Let us call the means that interpret the functions enclosed between sections  $S_2$  and  $S_4$  in fig. 2 an interface card.

As follows from [10-12], as a function of the number of interface functions and complexity of generated protocols, hardware implementation of the interface card (IK) requires 40-60, and for complex instruments up to 80 packages of microcircuits and a number of other components. In reconfiguring the system, the matching functions of the new processes most often do not coincide with the similar functions of the preceding ones, which requires replacement of the interface card. Reworking of interface cards in the case of their hardware implementation requires large inputs of labor and time and is unacceptable. The optimal solution lies in developing a universal interface card that provides for matching of processes flowing in fundamentally different instruments. It is not possible to solve this problem by hardware implementation of the functions because of the complexity of such a device, in particular the circuits for implementation of the protocols. This problem has not been solved even with the emergence of LSI circuits (BIS) for hardware interpretation of interface functions described in [13]. These LSI circuits, though they do reduce to 10-15 packages the amount of apparatus that interprets the functions enclosed between sections  $S_3$  and  $S_4$  in fig. 2, have almost no effect on the amount of apparatus that interprets the functions between sections  $S_2$  and  $S_3$ . Despite the fact that attempts at developing universal interface cards for narrow

## FOR OFFICIAL USE ONLY

classes of instruments were quite successful [12, 14], they do not solve the problem posed as a whole. It can be solved only under the condition of application in interface cards of the most modern developments of electronic components: microprocessors and LSI microprogrammable logic. In the general case, the universal interface card that implements matching of the overwhelming majority of instruments applied within LSRAS must ensure execution of all the functional capabilities offered by the IEC bus and compatibility at the electrotechnical and mechanical levels. With respect to the instrument, it must provide the capability of input and/or output of command words and data with a size of no less than 40 bits, manual addressing under the conditions of no addresses and easy changing of the instrument address in the process of system operation. It must also provide the capability of forming any protocols permitted by the standard and all conversions of data and instrument commands with that, including calculation, as well as indication of extreme operating conditions (no-address and malfunction situations). All necessary functions of interface card inputs/outputs with respect to an instrument must be performed in the process of interpreting FSF [format match functions], and communications by direct electrical connections of the corresponding inputs/outputs of the interface card and the instrument. It is also necessary to ensure the maximum exchange rate.

From these requirements, it is clear that a universal interface card must contain at least storage for programs that interpret functions, working storage for intermediate values of auxiliary variables used in forming protocols, I/O hardware for communication with an instrument, apparatus for matching with the IEC bus at the electrotechnical and mechanical levels, as well as a processor that executes the instructions of the interpreting program. However, in this case it will not be possible to ensure the maximum possible speed; therefore, it is advisable to incorporate in the universal interface card a microcircuit for hardware interpretation of interface functions. Shown in fig. 3 is the structure of a universal interface card built with nine microcircuits. Instructions in the programs that interpret protocol matching functions (and when necessary, the extended instrument functions too) and are stored in a ROM (PZU) with a size of 2K bytes are executed by the central processor [CPU] (TsP). Used for communication with instrument functions are two microcircuits (MC), each of which contains 256 bytes of working storage and three programmable I/O ports: two with 8 bits each (A and B) and one with a length of 6 bits (C). Each port can be programmed for input or output by setting the appropriate bits in the internal status register (STAT) in the microcircuit. Six-bit ports, in addition to data I/O, can perform the functions of synchronizing registers for asynchronous exchange of data with an instrument. The microcircuits also contain timers (TIM) and can generate requests for interruption of the CPU when the eight-bit registers are full or empty or upon expiration of a time computed by the timer. Used for interpretation of interface functions is a separate microcircuit (MIF) that has logic circuits and also 18 control and status registers accessible for CPU reads or writes. The registers are used for interaction between the CPU and the interface function interpretation circuits. The MIF has the capability of interrupting CPU operation for a number of internal reasons by sending an INT signal to output. The CPU can store in the MIF the addresses of acceptors and sources assigned to processes being matched by using the interface card, data and status bytes for transmission to the IEC bus; and assign the code for the line end symbol, the mode of operation for an exchange (acceptor or source), masks for interruptions, commands and data to ensure the appropriate modes of

FOR OFFICIAL USE ONLY

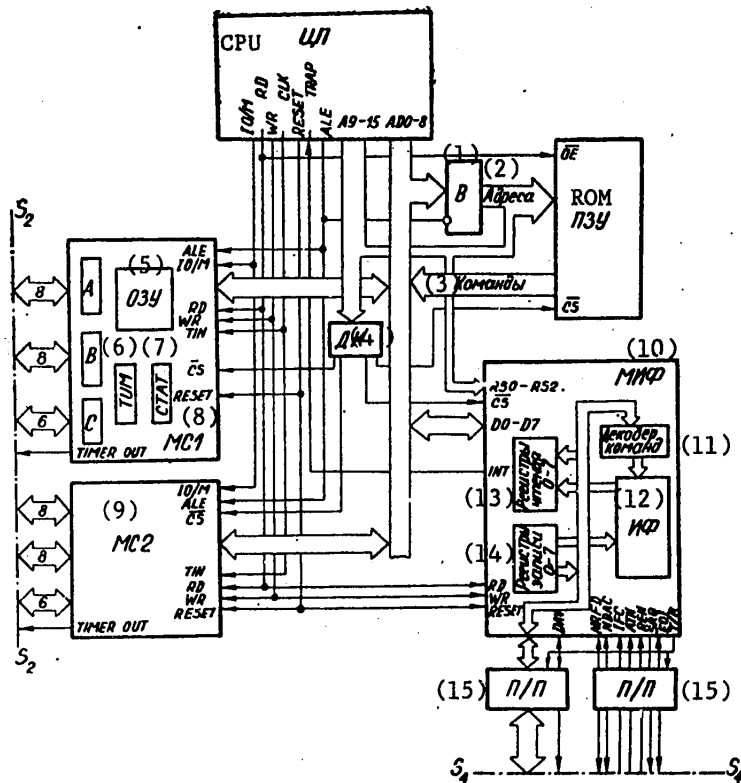


Fig. 3. Simplified structure of a universal interface card

Key:

- |                           |  |
|---------------------------|--|
| 1. V [gate]               | 9. MS2 [microcircuit 2]  |
| 2. addresses              | 10. MIF [microcircuit for interpretation of interface functions] |
| 3. commands               | 11. command decoder  |
| 4. DK [decoder]           | 12. IF [interface functions]                                     |
| 5. OZU [working storage]  | 13. read registers, 0-7  |
| 6. TIM [timer]            | 14. write registers, 0-7   |
| 7. STAT [status register] | 15. P/P [transceivers]   |
| 8. MS1 [microcircuit 1]   |  |

operation. The CPU can read from the registers bytes of data obtained from the IEC bus, interruption status bytes, addressings and statuses sent to the bus during serial polling (STB), as well as current values of addresses of the process being matched, bytes of multiline commands not understood by the circuits interpreting interface functions and bytes of secondary addresses that are recognized by the software method. Among the features of the structure of the suggested universal

FOR OFFICIAL USE ONLY

## FOR OFFICIAL USE ONLY

interface card is that the data transmission lines between the microcircuits are coincident with the low-order lines of addresses. Used to separate addresses and data is the ALE strobe sent by the CPU at the appropriate times. The microcircuits have the necessary circuits to realize separation of addresses and data, and for the ROM, an eight-bit microcircuit of strobed gates (V) is used. All commands fetched from the ROM and data stored in working storage and MIF registers have through addressing through the internal bus for the interface card. In the process, the physical addresses are distributed in the array of addresses (from 0 to 64K) generated by the CPU by the connection of the CHIP SELECT (CS) microcircuit inputs through a decoder of type 1 of 8 (DK) to the noncoincident lines of CPU addresses. Virtual addresses may be specified instead of physical addresses when the appropriate cross-assembler is available in the process of compiling the programs for interface function interpretation. The isomorphism between the virtual and physical addresses with regard to the features of the apparatus is established the following way:

name of variable EQU physical address  
and for the ROM  $A_p = A_c$ ,

$$\text{for OZU1 } A_p = A_c + D_1 = A_c + 1900_{16},$$

$$\text{for OZU2 } A_p = A_c + D_2 = A_c + 2000_{16},$$

$$\text{for MIF: } A_p = A_c D_3 + D_4 = A_c 100_{16} + 3800_{16}.$$

Here,  $A_p$  and  $A_c$  are the physical address of the first byte of the command or data and this same address within the array of addresses of the corresponding microcircuit and  $D_{1,2,3,4}$  is the displacement of addresses due to organization of communications in the interface card.

These addresses are accessible for processing by the usual CPU commands. The microcircuit I/O ports are used only by I/O commands. OZU [working storage] is shared through the IO/M inputs. The physical address of the port, status register or timer may be determined by the formula  $A_p = A_c + D_{mc}$ , where  $D_{mc}$  is the displacement of the address for the given microcircuit, equal for MC1 to  $18_{16}$  and for MC2 to  $20_{16}$ .

Matching with the IEC bus at the electrotechnical level is effected by using the LSI circuits of the bus transceivers (P/P) that can operate in four different modes as a function of what code is sent to the control inputs. For data lines, the transceiver operates in mode 1, and for command lines, mode 0. The type of plug and connecting cable stipulated in the standard is used for matching at the mechanical level.

The operator has the capability of turning on the power, making the initial setting and switching the LISTEN ONLY and TALK ONLY modes. Input of the address is effected by means of port B2 which is assigned as input during all interpretations. In doing so, input via the two high-order bits are the statuses of the LISTEN ONLY and TALK ONLY switches; the next two bits are allocated for the high-order decade

## FOR OFFICIAL USE ONLY

of the binary-decimal code of the address (maximum address does not exceed 31), and the last four bits are for the low-order decade of the address. Information for displays is output through the three high-order bits of port C2 which must be assigned as output with all interpretations. Remaining bits can be used to output instrument control commands. Other than those described above, no other restrictions are imposed on the interpretation of functions.

The interface card built that way provides the capability of interpreting the functions for coordination of the overwhelming majority of processes (from the simplest to the very complex) that make up an automated experiment in LSRAS on USSR AS ships.

With a high degree of confidence, one can state that what has been said is true too for the majority of LSRAS in general.

Let us consider the basic principles of development of programs for interpreting functions for coordination of processes by using the interface card described in the example of a laboratory pH-millivoltmeter. The instrument analyzes (measures) the characteristics of samples of sea water by using various electrodes. In doing so, the PF [instrument functions] generate a word of data that can be read on a digital display or sent outside in one of three modes initiated by using the appropriate controls. The instrument receives commands externally for start up, waiting and keeping results at output. The commands and data, intersecting section  $S_2$  in both directions for the pH-millivoltmeter, are shown in fig. 4. In analyzing the composition of signals, sent through section  $S_2$ , one can state that from the viewpoint of interaction in the system, the instrument is simple. Sufficient for such a system is the set of interface functions: AH1, SH1, T5, L2, SR1, DC2 and DT1. In the process, it will receive the capability of receiving multiline commands and addresses, sending data through the IEC bus, being started and put in the wait mode, and sending the controller status-bytes during serial polling and requests for service in event errors occur. In developing the interpreting program in the interface card, all ports for communication with the instrument except C2 should be designated as input. In the process, output through the high-order bits of C2 are data to the displays, while the low-order bits must be designated for output of the commands MEASURE, WAIT and NO DATA CHANGE. Decades of data are input through ports A1 (high-order decades) and B1. The high-order decade is sent first to the bus. To simplify the interpretation program, the sign is input through the low-order bit of port C1. Information on the mode of operation and availability of the instrument goes through port A2, and the values of the bits of the port are selected in accordance with the recommendations [7] on generating status-bytes. The three low-order bits are allocated for modes of measuring (polarization current, pH and millivolts, respectively), bit 6 for the measuring readiness flag, and bit 8 for the overflow flag. In addressing, the instrument will send to the IEC bus a message in the format FMMSDDDE, where F is the overflow flag (an S or blank in the absence of overflow), MM is the mode mnemonic (IP, pH or mV, respectively), S is the data sign (+ or -), DDDDD is the data field taking the floating point into account, and E is line end symbol (; or carriage return). The line end flag (END on line EOI) is sent to the bus simultaneously with the last symbol. All data bytes are coded in ASCII (KOI-7) seven-bit code. Two types of errors are introduced that require display and controller response: instrument errors (no mode set, instrument not turned on or not working) and IEC bus errors (instrument is addressed as a data source, but there are no addressed receivers on the bus). Shown in fig. 5 are the contents of the MIF registers suggested for the described

## FOR OFFICIAL USE ONLY

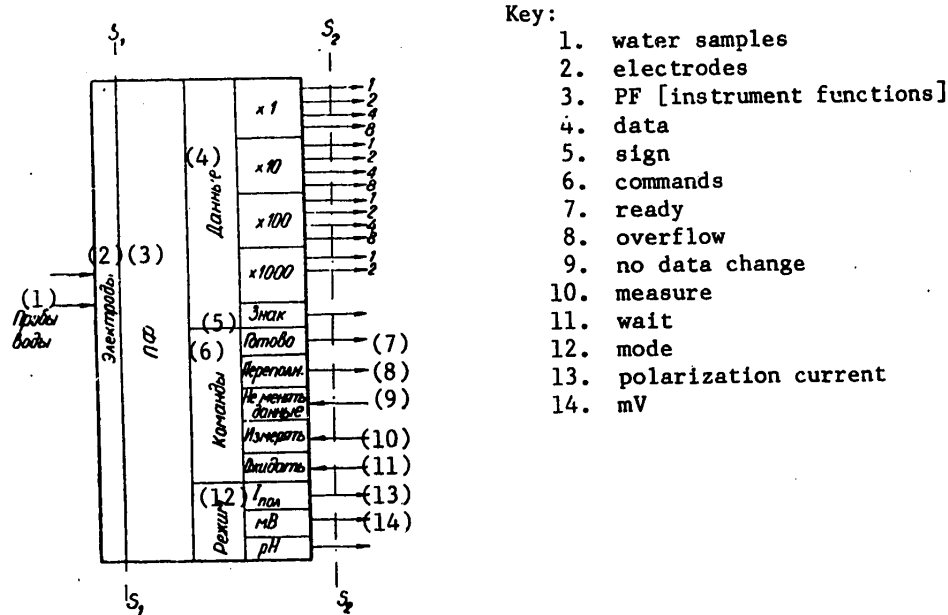


Fig. 4. Interaction of laboratory pH-millivoltmeter with system and external environment

pH-millivoltmeters. Registers are grouped in pairs so that each pair corresponds to one address  $A_c$ , and one register is used only for writing and the other only for reading of data. The addresses  $A_c$  are indicated along with each pair. The purpose of the registers and their individual bits used in interpretation of FSF [data format matching] is as follows. The output register is used to send the MIF data bytes in a series defined by the format shown above. The MIF then sends these bytes to the IEC bus, matching the transmission of each byte with the receivers. The data input register is not used. The interrupt mask and status registers are used for output of CPU interruption signals under conditions (bits) specified in the mask registers, when the bit in the status register is set. Bits are set in status registers by MIF apparatus independently of bits in mask registers. GET, DEC and ERR designate, respectively, multiline bus commands for starting the instrument, setting it in the initial state (waiting) and the occurrence of bus errors. BO is the next byte output to the bus. INT is the status of output INTERRUPTION (INT) MIF. SPAS is the status "serial polling activated" of interface function T. SPASC and ADSC are respectively the change in status of serial polling and addressing of the instrument on the bus. The registers for the mode and status of serial polling are used to send to the IEC bus the status-byte with the capability of its storage and reading in the MIF. In addition to the instrument mode bits described above, bit 7 in the register for status of serial polling is used for writing a request for service, which the SR interface function sends to line SRQ of the IEC bus and sets in the process the SRQS flag in the status register; bit 4 used for error display and bit 5 for the wait mode. Registers for the mode and status of addressing are used to indicate the mode of addressing of the

## FOR OFFICIAL USE ONLY

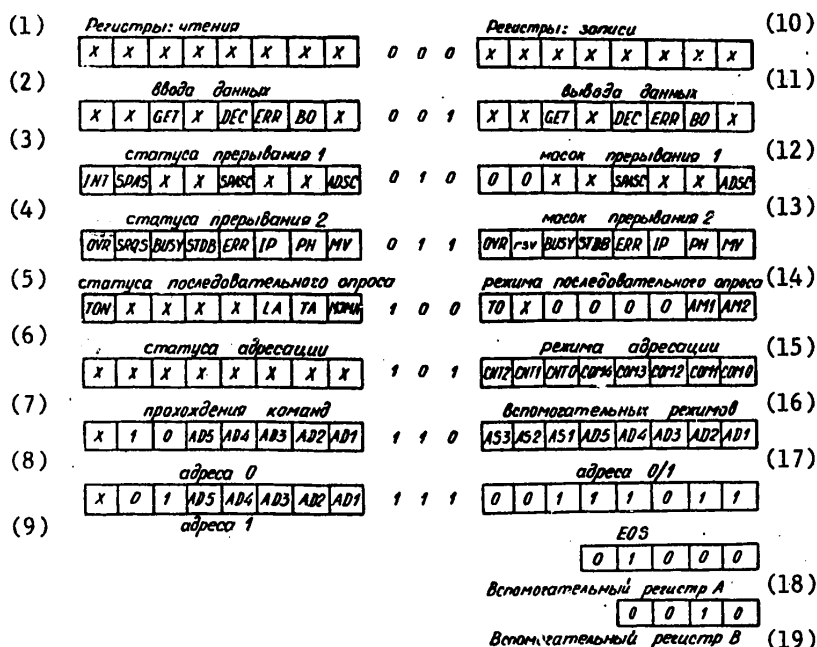


Fig. 5. Contents of MIF [microcircuit for interpretation of interface functions] registers during interpretation of functions for interface of pH-millivoltmeter

## Key:

- |                             |                             |
|-----------------------------|-----------------------------|
| 1. registers: reading       | 11. data output             |
| 2. data input               | 12. masks of interruption 1 |
| 3. status of interruption 1 | 13. masks of interruption 2 |
| 4. status of interruption 2 | 14. mode of serial polling  |
| 5. status of serial polling | 15. mode of addressing      |
| 6. status of addressing     | 16. auxiliary modes         |
| 7. passage of commands      | 17. address 0/1             |
| 8. address 0                | 18. auxiliary register A    |
| 9. address 1                | 19. auxiliary register B    |
| 10. registers: writing      |                             |

interface functions T and L. Ton is talk only (manual addressing), AM=01 is the address in the address registers, LA and TA mean that the instrument is active on the bus as either a data listener or talker, and bit MJMN indicates just which address is activated. Auxiliary command register is used to store information in auxiliary registers A and B (100 and 101 in field CN, data in field CO) and for issuing several auxiliary MIF commands. The command passage register is not used. Through the address 0/1 register, the CPU can store the addresses of the acceptor and (or) the source in MIF address registers and indicate which address pertains to interface function 1, and which to T. The line end symbol code E can be stored

## FOR OFFICIAL USE ONLY

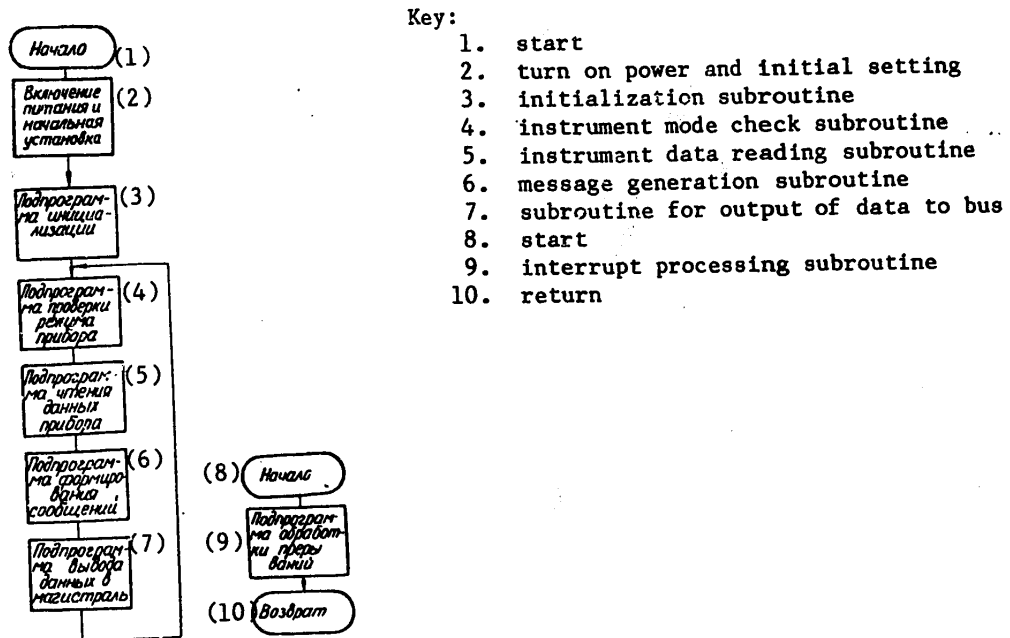


Fig. 6. Consolidated structure of the program for interpretation of functions for interface of laboratory pH-millivoltmeter

in the EOS register. Bits in the auxiliary registers A and B in the given interpretation are set in such a way that the MIF puts out the END flag together with the status-bytes and each byte that coincides with the contents of the EOS register.

Thus, the task of interpretation is reduced to forming the initial configuration of the hardware for the interface card by storing the necessary data in the appropriate registers, providing for transmission of bus commands to inputs MEASURE, WAIT and NO DATA CHANGE, display of errors and generating lines FMMDDDDDE of data words shown in fig. 4. In forming the initial configuration, it is necessary to enter data in the addressing mode register and the address registers. The structure of the interpreting program must be built in such a way that precludes the effect of a possible operator error or other actions that would lead to an unauthorized change of the instrument address in the set of addresses in the process of performing the experiment. The structure of the program for interpretation of the FSF for the pH-millivoltmeter is shown in fig. 6. The program cyclically polls the instrument and as measurements are available generates and outputs lines FMMDDDDDE to the bus. All actions for issuing commands to the instrument and sending to the bus of status-bytes are performed by the interrupt processing program; control is transferred to its starting address (24<sub>16</sub>) in each interrupt situation. If any error occurs, the interface card sends to the bus a request for service and lights the error display, and program execution is terminated. The initial sector of the program is loaded at address 0. Control is transferred to

## FOR OFFICIAL USE ONLY

this address right after the initial setting for the interface card apparatus when power is turned on. Taking the port B2 read commands to the initial sector makes it possible to eliminate the undesirable effect of an unauthorized address change, which can now be done only after pressing the initial setting button, which is highly improbable. The actions performed by the subroutines shown in fig. 6 are clear from their titles. The subroutines contain waiting peaks and internal cycles and perform the required calculations to determine the place of the point in the data field.

In conclusion, let us note that organization of instrument-computer interaction in LSRAS must be performed on the basis of using standard interfaces; of these, the IEC bus is preferred for the majority of ship scientific research automation systems. To match instruments with this bus within the LSRAS, it is advisable to have several universal interface cards on a base of microprocessors and LSI programmable logic. The suggested structure of the interface cards allows matching with the IEC bus any instruments with parallel or serial input and (or) output of data used in oceanologic research, and also allows expanding the instrument functions when necessary. The suggested interface card is used in several laboratories on the "Akademik Mstislav Keldysh" scientific research ship to interface various measuring instruments and sounding devices to computers. The suggested structure of the program that interprets the FSF [format matching functions] provides protection from an unauthorized change to the instrument address without reducing the flexibility of the system as a whole.

## BIBLIOGRAPHY

1. Yakubaytis, E. A., "Problems of Developing Computer Networks," AVT, No 1, 1980, pp 3-10.
2. Tannenbaum, E., "Mnogourovnevaya organizatsiya EVM" [Multilevel Organization of Computers], Moscow, Mir, 1979, 547 pages.
3. "A Modular Instrumentation System for Data Handling, CAMAC System, IEC Standard, Publication 516," 1st ed., Geneva, IEC, 1975, 65 pages.
4. "Multiple Controllers in a CAMAC Crate," EUR 6500, ECSC-EEC-EAEC, Brussels-Luxemburg, 1978, 32 pages.
5. "CAMAC. The Definition of IML. A Language for Use in a CAMAC System Endorsed by the ESONE Committee and the EAC NIM Committee," ESONE/IML/01, ESONE Committee, B2440 Geel, Belgium, October 1974, 36 pages.
6. "IEEE Standard Digital Interface for Programmable Instrumentation," IEEE Std. 488-1978, IEEE, NY, Nov. 30, 1978, 83 pages.
7. "Interface System for Programmable Measuring Apparatus, Byte Serial Bit Parallel, Code and Format Convention," (Draft), 1976, N 17, IEC, TC66/WG3.
8. Kolpakov, I. F., "Selection Criteria of Standard Interfaces," 1st Europ. Symp. on Real-Time Data Handling and Process Control, (West) Berlin, Oct. 1979, 5.1.a-4.

FOR OFFICIAL USE ONLY

9. Benes, E.; Harms, K. and Wimmer, L., "A Microprocessor-Oriented Measurement and Control System," in "Microcomputer Architectures," 3rd EUROMICRO Symp. on Microprocessing and Microprogramming, October 3-6, 1977, Amsterdam, North-Holland Publishing Company, 1977, pp 143-150.
10. Gorelikov, N. I.; Domaratskiy, A. N.; Domaratskiy, S. N.; Ponenko, N. V. and Sitnikov, L. S., "Requirements for System Functions of Measuring Instruments according to the IEC Standard," PRIBORY I SISTEMY UPRAVLENIYA, No 3, 1980, pp 15-19.
11. Domaratskiy, A. N.; Domaratskiy, S. N.; Liskin, V. A.; Ponenko, N. V. and Sitnikov, L. S., "Interface Cards according to the IEC Standard for Perforator and Photo Reader," PRIBORY I TEKHNIKA EKSPERIMENTA, No 4, 1979, pp 109-118.
12. Domaratskiy, A. N.; Domaratskiy, S. N.; Ponenko, N. V. and Sitnikov, L. S., "Interface Cards for Voltmeters and Multimeters for Instrument Bus according to the IEC Standard," PRIBORY I TEKHNIKA EKSPERIMENTA, No 5, 1980, pp 74-79.
13. Pieper, I. and Grossi, R. I., "LSI Streamlines Instrument Interface with Standard IEEE-488 Bus," ELECTRONICS, April 26, 1979, pp 145-150.
14. "Five More DVM's Compatible with IEEE-488," THE FLUKE REVIEW, June 1979, Fluke (Holland) BV, Filburg, The Netherlands, 4 pages.

COPYRIGHT: Izdatel'stvo "Zinatne", "Avtomatika i vychislitel'naya tekhnika", 1981

8545

CSO: 8144/0128

FOR OFFICIAL USE ONLY

UDC 681.32:551.46:53.08

INTERACTION OF COMPUTING PROCESSES IN AUTOMATED RESEARCH VESSELS

Riga AVTOMATIKA I VYCHISLITEL'NAYA TEKHNKA in Russian No 1, Jan-Feb 82  
(manuscript received 30 Mar 81) pp 12-21

[Article by O. S. Zudin, S. N. Domaratskiy and I. Lindfors: "Organizing the Interaction of Computing Processes in Variable-Structure Systems for Automating Scientific Research"]

[Text] The most important indicators of the efficiency of multipurpose scientific research vessels for studying the world ocean are the volume and quantity of data collected and processed during a cruise and expenditures for reorganizing the program of the cruise and essential downtime between cruises. Solving the problems of data collection and processing is inconceivable today without automation of research, without installing measurement and computer hardware combined into a unified system for automation of scientific research (SANI) on the ship. Automation of research on multipurpose scientific research vessels is made more complex by the unique character of particular experiments, the necessity of collecting data from large areas over long periods of time and in a broad range of studies, the existence of a large number of measured parameters and measurement techniques, the diversity of algorithms for recording and processing data using deck, towed, and sounding equipment, the necessity of rapidly restructuring the automation system to conform to the requirements of new experiments, heightened requirements for system reliability, and the like. This task is made even more complex by the fact that the research contingent is not constant from one cruise to another, while the data recorded both during the cruise and after its completion must be accessible and understandable to a broad range of specialists in different fields of science who did not participate in preparation for and actual conduct of the particular experiment.

Meeting these sometimes conflicting requirements makes it necessary to design a SANI with flexible and quickly reorganizable structure, easy to master, simple to use, with graphic representation of intermediate and final results.

Work [1] reviewed the basic principles of constructing SANI's for multipurpose research ships using the example of the integrated system for automation of scientific research of the research vessel Akademik Mstislav Keldysh, which was built for the USSR Academy of Sciences at the Hollming AO shipyard in Finland.

This system consolidates measurement and computer instruments and hardware, devices for sounding the body of water, and devices to measure different parameters of the environment, with subsystems for data recording and processing, into a

## FOR OFFICIAL USE ONLY

single integrated complex. The final product of recording is files in standard format with data in the form of values of the measured and computed parameters. The information contained in these files may be subjected to further directed processing in the ship's processing subsystem and at on-shore computer centers. The values of the recorded parameters are fed to the system both directly from various sensors, measuring instruments, and subject subsystems and manually, using a keyboard, by operators of laboratory computers based on the results of visual observations of the state of the environment or laboratory analyses of samples taken.

Let us dwell in greater detail on the methods and procedures which are the basis for formulating the software of the SANI and make it possible to restructure the system for new experiments in a fairly flexible way with minimum expenditures. The basis for this is including the appropriate resources in the recording subsystem: system tables, means of generating, maintaining, and updating them, and certain procedures for organizing interaction of computing processes taking place at different levels of the system hierarchy. In this case, according to [1], we will bear in mind that the state of the computing processes in the system at any moment in time is determined by the program, the current steps of this program, and the state of program variables and input-output units.

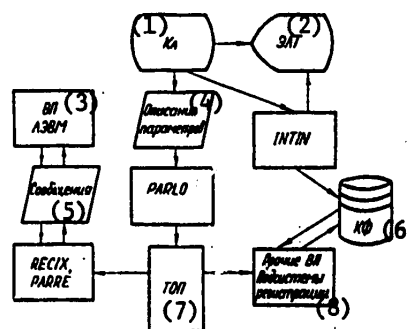
One of the most important resources of the system is the Table of Parameter Descriptions (TOP), which makes it possible to break the full set of parameters recorded in the SANI down into subsets assigned to definite laboratories or subject subsystems and to describe each element of them. The TOP is generated or updated during adjustment of the system for a certain group of experiments. The recording subsystem insures recording of the values of those, and only those, parameters whose descriptions are contained in the TOP at the current moment. The elementary TOP entry, describing one parameter, contains mandatory and optional fields. The mandatory field includes, as a minimum, the name of the parameter and units of measure of its values, the type of sensor or measuring instrument, the format and type of values obtained, and a description of its subset affiliation and reference to use in other resources. The subset affiliation is described by a composite code whose first two characters are a mnemonic abbreviation of the subset name; the next four digits indicate the ordinal number of the parameters in the subset, if other methods of ordering elements are not used. The optional fields appear in TOP's when they are oriented to standard formats for records of finite files with data. Table 1 below shows the format of the elementary TOP entry and an example of recording one of the parameters recorded by the automatic weather station of a synoptic weather laboratory compiling a finite file in a format close to that of work [2].

As a rule the SANI is restructured for new experiments by connecting equipment to it to measure new parameters, which also requires a certain restructuring of programs at all levels of the hierarchy. To minimize expenditures for reconfiguration the software of the Integrated System of the research ship Akademik Mstislav Keldysh is built on the modular principle. The functions of primary processing, transmission, sorting, and storage of data are distributed among the computing processes, which are defined by particular program modules so that the required changes touch the minimum number of these modules.

FOR OFFICIAL USE ONLY

## FOR OFFICIAL USE ONLY

Figure 1. Structure of Interaction of Computing Processes During Generation and Updating of TOP and Formation of Files.



Key: (1) Keyboard; (2) Cathode Ray Tube (Display); (3) Computing Process of Laboratory Computer; (4) Parameter Description; (5) Messages; (6) Finite File; (7) TOP; (8) Other Computing Processes of Recording Subsystems.

Figure 1 shows the structure of interaction of computing processes during generation (updating) of the TOP, transmitting information on a parameter from the recording subsystem to the laboratory computer at the request of an operator, and formulating new files. The computing process defined by the PARLO program receives entries on new or changeable parameters from the terminal in the format shown in Table 1 and structures the TOP in the computer memory of the recording subsystem. The volume of the TOP is defined by the program of the cruise and does not exceed 300-500 entries in the system under description. The computing process defined by the PARRE program, when requested by the laboratory computer, finds the necessary description by its composite code and sends the laboratory computer a message which contains information on the queried parameter.

Table 1.

No.	Content of Field	Primary Field	Length, bytes	Displacement from Start, bytes
1	Code of parameter by classifier	No	4	0
2	Name of parameter	Yes	15	4
3	Code of unit of measure	No	3	19
4	Name of unit of measure	Yes	11	22
5	Scale 1	No	8	35
6	Scale 2	No	8	41
7	Attribute 1	Yes	7	49
8	Definition of attribute 1	Yes	11	56
9	Attribute 2	No	7	67

[Table continued, next page]

## FOR OFFICIAL USE ONLY

[Table 1 continued]

No.	Continent of Field	Primary Field	Length, bytes	Displacement from Start, bytes
10	Definition of attribute 2	No	11	74
11	Type of sensor	Yes	10	85
12	Code of measurement technique by classifier	No	2	95
			1	97
13	Number of characters after comma	No	1	97
14	Total length of value in characters	Yes	2	98
15	Format identifier	Yes	1	100
16	TSS index	Yes	4	101
17	Composite code of parameter in SANI	Yes	6	105
18	Reserve	No	3	111
19	Word description of measurement technique	No	29	114

Example of recording the parameter of air temperature measured with a precision down to tenths of a degree using a sensor of an automatic weather station installed at a height of 20.5 meters from the deck on the starboard side:

000000	GATE CODE:	5000
000001	PARAMETER NAME:	AIR TEMP SR
000002	UNIT CODE:	500
000003	UNIT NAME:	DEG C
000004	SCALE 1:	1.000000
000005	SCALE 2:	0.000000
000006	ATTRIBUTE 1:	20.5
000007	DEFINITION 1:	HEIGHT, M
000008	ATTRIBUTE 2:	-
000009	DEFINITION 2:	-
000010	SENSOR:	DTS-11
000011	METHOD CODE:	80
000012	LENGTH OF DEC.:	1
000013	TOTAL LENGTH:	06
000014	VALUE TYPE:	F
000015	STATE TABLE IND.:	0059
000016	COMPOSITE CODE:	MS0021
000017	RESERVED:	
000018	METHOD DESCR.:	PLATINUM RESIST. OF WEATHER ST

## FOR OFFICIAL USE ONLY

The programs which provide for transmission of data among subsystems of different levels are singled out in a separate group. The formats of the fields of data of transmitted messages have been standardized so that the modules of the communications programs can remain constant when the subsystem is adjusted for different experiments. The protocols selected for the communications lines between laboratory computers and the recording subsystems are subsets of well-known standards ISO-1745 and X.25, while the communications lines for subject subsystems of the automatic weather station type use simplified procedures that resemble the BSC [3].

Because the protocols do not affect the essential features of the messages themselves, we will describe here some principles of formulating them that make it much simpler both as a problem of reconfiguration of software when the system is adjusted for new experiments and a problem of retrieving recorded data. Whereas the water sounding experiment cited in [1] changed the set of sensors and adjusted the work of the submarine and deck units, with traditional procedures that depersonalize data and give the right to identify it to the computing process defined by the recording program it is necessary to make changes in practically all programs related to the experiment. To avoid this, the system being described realizes the principle of data self-identification [4], where all data being received are given tags that indicate their type, properties, time and place of recording, and so on.

Tagging data in the SANI's of multipurpose scientific research vessels should be done beginning from the lowest levels of the hierarchy. At each level, as the result of the operation of the corresponding computing process, the data that are transmitted to the higher level are formulated. Tags are added to these data. Their principal purpose is to organize the interaction of computing processes taking place at the next hierarchical level of the system. We will identify two levels of tags conforming to their purposes. First-level tags (developer tags) are designated for controlling interaction of computing processes defined by known program modules in the process of recording data. Second-level tags (user tags) are designated to give greater informational value to data during subsequent processing and for control of the processes of sorting and retrieving needed elements of a set of recorded data. The programs of these processes are determined by the user and may be unknown in the stage of system development.

The number and composition of developer tags transmitted with the data from certain computing processes to others at different levels of the hierarchy depends on system structure. For instruments and sensors only the simplest developer tags are needed, such as the tags for type and quality of data, for example the code of the RR regime and the overflow sign P in the message PRRZDDDDK for laboratory pH-millivolt meters [5]. Other tags of this type include the code of the quantity being measured or the number of the sensor in a set where there is a large number of similar sensors. We consider information on physical overloading of an instrument and on a quantity going outside the boundaries of the measurement range to be quality tags that describe the degree of suitability of the data for processing; in the case of more complex microprocessing instruments such tags may be data on errors that are recognized. When a new instrument is connected to the laboratory level in a laboratory computer the computing process that receives incoming data must be determined. This computing process

## FOR OFFICIAL USE ONLY

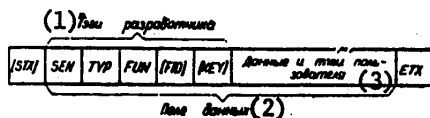
may be expanded into a series of simpler processes, each of which corresponds to one program module and performs one particular operation. For example, for the laboratory pH-millivolt meter data may be dumped in a dump file based on the value of quality tag S by computing process No 1 that makes a quality check, while on the basis of the value of an MV type tag the data are transferred to computing process No 2, which receives the data measured in volts (or millivolts). When the processes are expanded by the values of user tags the new computing process may be defined so that it includes primarily program modules that already exist, with a small number of new (or modified) modules. This greatly reduces the time required for reconfiguration of software at the level of the laboratory computer. We should note that at this level in the stage of preliminary data processing user tags with values of recording time are added to them. In our opinion, this is essential for the SANTI's of multipurpose scientific research vessels.

In order to speed up the reconfiguration of software in the messages being transmitted to the recording subsystem, there must be the following developer tags at a minimum: the sender tag, which indicates precisely which one of the similar computing processes originated the message that has arrived; the type tag, which describes the affiliation of the process to a certain group of computing processes of the recording subsystems; and, the tag for the message function in the subsystem. In addition, for data from prolonged measurements there must be a tag to indicate the name of the file for recording, while for data from one-time measurements a key parameter tag is needed to show the subset of recorded parameters with which the particular message should be associated. Figure 2 shows the structure of a field of data messages transmitted to the recording subsystem of the Integrated System of the scientific research ship Akademik Mstislav Keldysh, while Table 2 indicates the values of the developer tags for all types of system messages. The data in the messages are encoded with characters of the standard seven-bit code ISO-646 (Soviet analog KOI-7 GOST 13502-74). When the composition of the available subsystems is changed this set of developer tags makes it possible to limit changes in the recording subsystem to simply editing the TOP, and when a new subsystem is connected to the SANTI the only thing necessary is to develop one more program for receiving messages, without significant changes in existing software.

The most frequently used user tags are parameters such as the date, time, and place (latitude and longitude) of the experiment, the identifier of the researcher, and parameters that describe the environment: direction and velocity of wind, air temperature and humidity, sea state, direct and reflected solar radiation, and the like. Second-level tagging requires inclusion of another resource in the structure of the recording subsystem: internal memory, a supervisor Table of the State of the Ship, system, and environment (TSS). This resource is structured and modified concurrently with the TOP and contains the current values of parameters that can potentially be used as user tags. Figure 3 below shows the structure of the TSS. The names of the parameters whose values form the TSS are defined in the TOP by non-empty values of the TSS index (see Table 1 above). All elements of the table are put in order according to the value of the index. Because the format of parameter values is not known in advance and may change many times in the TOP during the life of the system, a two-level structure is used for the TSS that makes it possible to modify its format and dimensions on an operational basis.

## FOR OFFICIAL USE ONLY

Figure 2. Format of the Field of Data Messages Transmitted to the Recording Subsystem.



Key: (1) Developer Tag;  
 (2) Data Field;  
 (3) Data and User Tags;  
 (STX) and (ETX) Control Characters of ISO646 Code;  
 (SEN) Tag of Message Sender;  
 (TYP) Tag of Message Type;  
 (FUN) Tag of Message Function in Recording Subsystem;  
 (FID) Tag of Name of Data Recording File;  
 (KEY) Tags of Key Parameters.

Table 2.

No.	Character Before Data Field	Value of TYP Tag	Value of FUN Tag	Designation
1	STX	0	-	Control message
2	STX	1	1	Sequential reading of values of TSS parameters
3	STX		2	Reading value of TSS parameter
4			3	Entering the value of TSS parameter
5	STX	2	-	Setting up data files
6	STX	3	0	Position during experiment
7			1	Position at start of experiment
8			2	Position at end of experiment
9			3	Environment at start of experiment
10			4	Environment during experiment
11			5	Environment at end of experiment
12			6	Request for description of parameters
13			7	Final request for description of parameters
14	STX	4	1	Data from prolonged measurements - parameters of a cycle
15			2	Data from prolonged measurements - parameters of entry
16			3	End of recording data from prolonged measurements
17	STX	5	1	Data from one-time measurements
18			2	End of recording of data from one-time measurements

[Table 2 continued, next page]

## FOR OFFICIAL USE ONLY

[Table 2 continued]

No.	Character Before Data Field	Value of TYP Tag	Value of FUN Tag	Designation
19	STX	6	1	Starting process in recording subsystem
			2	Stopping process in recording subsystem
20	STX	7	-	Transition of laboratory computer to regime of recording subsystem terminal
21	STX	8	0	Formation of finite files without entry in SZF [possibly locking filter bay]
22			1	Formation of finite files with entry in SGF [expansion unknown]
23	STX	B	1	SZF entry for trans
24			2	SZF entry for DBACK
25		G	0	Starting DBACK process
26			1	Stopping DBACK process
27		TYP	FUN	Response message on receipt
28	S	TYP	FUN	Response message on error

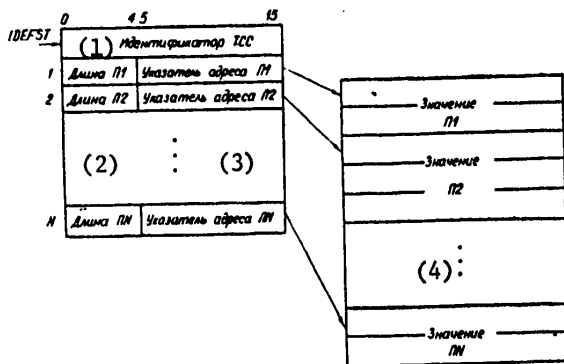


Figure 3. Structure of the TSS.

$\Pi$  are parameters included in the TSS.  
 $1 \leq i \leq N < k$  ( $k$  is the number of parameters in the TOP)

Key: (1) Identifier of TSS;  
 (2) Length [of  $\Pi_1, \Pi_2 \dots$ ];  
 (3) Indicator of [address of  $\Pi_1 \dots$ ];  
 (4) Value [of  $\Pi_1 \dots$ ].

The first part of the TSS contains  $N+1$  words where  $N$  is the number of parameters of the Table (for the system being described  $N = 200$ ) and begins at the heading IDEFST, which occupies one word and makes it possible to localize its position in memory. The  $N$  words that follow contain fields with an indication of length in machine words and the addresses of the first word for the value of each TSS parameter. The second part has variable length and contains as many words as are occupied by all the values of the parameters included in the Table at the particular moment of time taken together. The values of the parameters in the second part of the TSS are periodically updated. Most of them are measured by subject

## FOR OFFICIAL USE ONLY

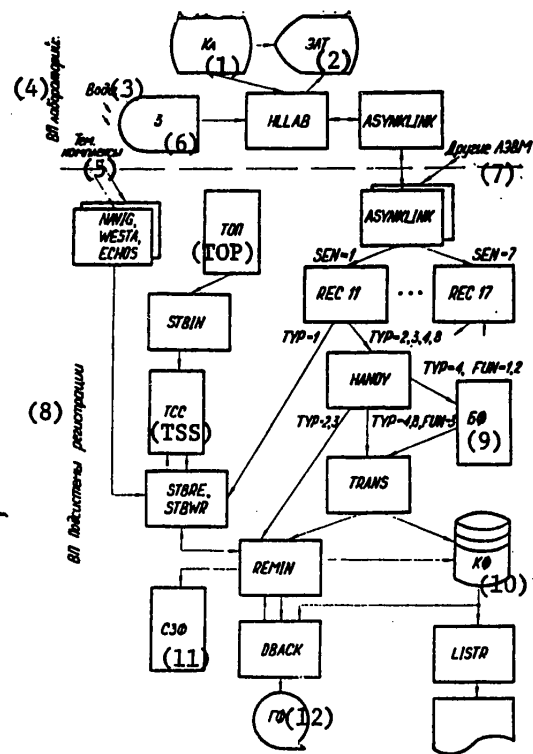
complexes during the entire cruise independently of other experiments, while the rest are obtained as the result of laboratory experiments and observations. Updating times are assigned when the corresponding computing processes are initialized and may be chosen from the set of permissible values for the purpose of increasing system flexibility.

Figure 4 below shows the structure of interaction of computing processes during generation and updating of the TSS, and during recording of data from prolonged measurements of parameters of the water using the hydrologic laboratory equipment in the experiment given in work [1]. Any change in the set of sensors in the underwater unit necessitates an updating of the TOP. For the sake of brevity in describing the interaction of computing processes we will designate each process with the name of its defining program. After each updating the TOP must be analyzed by the computing process defined by the STBIN program, which constructs the internal memory, the supervisory TSS in conformity with the structure shown in Figure 3 above. Parameters are taken from the TOP according to the value of the TSS index. The values of the TSS parameters are updated using the NAVIG, WESTA, ECHOS processes which receive messages from the navigating system (updated at periods of 10 seconds), the automatic weather station (periodicity of 1-10 minutes), the echosounder subsystem of the geophysical laboratory (periodicity of less than one second), and also from the computing processes activated by the programs of the laboratory computers and REC11-REC17 and STBWR programs in the recording subsystem, for example in the case of feeding visual observation data from the keyboard of the synoptic meteorology laboratory computer. The computing processes of the laboratory computers should prepare messages that contain the composite codes of parameters and their values accompanied by the values of the developer tags TYP=1 and FUN=3. When it is necessary to obtain the values of user tags from the TSS by the processes of the laboratory computers, the latter are sent to the message recording subsystem with developer tag values of TYP=1 and FUN=1, 2 (see Table 2 above). Program semaphore engineering is used to protect the TSS against simultaneous access by different computing processes; in this case the next computing process receives access to the resource only after the preceding one has completed its use and thrown the semaphore [6].

When recording data from prolonged measurements a file must first be set up for these data in the recording subsystem. This is done by a statement from the recording subsystem terminal with the help of the INTIN process (see Figure 1 above). Then the computing process of the laboratory computer is activated and, together with the REMIN process, shapes the structure of the file and enters its titles, sending a message with the values of the tags TYP = 2, 3. The necessary user tags may also be put in the file as parameters of the cycle and as recording parameters. This is determined by the content of the message on setting up the file (TYP = 2) which the REMIN process uses to structure the file. The title includes information on the location of the ship and state of the environment. Data for a heading are taken from the TSS by the REMIN process. The computing processes defined by the ASYNKLINK programs transmit messages on communications lines following protocol ISO-1745. After the file is structured the computing programs of the laboratory computers go into operation. In the case of sounding the water with hydrologic laboratory equipment (HLLAB) they request values of the measured parameters from the deck sounding unit, perform preliminary processing and computation of calculated parameters, form messages with data and the values of the developer tags TYP = 4 and FUN = 1, 2, and copy them using the

**Figure 4. Structure of Interaction of Computing Processes During Generation of TSS and Recording the Data of Prolonged Measurements of Environmental Characteristics.**

- Key:**
- (1) Keyboard;
  - (2) Cathode Ray Tube;
  - (3) Water;
  - (4) Laboratory Computing Processes;
  - (5) Subject Complexes;
  - (6) Probe Submerged in Water (Submarine and Deck Units);
  - (7) Other Laboratory Computers;
  - (8) Computing Processes of Recording Subsystem;
  - (9) Buffer File;
  - (10) Finite File;
  - (11) List of Completed Files;
  - (12) Ready File.



110

## FOR OFFICIAL USE ONLY

and set up a finite file, the tag values are TYP = 8, FUN = 1. These messages are transmitted to the TRANS process, which shapes the finite file in the format selected, putting in it entries from the buffer according to the tag value FID, which indicates belonging to a certain file. When a small number of sources are working at one time and the density of data flows is not great, the software can be generated in such a way that messages from the HANDY process can go to the TRANS process, bypassing the stage of storage in the buffer file. In this case, the values of the FID tags are used to record data in the required open finite file.

When receiving a message with the tags TYP = 8, the TRANS closes the file identifiable by an accepted value of the tag FID and immediately sets up and structures a new file, free and ready to receive data, under the same identifier. This permits minimizing the fairly protracted and labor-intensive operations of setting up and structuring files. The user performs these operations just once for each type of file structure.

The interaction of computing processes on different levels of the hierarchy is carried on according to this description, as is interaction when recording data from one-time measurements. But in this case user tags are used as key parameters and play a more important role in shaping the finite file. Requests in the form of composite codes of parameters to add to the values of the user tags selected from the TSS are, by the choice of the laboratory operator (user) included in messages received by the processes REC11-7. The data together with the values of these tags are first stored in a structure close to the data base [7]. Then, based on requests structured according to different user criteria, they may be selected by values of key parameters and grouped in finite files similar to files with data from prolonged measurements.

After completion of a finite file it may be stored on a magnetic disk for some time so that the computing processes of the processing subsystem can request the data stored in it. When the need for this is over, the DBACK process is activated and copies the finite file onto magnetic tape, adding essential information on the cruise, organization, leader of the expedition and experiment, and so on to the title. The ready file is stored on magnetic tape and may be used in the processing system at a later time or transmitted to shore-based computer centers for processing. The LISTR process makes it possible to output a finite file to a display screen or print it for visual monitoring and maintaining the archives.

When forming the finite file the REMIN process makes an entry about it in the third resource of the system, the list of completed files in the format shown in Table 3 below. When it is necessary to get access to data recorded in different finite or ready files, the user scans the contents of the entries in the list of completed files on a screen or initiates a computing process that selects the necessary files according to the contents of the entries. After selecting the necessary files their contents can be manipulated both in the processing subsystem and at shore-based computer centers with the help of computing processes defined by applied programs, making broad use of the values of user tags recorded in the files together with the data.

FOR OFFICIAL USE ONLY

## FOR OFFICIAL USE ONLY

Table 3.

No.	Content of Field	Length, Bytes	Displacement from Start, Bytes
1	Name of Station	6	0
2	Name of Experiment	6	6
3	Name of Medium	12	12
4	Name and Version of File	12	24
5	Time of Creation	13	36
6	Time of Completion	12	48
7	Latitude	7	60
8	Longitude	8	67
9	Number of Parameters	2	75
10	Composite Code $\Pi_1$	6	77
11	Composite Code $\Pi_2$	6	83
12	...		
k+9	Composite Code $\Pi_k$	6	77+6(k-1)

$\Pi_k$  is parameter k recorded in the file.

#### Conclusions

1. The structure of the SANI software of multipurpose scientific research ships must be flexible, easily restructured, accessible for quick assimilation, simple to use, and be able to represent results in graphic form.
2. The flexibility of software structure and possibility of quickly adjusting the SANI to a new group of experiments can be accomplished by introducing three system tables in the recording subsystem (the table of parameter descriptions, the table of the state of the system, ship, and environment, and the list of completed files), as well as means to generate, update, and maintain them.
3. It is advisable to tag data in the SANI of multipurpose research ships beginning from the lowest levels of the hierarchy. Two levels of tags can be identified in such systems. First-level tags are developer tags, designed to control the interaction of data recording processes; second-level tags are user tags, designed to give the data greater informational value in subsequent processing and to control the processes of sorting and retrieving elements of a set of recorded data.
4. The number of developer tags transmitted with the data from certain processes to others at different levels of the hierarchy depends on the structure of the system. With an eye to stepping up the reconfiguration of software it is essential to standardize the formats of the data fields of all messages. Among the developer tags transmitted to the recording subsystem there should be tags for the sender, type and function of the message, recording file, and key parameters. The current values of user tags should be kept in the state table.

FOR OFFICIAL USE ONLY

FOOTNOTES

1. O. S. Zudin, S. N. Domaratskiy, I. P. Kotik, G. N. Kuklin, A. A. Novikov, L. S. Sitnikov, O. Laaksonen, and R. Aarinen, "Integrated Systems of Automatic Scientific Research on Multipurpose Research Vessels," AVT. 1981, No. 6, pp 72-80.
2. "The International Data Management Plan for the GARP Atlantic Tropical Experiment. Part 1. General Description of the GATE Data Management Scheme and Its Specification," Geneva, 1974, April, (GATE Report No 13.)
3. A. Butrimenko, and Dzh. Sekston, "Protocols in Communications Networks for Transmitting Digital Information," AVT, 1978, No 6, pp 56-65.
4. G. I. Marchuk, and V. Ye. Kotov, "Problems of Computer Technology and Pure Research," AVT, 1979, No 2, pp 3-14.
5. S. N. Domaratskiy, O. S. Zudin, and O. Vaynio, "The Organization of Interaction of Instruments and Computers in Variable-Structure Systems To Automate Scientific Research," AVT, 1981, No 3, pp 81-91.
6. E. W. Dijkstra, "Cooperating Sequential Processes in Programming Languages," "Academic Press", 1968 pp 43-112.
7. J. Martin, "Computer Data-Based Organization," 2nd Ed, "Prentiss-Hall Inc.", Englewood Press, N. J., 1977, pp 451-487.

COPYRIGHT: Izdatel'stvo "Zinatne", "Avtomatika i vychislitel'naya tekhnika", 1982

11,176

CSO: 1863/120

## FOR OFFICIAL USE ONLY

UDC 551.46(262.5)

## BLACK SEA HYDROPHYSICAL, HYDROCHEMICAL EXPEDITION RESULTS

Kiev KOMPLEKSNIYYE OKEANOGRAFICHESKIYE ISSLEDOVANIYA CHERNOGO MORYA in Russian 1980  
(signed to press 24 Oct 80) pp 2, 237-238

[Annotation and table of contents from book "An Overall Description of Research Conducted on Aspects of the Black Sea", by Sergey Grigor'yevich Boguslavskiy, Viktor Aleksandrovich Zhorov, Leonid Vasil'yevich Cherkesov, Vladimir Vasil'yevich Yefimov, Geliy Grigor'yevich Neuymn, Nikolay Nikolayevich Karnaushenko, Gennadiy Stepanovich Dvoryaninov, Aleksey Yevtikhiyevich Bukatov, Vladimir Ivanovich Lopatnikov, Valeriy Nikolayevich Yeremeyev, Gennadiy Fedorovich Batrakov, Arnol'd Anatol'yevich Berezovskiy, Svetlana Vasil'yevna Lyashenko, Tamara Nikolayevna Abakumova, Vera Pavlovna Ronkova, Yuriy Mikhaylovich Belyakov, Leonid Anatol'yevich Koveshnikov, Anatoliy Dmitriyevich Zemlyanoy, Lyudmila Alekseyevna Korneva and Lyudvig Dmitriyevich Pukhtyar, Institute of Marine Hydrophysics, UkSSR Academy of Sciences, Izdatel'stvo "Naukova dumka", 1000 copies, 240 pages]

[Text] Problems associated with the hydrophysics and hydrochemistry of the Black Sea are examined on the basis of materials from the latest expeditions, natural experiments and mathematical simulation: small-scale dynamic and thermal interaction between the sea and atmosphere, surface and internal waves, the vertical structure of water, mixing, the light and electromagnetic fields, and aquatic geothermy and hydrochemistry.

This book is intended for a broad range of specialists in ocean science and geophysicists.

Thirty one tables, 108 figures; bibliographies follow each chapter.

	CONTENTS	Page
Foreword . . . . .		3
Chapter 1. Investigation of the Structure of the Boundary Layers of the Atmosphere and Sea		
1.1. Introduction . . . . .		5
1.2. Methods and Apparatus of Traverse Explorations . . . . .		6
1.3. Spectral Characteristics of the Velocity Field and of Prominences in the Wind Wave Layer . . . . .		12
1.4. A Model of the Dynamics of the Turbulent Layer of Wind-Induced Mixing . . . . .		24

114  
FOR OFFICIAL USE ONLY

## FOR OFFICIAL USE ONLY

1.5.	Solution of the Problem for a Dynamic Field. Analysis of Results . . . . .	29
1.6.	A Model of a Surface Thermal Film. Its Influence on Heat Diffusion . . . . .	44
1.7.	The Mechanism of Transfer of Heat by Waves . . . . .	49
Chapter 2.	Wind Waves	
2.1.	Marginal Theoretical Distributions of Heights and Periods . . . .	59
2.2.	Calculation and Analysis of Theoretical Distributions of Frequencies, Lengths and Wave Numbers, and Their Statistics . . .	63
2.3.	Procedure for Calculating Statistical Characteristics and the Confidence Interval of Experimental Data . . . . .	71
2.4.	Development of a Method of Preliminary Calculation of the Elements of Irregular Waves . . . . .	74
2.5.	Experimental Confidence and Conditional Distributions of Wind Waves . . . . .	77
2.6.	Calculation of an Experimental Curve for Distribution of Wave Steepness . . . . .	83
2.7.	Spectral Analysis of Wavegrams . . . . .	87
2.8.	Distribution of the Energy of Waves Visible on the Surface With Respect to Frequencies . . . . .	89
2.9.	Laws and Variability of Experimental Statistical Characteristics.	92
2.10.	Laws and Variability of Spectral Characteristics . . . . .	95
2.11.	Calculation and Mapping of Spectral Characteristics in Relation to the Wind Field . . . . .	98
Chapter 3.	Internal Waves	
3.1.	Typical Oscillation Periods and Generation Mechanisms of Internal Waves . . . . .	103
3.2.	Influence of Horizontal Density Diffusion on Internal Waves Depending on Periodic Atmospheric Perturbations . . . . .	110
3.3.	Influence of Vertical Change in Horizontal Density Diffusion on Internal Waves Caused by Periodic Perturbations . . . . .	115
3.4.	Basic Equations Taking Account of the Vertical Structure of the Velocity, Density and Turbulent Diffusion Fields . . . . .	120
3.5.	Theoretical Models of Continuous Distribution of Current Velocities, Density and Horizontal Density Diffusion . . . . .	122
3.6.	Results of Analyzing Internal Waves in the Central Region of the Black Sea . . . . .	125
Chapter 4.	Hydrological Problems of the Black Sea	
4.1.	Vertical Structure of the Water . . . . .	136
4.2.	Surface Currents in the Black Sea . . . . .	147
4.3.	Vertical Transfer Processes in the Black Sea . . . . .	150
4.4.	Heat Transfer by Currents in the Black Sea Basin . . . . .	155
Chapter 5.	Hydrochemical Cycles of the Black Sea	
5.1.	Equilibrium Elements of the Carbonate System . . . . .	163
5.2.	Vertical and Horizontal Distribution of Hydrochemical and Hydrological Parameters . . . . .	174

FOR OFFICIAL USE ONLY

FOR OFFICIAL USE ONLY

Chapter 6.	Spatial and Temporal Variability of the Black Sea's Radioactive Field	
6.1.	Experimental Results . . . . .	189
6.2.	A Model of Formation of the Black Sea's Radioactivity Field . . .	191
6.3.	Objective Analysis of the Black Sea's Radioactivity Field . . . .	193
Chapter 7.	Optical Characteristics of the Waters of the Black Sea	
7.1.	Vertical Distribution of Optical Properties . . . . .	199
7.2.	Horizontal Structure of Optical Properties . . . . .	206
7.3.	Characteristics of the Light Fields . . . . .	208
Chapter 8.	The Electromagnetic Field in the Black Sea	
8.1.	The Black Sea's Electrotelluric Field . . . . .	216
8.2.	Electromagnetic Pulsations . . . . .	226

COPYRIGHT: Izdatel'stvo "Naukova dumka", 1980

11004

CSO: 1865/100

## FOR OFFICIAL USE ONLY

UDC 621.370/550.837

## MARINE GEOPHYSICAL EXPLORATION

Kiev MORSKAYA GEOFIZICHESKAYA RAZVEDKA in Russian 1978 (signed to press 16 Dec 77)  
pp 2, 162-163

[Annotation and table of contents from book "Marine Geophysical Exploration" by Vladimir Ivanovich Gordiyenko, Institute of Physico-Mechanics, UkSSR Academy of Sciences, Izdatel'stvo "Naukova dumka", 1000 copies, 164 pages]

[Text] This monograph examines problems associated with developing the theoretical principles of designing systems intended for marine electromagnetic geophysical exploration. A new theory of marine electromagnetic exploration based on a consideration of slow motion of the marine environment is presented, and the limits of its applicability are defined. A theory of contactless electromagnetic field emitters and a theory of contactless measurement of a low frequency electric field are developed, the possible geometries of systems for marine electromagnetic exploration are analyzed, and the most effective units are selected. The general properties of electromagnetic fields are formulated, and the possibility of their reflection and reproduction by real monitoring and measuring devices is analyzed.

The monograph is intended for specialists dealing with the problems of exploratory geophysics and geophysical instrument making.

Thirty-five figures, 14 tables, 132 bibliographic references.

CONTENTS	Page
Foreword . . . . .	3
Chapter 1. Principles of the Theory of Propagation of an Electromagnetic Field in Slowly Moving Media . . . . .	9
1. The Basic Equations of an Electromagnetic Field . . . . .	9
2. Vector and Scalar Potentials of an Electromagnetic Field . . . . .	13
3. Propagation of Flat, Cylindrical and Spherical Waves . . . . .	19
4. Limits of the Theory's Applicability . . . . .	31
Chapter 2. Electromagnetic Field Emitters for Marine Geophysical Exploration . . . . .	34
1. The Electromagnetic Field of an Electric Emitter . . . . .	34
2. The Electromagnetic Field of a Toroidal Induction Coil . . . . .	39
3. The Electromagnetic Field of a Magnetic Emitter--a Magnetic Dipole . . . . .	51

## FOR OFFICIAL USE ONLY

4. Effectiveness of Using Electromagnetic Emitters . . . . .	55
5. Secondary Electromagnetic Field Emitters . . . . .	58
Chapter 3. Electromagnetic Field Receivers for Marine Geophysical Exploration . . . . .	71
1. Inductive Magnetic Field Receivers . . . . .	71
2. Principle of Operation and Basic Dependencies of Inductive Electric Field Receivers . . . . .	73
3. Deformation of an Investigated Field by the Housing of an Inductive Electric Field Receiver . . . . .	76
4. Inductive Receivers With Axial Cores . . . . .	79
5. An Inductive Electric Field Receiver With a Compound Core . . . .	84
6. Ways of Raising the Sensitivity of Inductive Electric and Magnetic Field Receivers . . . . .	87
7. Measurement of Electric and Magnetic Fields in Slowly Moving Media . . . . .	96
Chapter 4. Properties of Electromagnetic Fields . . . . .	101
1. Properties of Spherical and Cylindrical Electromagnetic Fields.	101
2. General Properties of Electromagnetic Fields . . . . .	111
3. Determination of the Distance to an Electromagnetic Field Emitter . . . . .	114
4. Reflection and Reproduction of the Properties of an Electro- magnetic Field . . . . .	117
Chapter 5. Analysis of the Geometry of Apparatus Used in Marine Geophysical Electromagnetic Exploration . . . . .	124
1. Analysis of the Geometry of Apparatus for Marine Electro- magnetic Exploration Containing Single and Differential Primary Electromagnetic Field Receivers . . . . .	124
2. Analysis of the Geometry of Apparatus for Marine Electro- magnetic Exploration Containing a Single and Differential Field Receiver in the Presence of Spherical Abnormal Bodies . .	136
Bibliography . . . . .	155

COPYRIGHT: Izdatel'stvo "Naukova dumka", 1978

11004

CSO: 1865/98

FOR OFFICIAL USE ONLY

UDC 502.3:629.78

ANNOTATION, ABSTRACTS OF ARTICLES IN COLLECTION 'PHYSICAL ASPECTS OF REMOTE SOUNDING OF OCEAN-ATMOSPHERE SYSTEM'

Moscow FIZICHESKIYE ASPEKTY DISTANTSIONNOGO ZONDIROVANIYA SISTEMY OKEAN-ATMOSFERA in Russian 1981 (signed to press 23 Apr 81) pp 2, 213-216

[Annotation and abstracts of articles in collection "Physical Aspects of Remote Sounding of Ocean-Atmosphere System", edited by Doctor of Physical and Mathematical Sciences M. S. Malkevich, Institute of Oceanology imeni P. P. Shirshov, USSR Academy of Sciences, Izdatel'stvo "Nauka", 850 copies, 216 pages]

Annotation

[Text] This collection is devoted to space, aircraft, ship and terrestrial exploration of the sea surface and the atmosphere with the purpose of remote sounding of the ocean and of the atmosphere above the ocean. Much attention is devoted to transformation of visible and infrared radiation in the atmosphere and to analysis of the dependencies between ocean parameters and emission characteristics of the "ocean-atmosphere" system.

This collection is intended for specialists in oceanology, atmospheric physics and meteorology, and other specialists using the results of studying earth from outer space.

THERMAL SOUNDING OF THE 'OCEAN-ATMOSPHERE' SYSTEM FROM SPACE: STATE OF THE PROBLEM

[Abstract of article by M. S. Malkevich]

[Text] The problem of determining the temperature of the ocean surface and the vertical temperature profile of the atmosphere by remote methods is examined. The possibility of attaining precision in such a determination necessary for solution of fundamental and applied problems in research on the ocean and atmosphere is discussed. Emphasis is laid upon the importance of the integral problem of simultaneously determining, by satellite, both the thermal characteristics and the parameters of the ocean atmosphere upon which measured radiation depends and consideration of which is necessary for solution of this integral problem on the basis of an analysis of the relationships of emissions of the "ocean-atmosphere" system and its other parameters. Four figures, 33 bibliographic references.

FOR OFFICIAL USE ONLY

FOR OFFICIAL USE ONLY

DETERMINATION OF OCEAN TEMPERATURE ON THE BASIS OF RADIATION IN AN 8-12 MICRON  
ATMOSPHERIC TRANSPARENCY WINDOW

[Abstract of article by A. K. Gorodetskiy, A. P. Orlov and B. Z. Petrenko]

[Text] The problem of determining the temperature of the ocean surface by measuring infrared radiation escaping the earth is examined. The influence of the atmosphere (aerosol attenuation and absorption by water vapor) on the error of establishing the temperature of the ocean on the basis of radiation measurements is discussed. The authors perform a numerical experiment to evaluate the aerosol effect. They conclude from this experiment that synchronous information concerning different atmospheric parameters influencing transformation of radiation in earth atmosphere must be acquired. Two tables, 10 bibliographic references.

RADIATION CYCLE AND EMISSIVITY OF THE WATER SURFACE IN THE INFRARED RANGE

[Abstract of article by A. K. Gorodetskiy and A. P. Orlov]

[Text] The relationship between the radiation and thermodynamic temperatures of the surface water layer of the ocean is analyzed. Measurements of the intensity of emission by the water surface and atmosphere, made from aboard a vessel with a radiometer with 10-12  $\mu$  spectral sensitivity, are the experimental basis for this comparison.

By combining radiation and contact measurements of the temperature of surface water the authors were able to reveal a strong dependence between angle of emission and the emissivity of the water surface, and isolate radiation from the water surface specifically and reflected atmospheric back radiation from the total intensity of radiation escaping the water-air interface. The mean effective hemispherical emissivity of water,  $\epsilon_0' = 0.96$  was also determined. Variations in the reflected flux total 1.2-3.2 percent. Two figures, 16 bibliographic references.

VERTICAL STRUCTURE OF ATMOSPHERIC TRANSFORMATION OF THE OCEAN'S INFRARED RADIATION

[Abstract of article by V. V. Badayev, A. K. Gorodetskiy, L. G. Istomina, Ye. M. Kozlov, M. S. Malkevich and A. P. Orlov]

[Text] This paper presents the results of integrated research on the vertical structure of factors transforming infrared radiation in an 8-12  $\mu$  transparency window, obtained by both direct measurement methods (by aircraft) and by indirect methods (from aboard ship), and the results of analyzing high-altitude transformation of three-dimensional nonuniformities in the temperature field of the ocean surface. It is demonstrated that the principal substance responsible for transformation of free radiation in the atmosphere is aerosol, the contribution of which to attenuation of infrared radiation in the atmosphere may be evaluated indirectly from shipboard measurements of the angular profiles of the air's emissivity and simultaneous determination of vertical thermal and moisture stratification of the atmosphere, using the concentration of "minimal values" of the effective coefficient of absorption of water vapor for this purpose. Nine figures, 16 bibliographic references.

FOR OFFICIAL USE ONLY

ABNORMAL PROPERTIES OF ATMOSPHERIC TRANSMISSION IN THE 9.6 MICRON OZONE BAND

[Abstract of article by M. S. Malkevich, L. M. Shukurova and A. I. Chavro]

[Text] Research on abnormalities in the transmission function of the atmosphere in the 9.6  $\mu$  ozone band is presented, and the causes are examined. The hypothesis that reactions of ozone with gaseous impurities and aerosol absorption bands in this interval of the spectrum have an influence on the course of the transmission function is discussed. The possibility of determining vertical concentration profiles and the total mass of ozone by measuring emissions in the ozone band is examined. Two tables, 6 figures, 26 bibliographic references.

ATMOSPHERIC ATTENUATION OF RADIATION IN WINDOWS IN THE 8-21 MICRON RANGE OF THE SPECTRUM ON THE BASIS OF MARINE AND CONTINENTAL MEASUREMENTS

[Abstract of article by A. Kh. Shukurov and A. I. Chavro]

[Text] Measurements of atmospheric transmission above the ocean in the equatorial zone of the Atlantic are presented and compared with similar measurements made on the ground. This permitted consideration of the maximum range of variations in humidity and temperature. Estimates of the aerosol and water vapor components of the optical thickness of the atmosphere are presented. One table, 2 figures, 9 bibliographic references.

DETERMINATION OF THE CONTRIBUTION BY WATER VAPOR AND AEROSOL TO THE CONTINUUM

[Abstract of article by V. V. Badayev, A. K. Gorodetskiy and A. P. Orlov]

[Text] The influence of aerosol and water vapor on continual light absorption in the atmosphere is analyzed on the basis of data acquired from shipboard and aircraft experiments (correspondingly involving large and small water vapor partial pressures) conducted with the purpose of studying variations in transmission of infrared radiation. These data were obtained with a spectrometer in the 9-15  $\mu$  region of the spectrum, and with a radiometer with 10-12  $\mu$  spectral sensitivity. Using the principle of selecting the least optical thicknesses for the given mass of water vapor, the authors evaluate the maximum possible values for the coefficients of absorption by water vapor specifically. One table, 4 figures, 16 bibliographic references.

DETERMINATION OF BRIGHTNESS TRANSFORMATION CHARACTERISTICS IN THE VISIBLE AND NEAR-IR REGIONS OF THE SPECTRUM

[Abstract of article by V. V. Badayev, A. K. Gorodetskiy, Ye. M. Kozlov and B. Z. Petrenko]

[Text] The results of aircraft synchronous vertical measurements of sky brightness and of the "water surface-atmosphere" system and the optical thicknesses of attenuation and scattering in the 0.61, 0.74, 1.01 and approximately 2  $\mu$  portions of the spectrum are presented. It is demonstrated that spectral contrasts of the water surface measured through the atmosphere depend on the contrast properties of the atmosphere and on residual absorption of radiation by the small particle size fraction of aerosol. An approximate formula accounting for atmospheric

FOR OFFICIAL USE ONLY

effects associated with remote determination of the brightness characteristics of weakly reflecting surfaces is proposed for transparency windows in the visible range of the spectrum. Two tables, 6 figures, 26 bibliographic references.

SPECTRAL BRIGHTNESS OF THE 'OCEAN-ATMOSPHERE' SYSTEM

[Abstract of article by M. S. Malkevich and L. G. Istomina]

[Text] The results of calculating the statistical characteristics of the spectral structure of the brightness field of the ocean and the atmosphere above it are presented. These calculations were made on the basis of aircraft measurements of incident solar radiation and that reflected from the ocean made at two altitudes in the atmosphere above the ocean (0.3 and 10 km). The statistical stability and reliability of the obtained data on transformation of the density distribution of the ocean's brightness in the atmosphere are examined, the mean spectral distributions of ocean and atmospheric brightness are analyzed, and the atmosphere's transfer function and transformation of albedo and spectral contrasts of the ocean in the atmosphere are analyzed. The correlation between variations in brightness of the ocean, the atmosphere and the "ocean-atmosphere" system in individual spectral intervals and the mutual correlations of the spectrums of incident and reflected radiation are evaluated.

The reasons for the opposite nature of the mutual correlation revealed at the two altitudes are discussed, and recommendations are provided on accounting for atmospheric effects when solving remote sounding problems. Five tables, 18 figures, 19 bibliographic references.

DETERMINATION OF OPTICAL CHARACTERISTICS OF THE 'SURFACE-ATMOSPHERE' SYSTEM IN THE VISIBLE SPECTRUM

[Abstract of article by Ye. M. Kozlov and V. V. Badayev]

[Text] The results of measurements, made by aircraft above the sea, of the absolute brightnesses of the path of the sun, the indicatrices of the brightness of the sky and the vertical profile of attenuation by an aerosol atmosphere in the 0.61, 0.744, 0.762 and 1.04  $\mu$  portions of the spectrum in an altitude interval of 0.1-3 km are presented. The aircraft photometer is described. The obtained data are used to analyze high-altitude transformation of the indicatrix of scattering and reflection depending on the optical state of the atmosphere and the water surface. Six figures, 15 bibliographic references.

OPTICAL CHARACTERISTICS OF CLOUDS

[Abstract of article by M. S. Malkevich, V. S. Malkova and V. I. Syachinov]

[Text] Using optical measurements of a number of portions of the visible and near-IR spectrums made by the satellite "Kosmos-320", the authors examine the possibility of determining specific absorption by a cloud mass. Papers associated with the research on absorption of solar radiation by clouds are reviewed. The nature of substances in clouds responsible for absorption is discussed. Six tables, 39 bibliographic references.

FOR OFFICIAL USE ONLY

INTEGRATED METHOD OF DETERMINING THE PHASE STATE OF WATER IN CLOUDS

[Abstract of article by A. K. Gorodetskiy, A. P. Orlova, V. I. Syachinov and D. T. Matveyev].

[Text] The experimental results of synchronous measurements made by the satellite "Kosmos-384" in the infrared (10-12  $\mu$ ) and microwave (0.8 cm) ranges are analyzed, as are simultaneous measurements of cloud brightness in the near-IR range of the spectrum (0.951 and 1.03  $\mu$ ) and cloud emissions in the 10.5-11.5  $\mu$  transparency window made by the satellite "Kosmos-320."

Basing themselves on an analysis of experimental data using television cloud cover images obtained by "Meteor" and ESSA satellites and synoptic maps, the authors propose a method of determining one of the basic parameters--the phase state of water in clouds--on the basis of simultaneous measurements of cloud brightness in the near-IR portion of the spectrum, in the 10-12  $\mu$  transparency window and in the microwave range. One table, 3 figures, 13 bibliographic references.

RADIATION CHARACTERISTICS OF CLOUDS

[Abstract of article by A. K. Gorodetsky and A. P. Orlov]

[Text] Measurements of free radiation in clouds in the descending and ascending directions are presented. The measurements were made with a radiometer sensitive to the 10.5-12  $\mu$  portion of the spectrum. The angular path of radiation through dense clouds is close to isotropic, with the deviations being up to 2-3 percent. The emissivity of dense clouds in the low and middle strata, which is  $0.96 \pm 0.04$ , is determined. Two tables, 4 figures, 30 bibliographic references.

INFORMATION CONTENT OF BACK SCATTERING SIGNALS PICKED UP BY LASER SOUNDING OF QUASIUNIFORM CLOUDS

[Abstract of article by A. K. Gorodetskiy, Yu. A. Gol'din and V. S. Malkova]

[Text] The relationship between the characteristics of a reflected back scattering pulse and the parameters of the cloud layer is examined. Back scattering by clouds and mists is subjected to numerical simulation and experimental analysis with this purpose, using pulsed lasers mounted on an airplane and a ship. The calculations resulted in a large quantity of data on the temporal dependence of a pulse of reflected radiation in relation to different cases of single and double layer cloud cover. Examples of aircraft sounding of stratified cloud cover above the sea are also analyzed, and the possibilities of studying a nonuniform cloud layer and determining its structure are discussed. Six figures, 21 bibliographic references.

**FOR OFFICIAL USE ONLY**

COMPLEX OPTICAL INSTRUMENTATION FOR ANALYZING ATMOSPHERIC SPECTRAL TRANSMISSIONS  
ALONG INCLINED AND HORIZONTAL FLIGHT PATHS IN THE ULTRAVIOLET, VISIBLE AND INFRARED  
RANGES OF THE SPECTRUM (0.3-25 MICRONS)

[Abstract of article by P. P. Anikin, A. I. Chavro and A. Kh. Shukurov]

[Text] Complex optical instrumentation permitting synchronous measurement of spectral atmospheric transmission on inclined flight paths in a broad range of the spectrum is described. The results of measuring spectral transmission by clouds with a system of five spectrometers are presented. The error of determining the relationship between optical thicknesses of different types of clouds is evaluated. Spectral attenuation of emissions by cumulus and cirrus clouds in the visible, infrared and ultraviolet ranges of the spectrum is compared. Eight figures, 10 bibliographic references.

COPYRIGHT: Izdatel'stvo "Nauka", 1981

11004

CSO: 1865/99

FOR OFFICIAL USE ONLY

TERRESTRIAL GEOPHYSICS

UDC 532.51:519.63

ONE-DIMENSIONAL COMPUTATIONS OF DISPLACEMENTS DURING BLAST IN PROBLEMS WITH WEAK TWO-DIMENSIONALITY

Moscow IZVESTIYA AKADEMII NAUK SSSR: FIZIKA ZEMLI in Russian No 1, Jan 82  
(manuscript received 18 Jul 80) pp 63-71

[Article by A. V. Zabrodin, V. V. Kadet, L. A. Pliner, I. F. Podlivayev and V. I. Selyakov]

[Text]

Abstract: A study was made of the possibility of using one-dimensional methods in investigating two-dimensional gas-dynamical problems. In the example of the problem of an unvented blast in a stratum it was possible to demonstrate the characteristic difference in the results of two- and one-dimensional computations. An upper estimate of the nonclosure between two- and one-dimensional computations was obtained; this was based solely on the information obtained when carrying out one-dimensional computations. The class of problems for which the estimate obtained in the study is correct is indicated. The theoretical estimate is compared with the real computed nonclosure. It is shown that the sectoral method makes it possible not only to clarify the principal features of solution of two-dimensional problems, but also to evaluate some purely two-dimensional effects, such as the phenomenon of pinching of strata during a blast in a stratified medium.

The use of unvented shots in the national economy has recently assumed increasingly broader scales. In particular, the task of augmenting the production of petroleum and gas by the setting off of strong shots in collectors is becoming increasingly timely.

The difference in the geophysical properties of the stratum and the surrounding rock mass leads to a need for taking into account non-one-dimensional effects when carrying out blasting work underground. Due to the costliness and great

## FOR OFFICIAL USE ONLY

amount of work involved in preparing and applying two-dimensional computation methods the question arises of the possibility of carrying out investigations of these effects on the basis of one-dimensional computations. The existing practice of computations, for example, in [1], revealed the effectiveness of application of one-dimensional methods in computations of problems involving blasts in a medium with an inhomogeneity.

However, there has been no mathematical validation of such a method for solving a definite class of problems. In this article we examine a class of problems related to the effect of a blast on a stratified medium. This class of problems is of the greatest practical interest because real rocks usually have a stratified structure.

The most significant manifestations of the two-dimensional effect can naturally be expected in the near zone of the blast, where the displacements are maximum. It is known that in this region the stresses exceed the strength constants of the medium, and accordingly, in the near zone the problem can be examined in a hydrodynamic approximation.

As an example we considered the problem of the initial stage in an unvented blast in a stratum whose properties differ from the properties of the surrounding rock mass. The stratum (regions I and II), axisymmetric relative to the Ox-axis, is filled with matter with the density  $\rho_1$  and with the initial speed of sound  $c_1$ , whereas the medium surrounding it (region III) is filled with matter with the density  $\rho_2$  and the speed of sound  $c_2$  (Fig. 1). The plane of mirror symmetry, perpendicular to the Ox-axis, intersects it at the point  $x = 0$ . At the initial moment in time in the cylindrical region I there is a release of energy with the volume density  $E_0$ , after which a shock wave is formed which propagates in the stratum and in the medium surrounding it.

The non-one-dimensionality of the problem is related both to the stratified structure of the medium and also the cylindrical shape of this charge. As a result of propagation of the shock wave in such a medium it is possible to observe the following physical effect: if the shock wave in the stratum "escapes" more rapidly than at the subsequent moments in time the pressure in the surrounding rock mass will exceed the pressure in the stratum and its pinching is possible. It is known that such phenomena are observed, for example, during blasts in tunnels [2].

The pinching effect will be the greater the greater the velocity of the shock wave in the stratum in comparison with the velocity of the shock wave in the surrounding medium and the greater the density of the rock matter in comparison with the density of stratum matter. For real rocks the ratio of the densities and the speeds of sound usually does not exceed 1.5 and 1.25 respectively. Moreover, it is known that the speed of sound is greater in the more dense material; accordingly, in order to obtain the maximum possible manifestation of the pinching effect in the model computations an "exotic" relationship of the parameters of the stratum and the surrounding rock mass is selected:  $\rho_1/\rho_2 = 0.66$ ;  $c_1/c_2 = 1.25$ .

The problem of shock wave propagation is described by a system of differential equations of conservation of mass, momentum and energy which can be represented in the form [3]:

## FOR OFFICIAL USE ONLY

$$\begin{aligned}
\frac{\partial v}{\partial t} + u \frac{\partial v}{\partial r} - v \frac{\partial u}{\partial r} - \frac{2uv}{r} &= -\frac{w}{r} \frac{\partial v}{\partial \theta} + \frac{v}{r} \frac{\partial w}{\partial \theta} + wv \frac{\operatorname{ctg} \theta}{r}, \\
\frac{\partial u}{\partial t} + u \frac{\partial u}{\partial r} + v \frac{\partial P}{\partial r} &= \frac{w}{r} - \frac{w}{r} \frac{\partial u}{\partial \theta}, \\
\frac{\partial w}{\partial t} + u \frac{\partial w}{\partial r} + \frac{w}{r} \frac{\partial w}{\partial \theta} + \frac{wu}{r} + \frac{v}{r} \frac{\partial P}{\partial \theta} &= 0, \\
\frac{\partial S}{\partial t} + u \frac{\partial S}{\partial r} &= -\frac{w}{r} \frac{\partial S}{\partial \theta}; \quad S = S(P, v).
\end{aligned} \tag{1}$$

Here  $t$  is time,  $r$  is radius,  $\theta$  is the polar angle,  $u$  and  $w$  are the radial and angular velocity components respectively,  $P$  is pressure,  $\rho$  is density,  $v = 1/\rho$  is specific volume,  $S$  is specific entropy.

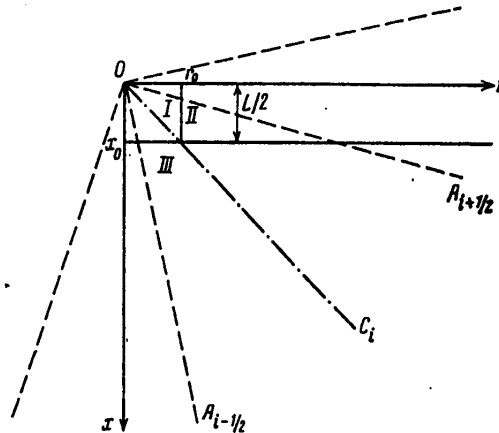


Fig. 1. Stratum in surrounding rock mass and discrimination of sectors for one-dimensional computations.

At pressures characteristic for the initial stage of a strong blast the equation of state will be determined by the thermal terms (4)

$$E = E_x + E_T \approx E_T = \frac{P}{\Gamma(\rho)\rho},$$

where  $E_T$  is the internal energy of thermal pressure per unit volume,  $E_x$  is the internal energy of "cold" pressure per unit volume,  $\Gamma(\rho)$  is the Grüneisen parameter, which in the gas-dynamical stage in the process can be identified with the parameter  $(\gamma - 1)$ ;  $\gamma$  is the adiabatic index. In practical computations an allowance for the "cold" component is usually made by employing a two-term equation of state [5, 6]:

$$E = \frac{P - c_0^2(\rho - \rho_0)}{(\gamma - 1)\rho},$$

## FOR OFFICIAL USE ONLY

where  $\rho_0$  is the initial density of matter,  $c_0$  is the initial speed of sound. System (1) was solved numerically by the method set forth in [5]. The computation method is based on a scheme of decay of an arbitrary fracture, and what is especially important, is adaptable to the conditions of the problem, that is, it is possible to discriminate and investigate in detail the characteristic features of the solution (shock wave fronts, contact boundaries, discontinuities, etc.).

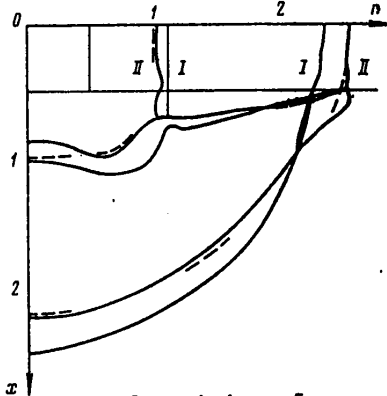


Fig. 2. Results of computation of position of wave front and boundaries of stratum. The dashed curve represents computations by the sectoral method. The solid curves represent two-dimensional computations.

One of the purposes of two-dimensional computations was a determination of the degree of pinching -- warping of the boundary of the stratum and the medium.

In order to make an independent investigation of the phenomena caused by inhomogeneity of the medium and the effects associated with the cylindrical form of the charge we examined two limiting cases: 1)  $\rho_1/\rho_2 = 1$ ;  $c_1/c_2 = 1$  -- the medium is isotropic and the non-one-dimensionality of the problem is related only to the cylindrical shape of the charge; 2) the ratios  $\rho_1/\rho_2 = 0.66$  and  $c_1/c_2 = 1.25$  assume values extremely possible for natural conditions and the effects associated with inhomogeneity of the medium are maximum.

The results of computations of these variants for some moment in time are represented in Fig. 2. In the computations it was assumed that  $\rho_1 = 1.4 \text{ g/cm}^3$ ;  $c_1 = 5 \text{ km/sec}$ ;  $E_0 = 2.5 \cdot 10^5 \text{ J/cm}^3$ ; the half-width of the stratum is  $0x_0 = 5 \text{ m}$ ; the radius of energy release is  $r_0 = 5 \text{ m}$ .

A comparison of computations of these variants shows that both effects, both inhomogeneity of the medium and the cylindrical shape of the charge, favor pinching of the stratum, but in general with the indicated relationship of parameters of the medium there is no significant geometrical pinching of the stratum (the pinching does not exceed 4%). An analysis of the velocity field shows that by the time for which the position of the boundary of the stratum is shown in Fig. 2 the movement of the segment of the boundary in the pinching region in a transverse direction virtually ceases and the dimensions of the pinching zone remain unchanged.

## FOR OFFICIAL USE ONLY

The absence of an essentially two-dimensional geometrical effect indicates the possibility of an approximate solution of this problem by means of the sectoral method, which is a combination of computations for nonmutually interacting sectors into which the region of interest to us is broken down. One of the possible variants of organization of the sectoral computations is as follows. The rays  $OA_{i-1/2}$ ,  $OA_{i+1/2}$  are drawn from the origin of coordinates, naturally coinciding with the discriminated point, of the blast epicenter type. These and similar rays bound the regions called sectors (Fig. 1). Within each sector we select still another ray -- its "representative." For example, in Fig. 1 the "representative" of the  $i$ -th sector ( $A_{i-1/2}OA_{i+1/2}$ ) is the ray  $OC_i$ . Such a ray can be, for example, the bisector of an angle. Boundaries of the layers are stipulated along these rays; these ensure an equality of masses and internal energies within the limits of the corresponding sector for the two-dimensional problem and the one-dimensional sectoral problem. If at the initial time the medium moves, a distribution of velocities maintaining the momenta is stipulated. A spherically symmetric problem with initial data obtained for the representative ray is computed for each sector.

In this study the computations were made for three sectors whose representative rays were the  $Ox$ ,  $Or$  axes or the bisector of the angle  $xOr$ . The sectors defined near the  $Ox$ - and  $Or$ -axes have an angle aperture  $30^\circ$ ; the aperture angle of the mean sector is  $60^\circ$ . The results of computations by the sectoral method are represented in Fig. 2 by dashed curves. The position of the front of these waves coincides with the results obtained in two-dimensional computations with an accuracy no worse than 1%; accordingly, the position of the boundaries of energy release at a particular moment in time differs by not more than 13%. The maximum error of the method in determining the geometrical parameters of the problem arises in a sector whose representative ray is the axis of symmetry.

## Evaluation of Error of Sectoral Method

An evaluation of the error in the sectoral method based solely on information obtained when making sectoral computations is of practical interest. Such an evaluation can be made for a class of problems whose solution is expanded into a quite rapidly convergent series in spherical harmonics so that already the first two terms of the expansion give the main part of the solution. A presentation of the solutions of two-dimensional gas-dynamical problems in the form of series in spherical functions and the derivation of a system of equations for the expansion coefficients is given in [7]. Since in a sectoral approximation the angular velocities are completely absent, for an evaluation of the main part of the error it is sufficient to compare the sectoral computations with the roughest approximation, containing angular velocities. It should be noted that when obtaining an evaluation the two-dimensional initial distribution can be replaced by the sum of the first two harmonics, but not in the entire region of determination of the problem, only in the region of sectors for which the evaluation of the nonclosure is made. Therefore, an increase in the number of the sectors leads to a considerable broadening of the class of problems for which the evaluation obtained in the study will be correct. In order to find the error in sectoral computations it is necessary to evaluate the parameters with the subscript  $\epsilon$ :

## FOR OFFICIAL USE ONLY

$$\begin{aligned}
u_i &= u_0 + u_1 \cos \Theta - u_i; \\
v_i &= v_0 + v_1 \cos \Theta - v_i; \\
P_i &= P_0 + P_1 \cos \Theta - P_i; \\
S_i &= S_0 + S_1 \cos \Theta - S_i; \\
W_i &= W_1 \sin \Theta.
\end{aligned}$$

The subscripts i denote the corresponding values in the sector i; the subscripts 0 and 1 were used for denoting the coefficients of the zero and first harmonics respectively; the remaining notations are as before.

Henceforth the evaluations of the errors are made in a Lagrangian coordinate system in the i-th sector; the mass coordinate m is introduced:  $dm = \rho r^2 dr|_{i=0}$ .

Omitting unwieldy computations, we will give the form of a system of equations in gas dynamics for coefficients of the harmonics:

$$\begin{aligned}
\frac{\partial u_0}{\partial t} + r_i^2 \frac{\partial P_0}{\partial m} &= \frac{r_i^2}{v_i} (u_i - u_0) \frac{\partial u_i}{\partial m} + r_i^2 \left( 1 - \frac{v_0}{v_i} \right) \frac{\partial P_i}{\partial m}; \\
\frac{\partial v_0}{\partial t} - r_i^2 \frac{\partial u_0}{\partial m} &= \frac{r_i^2}{v_i} (u_i - u_0) \frac{\partial v_i}{\partial m} - r_i^2 \left( 1 - \frac{v_0}{v_i} \right) \frac{\partial u_i}{\partial m}; \\
\frac{\partial S_0}{\partial t} &= (u_i - u_0) \frac{r_i^2}{v_i} \frac{\partial S_0}{\partial m}; \quad S_0 = F(P_0, v_0); \\
\frac{\partial u_i}{\partial t} + r_i^2 \frac{\partial P_i}{\partial m} + u_i \frac{r_i^2}{v_i} \frac{\partial u_i}{\partial m} + v_i \frac{r_i^2}{v_i} \frac{\partial P_i}{\partial m} &= 0; \\
\frac{\partial v_i}{\partial t} - r_i^2 \frac{\partial u_i}{\partial m} - \left( \frac{2v_i}{r_i} - \frac{r_i^2}{v_i} \frac{\partial v_i}{\partial m} \right) u_i - \\
- \left( \frac{2u_i}{r_i} + \frac{r_i^2}{v_i} \frac{\partial u_i}{\partial m} \right) v_i - \frac{2v_i}{r_i} w_i &= 0; \\
\frac{\partial w_i}{\partial t} + \frac{u_i}{r_i} w_i - \frac{v_i}{r_i} P_i &= 0; \\
\frac{\partial S_i}{\partial t} + u_i \frac{r_i^2}{v_i} \frac{\partial S_i}{\partial m} &= 0; \\
S_i &= \frac{\partial F(P_i, v_i)}{\partial P_i} P_i + \frac{\partial F(P_i, v_i)}{\partial v_i} v_i;
\end{aligned} \tag{2}$$

with the initial conditions

$$x_0(0, m) = \xi_0(m); \quad x_1(0, m) = \xi_1(m);$$

where  $x_0$  and  $x_1$  are elements of the normalized space of vector-solutions.

Here and in the text which follows  $F(P, v)$  is the equation of state. The system for the errors has the form

## FOR OFFICIAL USE ONLY

$$\begin{aligned}
\frac{\partial u_i}{\partial t} + r_i^2 \frac{\partial P_i}{\partial m} + \frac{r_i^2}{v_i} \frac{\partial u_i}{\partial m} u_i + \frac{r_i^2}{v_i} \frac{\partial P_i}{\partial m} v_i &= 0; \\
\frac{\partial v_i}{\partial t} - r_i^2 \frac{\partial u_i}{\partial m} - \frac{2u_i}{r_i} v_i + \left( \frac{r_i^2}{v_i} \frac{\partial v_i}{\partial m} - 2 \frac{v_i}{r_i} \right) u_i &= \\
= \cos \theta_i \left( \frac{r_i^2}{v_i} \frac{\partial u_i}{\partial m} v_i + \frac{2v_i}{r_i} w_i \right); & \\
\frac{\partial S_i}{\partial t} + \frac{r_i^2}{v_i} \frac{\partial S_i}{\partial m} u_i &= 0; \\
S_i = \frac{\partial F(P_i, v_i)}{\partial P_i} P_i + \frac{\partial F(P_i, v_i)}{\partial v_i} v_i; &
\end{aligned} \tag{3}$$

with the initial condition

$$x_i(0, m) = \xi_i(m).$$

It can be seen from the second equation in system (3) that the source of the inhomogeneity of the problem for errors is the continuity equation; the maximum inhomogeneity must be expected at the poles:  $\theta = 0, \pi$ .

The subsequent approach for computing evaluations of the errors is similar to that used in [8] and [9]. We will introduce Riemann invariants for systems (2) (the sectoral subscripts will be omitted in subsequent computations):

$$G_i = u_i + \frac{v}{c} P_i; \quad H_i = u_i - \frac{v}{c} P_i; \quad S_i; \quad w_i, \tag{4}$$

where

$$c = v \sqrt{\frac{\partial F(P, v)}{\partial v} / \frac{\partial F(P, v)}{\partial P}} -$$

is the speed of sound. We introduce the notations:

$$\begin{aligned}
\frac{r^2}{v} \frac{\partial u}{\partial m} &= \alpha_1; \quad \frac{r^2}{v} \frac{\partial P}{\partial m} = \alpha_2; \\
\frac{c}{v} \left( \frac{r^2}{v F_v'} \frac{\partial S}{\partial m} + \frac{2v}{r} - \frac{r^2}{v} \frac{\partial v}{\partial m} \right) &= \beta_1; \\
\frac{c}{v F_v'} \frac{\partial F_v'}{\partial t} = \beta_2; \quad \frac{c}{v} \left( \frac{2u}{r} + \frac{r^2}{v} \frac{\partial u}{\partial m} + \frac{1}{F_v'} \frac{\partial F_v'}{\partial t} \right) &= \beta_3; \quad \frac{2c}{r} = \beta_4; \\
\frac{\alpha_1}{2} \pm \frac{r^2 \frac{\partial}{\partial m} \left( \frac{c}{v} \right) - \alpha_2 \frac{v}{c}}{2} &= \gamma_1, \gamma_2; \quad \frac{\alpha_2}{F_v'} = \gamma_3; \\
\frac{\beta_1}{2} \pm \frac{\frac{v}{c} \frac{\partial}{\partial t} \left( \frac{c}{v} \right) + \beta_2 \left( \frac{c}{v} \right) - \beta_3 \left( \frac{v}{c} \right)}{2} &= \delta_1, \delta_2; \\
\frac{\beta_3}{F_v'} = \delta_3; \quad \beta_4 &= \delta_4; \\
A_{11} = \gamma_1 + \delta_1; \quad A_{12} = \gamma_2 + \delta_2; \quad A_{13} = \gamma_3 + \delta_3; \\
A_{14} = \delta_4; \quad A_{21} = \gamma_1 - \delta_1; \\
A_{22} = \gamma_2 - \delta_2; \quad A_{23} = \gamma_3 - \delta_3; \quad A_{24} &= -\delta_4;
\end{aligned} \tag{5}$$

## FOR OFFICIAL USE ONLY

$$A_{31} = \frac{r^2}{2v} \frac{\partial S}{\partial m}; \quad A_{32} = A_{31};$$

$$A_{41} = -\frac{c}{2r}; \quad A_{42} = -A_{41} = \frac{c}{2r}; \quad A_{44} = \frac{u}{r}.$$

The substitution of (4) into system (2), with (5) taken into account, gives

$$\begin{aligned} \frac{\partial G_1}{\partial t} + \frac{r^2 c}{v} \frac{\partial G_1}{\partial m} + A_{11}G_1 + A_{12}H_1 + A_{13}S_1 + A_{14}w_1 &= 0; \\ \frac{\partial H_1}{\partial t} - \frac{r^2 c}{v} \frac{\partial H_1}{\partial m} + A_{21}G_1 + A_{22}H_1 + A_{23}S_1 + A_{24}w_1 &= 0; \\ \frac{\partial S_1}{\partial t} + A_{31}G_1 + A_{32}H_1 &= 0; \\ \frac{\partial w_1}{\partial t} + A_{41}G_1 + A_{42}H_1 + A_{44}w_1 &= 0; \end{aligned} \quad (6)$$

Introducing the vector-column  $z_1 = (G_1/G_1^*, H_1/H_1^*, S_1/S_1^*, w_1/w_1^*)$ , where  $G_1^*, H_1^*, S_1^*, w_1^*$  is the characteristic value of the invariants, and the matrix

$$A = \begin{pmatrix} A_{11}; & A_{12}H_1^*/G_1^*; & A_{13}S_1^*/G_1^*; & A_{14}w_1^*/G_1^* \\ A_{21}G_1^*/H_1^*; & A_{22} & A_{23}S_1^*/H_1^*; & A_{24}w_1^*/H_1^* \\ A_{31}G_1^*/S_1^*; & A_{32}H_1^*/S_1^*; & 0; & 0 \\ A_{41}G_1^*/w_1^*; & A_{42}H_1^*/w_1^*; & 0; & A_{44} \end{pmatrix}$$

we write the system (6) in matrix form with the right part Q introduced for universality:

$$\frac{\partial z_1}{\partial t} + D \frac{\partial z_1}{\partial m} + Az_1 = Q, \quad (7)$$

where D is the symmetric matrix

$$D = \begin{pmatrix} r^2 c/v & 0 & 0 & 0 \\ 0 & -r^2 c/v & 0 & 0 \\ 0 & 0 & 0 & 0 \\ 0 & 0 & 0 & 0 \end{pmatrix}$$

Determining the scalar product and the vector norm

$$\|z\| = \sqrt{\int_0^M (z, z) dm}.$$

after multiplying (7) by  $z_1$  and integrating for m we obtain

$$\frac{\partial}{\partial t} \|z_1\|^2 = (z_1, Dz_1)|_{m=0} - (z_1, Dz_1)|_{m=M} +$$

## FOR OFFICIAL USE ONLY

$$+ \int_0^M (z_1, (D_m - 2A)z_1) dm + 2 \int_0^M (z_1, Q) dm.$$

Here  $M$  is the maximum value of the mass  $m$  used in the problem.

Now we will select the constants  $c_2$  and  $c_3$  in such a way that

$$|(z_1, Dz_1)|_{m=0} - |(z_1, Dz_1)|_{m=M} \leq c_2 \|z_1\|^2;$$

$$\int_0^M |(z_1, (D_m - 2A)z_1)| dm \leq c_3 \|z_1\|^2.$$

We use the notation  $c_1 = (c_2 + c_3)/2$  and employing the Cauchy-Bunyakovskiy inequality, we obtain

$$\frac{\partial}{\partial t} \|z_1\| \leq c_1 \|z_1\| + \|Q\|,$$

from which it follows that

$$\|z_1\| \leq \|z_1\|_{t=0} e^{c_1 t} + \int_0^t e^{c_1(t-\tau)} \|Q(\tau)\| d\tau. \quad (8)$$

The evaluation (8) of solution of system (2) has an auxiliary character and is necessary only to the extent that the  $z_1$  vector enters into the right part of system (3), the evaluation of whose solution is the final objective.

Similarly we obtain an evaluation of system (3)

$$\|z_2\| \leq e^{c_1 t} \left\{ \|z_2\|_{t=0} + \gamma_2 \|z_1\|_{t=0} \frac{e^{(c_1 - c_2)t} - 1}{c_1 - c_2} \right\}. \quad (9)$$

Here it is assumed that  $Q = 0$  and the  $\gamma_2$  value is selected from the expression

$$\|Q_2\| \leq \gamma_2 \|z_1\|.$$

For short times  $t < \min \{1/c_2, 1/(c_1 - c_2)\}$  the evaluation is simplified

$$\|z_2\| \leq \|z_2\|_{t=0} + \gamma_2 \|z_1\|_{t=0} t.$$

The initial vectors  $z_1(0, m)$  and  $z_2(0, m)$  are obtained from the functions  $\xi_1(m)$  and  $\xi_2(m)$ . As a parameter the constants  $\gamma_2$  and  $\|z_2\|_{t=0}$  include  $\cos \theta_1$ . In principle the choice of the initial formulation of the problem and the representative rays can be accomplished by minimizing the parameters  $\|z_2\|_{t=0}$  and  $\|z_1\|_{t=0}$  for all sectors.

It follows from (9) that the nonclosure increases exponentially with time. In actuality, as indicated by the computations, the nonclosure arises in the initial stage of the process during some characteristic time and thereafter in essence does not change. Therefore, for practical evaluations of the nonclosures it is evidently necessary to substitute  $t \approx \tau$  into (9), where  $\tau$  is the characteristic time of the problem.

## FOR OFFICIAL USE ONLY

In this case for the evaluation it was assumed that  $\tau = L/c$ , where  $L$  is the thickness of the stratum. The following values of the constants were obtained in this case:

$$c_1 \approx c_2 \approx 0.3; \quad \gamma_1 \approx 0.8; \quad \|z_1\|_{t=0} \approx 0.17; \quad \|z_2\|_{t=0} \approx 0.22.$$

Accordingly, the nonclosure value is  $\|z_{\varepsilon, p}\|_{t=\tau} \approx 1$ . A comparison of the numerical computations gives for this same moment in time the real error  $\|z_{\varepsilon, p}\|_{t=\tau} \approx 0.4$ , that is, the upper evaluation of the error in the method in this problem exceeds the real error by a factor of 2.5. An examination of the relative error  $\|z_{\varepsilon, p}\| / \|z_p\|$  shows that in this case it drops off because the norm of the solution vector  $\|z_p\|$  increases more rapidly than the nonclosure vector  $\|z_{\varepsilon, p}\|$ . By the selected moment in time  $\|z_{\varepsilon, p}\|$  increases by a factor of 2, whereas  $\|z_p\|$  increases by a factor of 2.5; accordingly

$$(\|z_{\varepsilon, p}\| / \|z_p\|)_{t=0} \approx 0.15, \text{ and } (\|z_{\varepsilon, p}\| / \|z_p\|)_{t=\tau} \approx 0.12.$$

Despite the fact that some two-dimensional effects are not determined formally by the sectoral method, they can be evaluated on the basis of sectoral computations. This sort of effects includes pinching of the stratum, determination of whose value was one of the principal purposes of two-dimensional computations. In order to obtain the magnitude of the displacement for the discontinuity of the media we will select two sectors between which the boundary to be investigated is situated. Using the results of sectoral computations it is possible to determine the radial velocities at the boundary and determine the pressure gradients  $\partial P / \partial \theta \approx \Delta P / \Delta \theta$ . Using the third equation of system (1), neglecting the squares of small values and employing Lagrangian coordinates, we obtain an equation for the angular velocity component:

$$\frac{\partial w}{\partial t} + \frac{u_{i+1/2}}{r_{i+1/2}} w = - \frac{v_{i+1/2}}{r_{i+1/2}} \frac{\Delta P_{i+1/2}}{\Delta \theta_i}, \quad (10)$$

where, for example, by the term  $u_{i+1/2}(t, m)$  is meant some mean value interpolated between  $u_i$  and  $u_{i+1}$ . Integrating this equation under the condition  $w|_{t=0} = 0$ , we obtain

$$w(t, m) = - \int_0^t \frac{v_{i+1/2}(\eta, m)}{r_{i+1/2}(\eta, m)} \frac{\Delta P_{i+1/2}(\eta, m)}{\Delta \theta} \exp \left\{ - \int_{\tau}^t \frac{u_{i+1/2}(\tau, m)}{r_{i+1/2}(\tau, m)} d\tau \right\} d\eta. \quad (11)$$

Knowing the radial and angular velocity components, it is easy to ascertain the boundary displacement. Computations using formula (11) give a pinching value  $\sim 2-3\%$ , which satisfactorily agrees with the precise solution.

Thus, our computations indicated that the sectoral method not only makes it possible to detect the principal features of solution of two-dimensional problems, but also to evaluate some purely two-dimensional effects.

It has been established that for real rocks the effect of pinching of strata in the dynamic stage is extremely small and for investigation of such a class of gas-dynamical problems (where  $\Delta \rho / \rho$  is of the order of several units) it is possible to apply the sectoral method. In this case the error of the sectoral method can be evaluated analytically by the method described in the article.

FOR OFFICIAL USE ONLY

BIBLIOGRAPHY

1. Terhune, R. W. and Shaw, J. G., "Calculation of Rock Fracturing From Multiple Nuclear Explosive Sources," PEACEFUL NUCLEAR EXPLOSIONS, 1974.
2. Crowley, B. K., Glenn, H. D. and Marks, R. F., "An Analysis of Marvel, a Nuclear Shock-Tube Experiment," PEACEFUL NUCLEAR EXPLOSIONS, 1974.
3. Stanyukovich, K. P., NEUSTANOVIVSHIYESYA DVIZHENIYA SPLOSHNOY SREDY (Unsteady Movements of a Continuous Medium), Moscow, Nauka, 1971.
4. Zel'dovich, Ya. B. and Rayzer, Yu. P., FIZIKA UDARNYKH VOLN I VYSOKOTEMPÉRATURNYKH GIDRODINAMICHESKIKH YAVLENIY (Physics of Shock Waves and High-Temperature Hydrodynamic Phenomena), Moscow, Nauka, 1966.
5. CHISLENNOYE RESHENIYE MNOGOMERNYKH ZADACH GAZOVOY DINAMIKI (Numerical Solution of Multidimensional Problems in Gas Dynamics), edited by S. K. Godunov, Moscow, Nauka, 1976.
6. TEORETICHESKIYE OSNOVY I KONSTRUIROVANIYE CHISLENNYKH ALGORITMOV ZADACH MATEMATICHESKOY FIZIKI (Theoretical Principles and Formulation of Numerical Algorithms in Problems of Mathematical Physics), edited by K. I. Babenko, Moscow, Nauka, 1979.
7. Podlivayev, I. F., PRIMENENIYE SFERICHESKIKH FUNKTSIY V GAZODINAMICHESKIKH ZADACHAKH (Use of Spherical Functions in Gas-Dynamical Problems), Moscow, Preprint IPM AN SSSR, No 91, 1975.
8. Kurant, R., URAVNENIYA S CHASTNYMI PROIZVODNYMI (Equations With Partial Derivatives), Moscow, Mir, 1964.
9. Godunov, S. K., URAVNENIYA MATEMATICHESKOY FIZIKI (Equations of Mathematical Physics), Moscow, Nauka, 1979.

COPYRIGHT: Izdatel'stvo "Nauka", Izvestiya AN SSSR, Fizika Zemli, 1982

5303

CSO: 1865/120

- END -